LUND UNIVERSITY

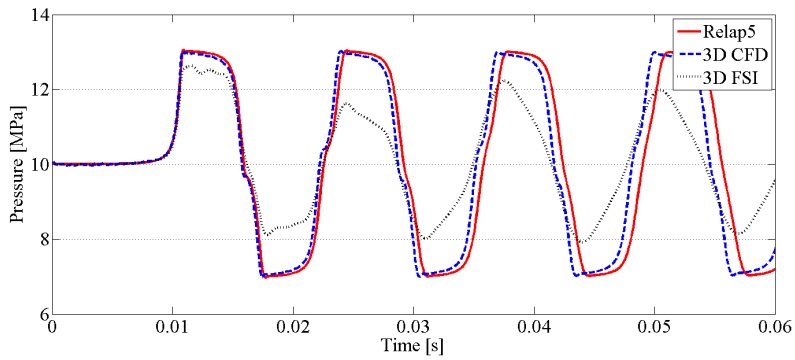

A COMPARATIVE STUDY OF COUPLED AND UNCOUPLED ANALYSIS METHODS FOR THERMOHYDRAULIC LOADS IN PIPE SYSTEMS

DAVID BJURHEDE and MATS HARRYSON

Structural Mechanics

Master's Dissertation

Department of Construction Sciences
Structural Mechanics

ISRN LUTVDG/TVSM--12/5178--SE (1-137)
ISSN 0281-6679

A COMPARATIVE STUDY OF COUPLED AND UNCOUPLED ANALYSIS METHODS FOR THERMOHYDRAULIC LOADS IN PIPE SYSTEMS

Master's Dissertation by

DAVID BJURHEDE and MATS HARRYSON

Supervisors:
Per-Erik Austrell *Senior Lecturer*,
Div. of Structural Mechanics, LTH, Lund

Per-Henrik Myrefelt, Johan Lundvall and Olof Dahlberg,
FS Dynamics Sweden AB

Examiner:
Kent Persson *PhD*,
Dept. of Construction Sciences, LTH, Lund

Printed by Media-Tryck LU, Lund, Sweden, December, 2012 *(Pl)*.

For information, address:
Division of Structural Mechanics, LTH, Lund University, Box 118, SE-221 00 Lund, Sweden.
Homepage: http://www.byggmek.lth.se

Preface

We begun work on our Master's dissertation in October 2010. Now, a little more than 2 years later it is finally finished. Both personal and proffesional reasons got in the way of the work. The work was carried out at the Department of Nuclear Engineering at FS Dynamics Sweden AB in Helsingborg and in collaboration with the Division of Structural Mechanics at Lund Institute of Technology. During this process we've learned to handle a lot of different commercial softwares and acquired an insight in to how the different theories behind the simulation methods work. We've also learned the value of planing your work and to make sure that you know what you need to do and what information you need to do it. We would like to extend our deepest thanks to everyone that have been involved.

Thanks to all our co-workers at FS Dynamics in Helsingborg. Special thanks to Per-Henrik Myrefelt, Johan Lundvall and Olof Dahlberg that have been a great support during this long process and helped us with their experience and knowledge. Also thanks to Per-Erik Austrell at the Division of Structural Mechanics for your patience.

David Bjurhede & Mats Harryson
Helsingborg, December 2012

Abstract

The structural integrity of the Swedish nuclear power plants continuously needs to be verified according to the standards decided by the Swedish Radiation Safety Authority. One part of the standard is to compute the stress response in the pipe systems and to verify them according to the current codes for the industry, such as the ASME code for boiler and pressure vessels. One method of performing these verifications is to use a 1-D fluid simulation software to calculate the forces within the pipe and then apply those forces on a pipe system stress calculation software where the pipes are regarded as beams. In this Master's dissertation, results from performing an evaluation according to the method above, using the 1-D fluid simulation software Relap5 and the pipe system stress calculation tool Pipestress, will be compared to performing the same evaluation using more refined simulation methods. The purpose is to evaluate whether or not a more refined simulation method will generate a lower stress response and to show if the Relap5 and Pipestress simulation method is conservative.

New forces will be calculated using a CFD-simulation software, ADINA CFD. More refined FEM-calculations, using ADINA FEM, will be performed using both the Relap5 and the ADINA CFD forces. Lastly, a Fluid Structure Interaction (FSI) simulation will be performed, connecting the ADINA CFD with the ADINA FEM code to run simultaneously and to interact with each other.

The pipe system examined in this Master's dissertation is a fictive setup, total of five meters long, running between two tanks. The pipe system is supported at five points along the pipe. A pressure wave propagation will be examined within the pipe system. The pressure wave will be initiated by a fast closing valve. The simulations will be performed at such a high pressure that cavitation will be avoided.

In this Master's dissertation it is shown that a more refined simulation method gives a lower stress response in two out of three evaluation points along the pipe system. However, the FSI simulation does not yield lower stress responses, this is because of how the pressure within the system is accounted for in the different methods. It is clear that the Relap5 and Pipestress simulation method is conservative. It is also observed that the frequency of the pressure waves and the forces are increased using the more refined simulation methods.

Keywords: Pipestress, Relap5, Fluid Structure Interaction, FSI, Nuclear engineering

Contents

Chapter 1

Introduction

This Master's dissertation is performed in the subject of structural mechanics. It is performed at the company FS Dynamics's office in Helsingborg. FS Dynamics is a company with about a total of 150 employees in Sweden, Denmark and Finland. The company head quarter is located in Gothenburg. FS Dynamics is a consultant company that performs fluid and structural calculations, either in projects in-house for clients or as support personnel at the client's location. One part of the company is the nuclear engineering department which performs simulations with one dimensional flow computational tools like Relap5 and stress evaluation tools like Pipestress. The results are evaluated according to the ASME code that are based on experimental testing of pipe systems and components. The company suspect there might be some conservatism with the current method. There have been discussion about however more detailed 3D simulations can be used to achieve more accurate results that might give lower utilization on the pipe system.

1.1 Purpose

The purpose of this Master's dissertation is to analyze the difference between a fully coupled Fluid Structure Interaction (FSI) simulation and uncoupled simulation methods for thermo hydraulic loads in pipe systems during sudden pressure surges such as fast closing valves or pipe ruptures. This in order to be able to establish whether or not the current method is

conservative and in some extension to quantify the conservatism. Another reason for this analysis is to decide if a fully coupled FSI simulation could be used as an additional tool when the current method does not provide sufficient results. Theoretically the most accurate simulation will be the one that is implemented with a fully coupled FSI simulation.

Acording to the articles [1] and [2], the results given by the FSI simulations goes well hand in hand with the results of the testing. The displacement and stress results of the experiments and the FSI simulations are generally below the results of the computational uncoupled simulations. The similarity of the FSI simulations to the experimental results are shown and there is a reason to believe that with FSI, a more realistic result will be obtained. Because of this, the Relap and Pipestress combination is assumed to be conservative.

Chapter 2

Method

2.1 Implementation

The dissertation emanate from the current simulation method which is to first calculate the time history load using the fluid simulation software Relap5 (Relap) using the pipe system as rigid boundaries. The force response is then applied on the pipe system using the stress evaluation tool Pipestress. The next step is to perform a refined 3D CFD simulation using the ADINA CFD code in order to calculate a time history load that accounts for some of the 3D effects in the fluid. For example, Relap does not model a bend in the system, it rather replaces it with a loss coefficient.

The calculated time history loads are applied on the pipe system using the Pipestress code which handles the pipe system according to classic beam theory and calculate the bending moments in the pipe due to the time history load. Pipestress uses mode supersposition to calculate the beam response. In order to quantify the conservatism a couple of sub-steps will be conducted before the fully coupled FSI simulation is implemented. The next step is to use the same time history loads on a 3D solid pipe system using the ADINA code. In this step the ADINA FEM code will be used with two methods, mode superposition and Direct integration. It is also important to account for different effects due to damping, such as modal and Rayleigh damping. Since Pipestress handles the pipe system as beams, applying the time history loads on a 3D solid pipe system should give a more accurate result. The final step is to implement a fully coupled

FSI simulation between ADINA CFD and ADINA FEM. In figure 2.1, it is shown how the results from different softwares and calculation methods are compared to each other. The single headed arrows represent input, the double headed arrows represent comparison.

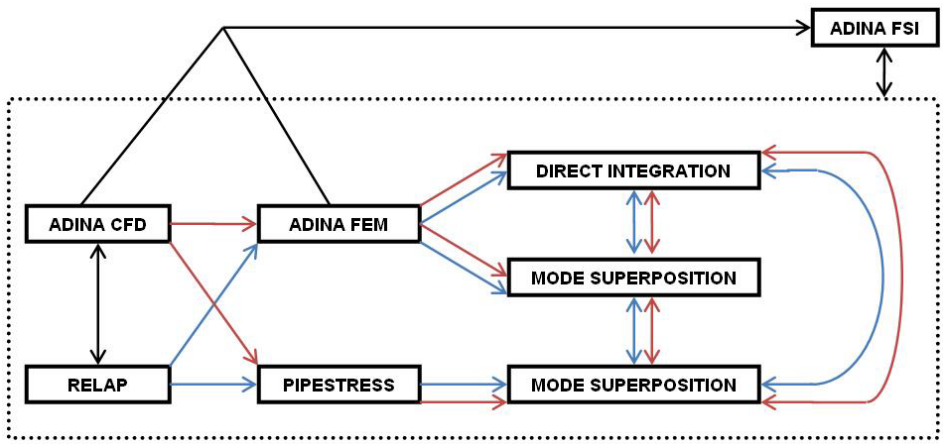

Figure 2.1: Scheme of the software combinations and result comparisons

2.2 Experimental Setup

The initial plan was to use an existing experimental setup with measured data to validate the results in this dissertation. Without such an experiment the task of quantifying the conservatism would be more difficult since it would be harder to determine whether or not the different results are closer or further away from the physically correct solution. Therefore, a lot of time was spent trying to find an experiment living up to the specifications needed such as rather simple geometry, fluid induced excitation of the system via valve opening or closing and good experimental data. However, finding such an experiment proved more difficult than estimated. Therefore the decision was made that focus in this dissertation would be to analyze the difference between the different solution methods without validating them against physical data since no experimental setup that suited the demands could be found. A fictional pipe system was created. A high frequency pressure wave is expected, $f >> 1$. The time of the simulations

will therefore be limited to 0.5 seconds which will be enough to see both the pressure wave in detail and the damping of the system with an acceptable CPU time. A sketch of the setup for the fictional experiment can be seen in Figure 2.2.

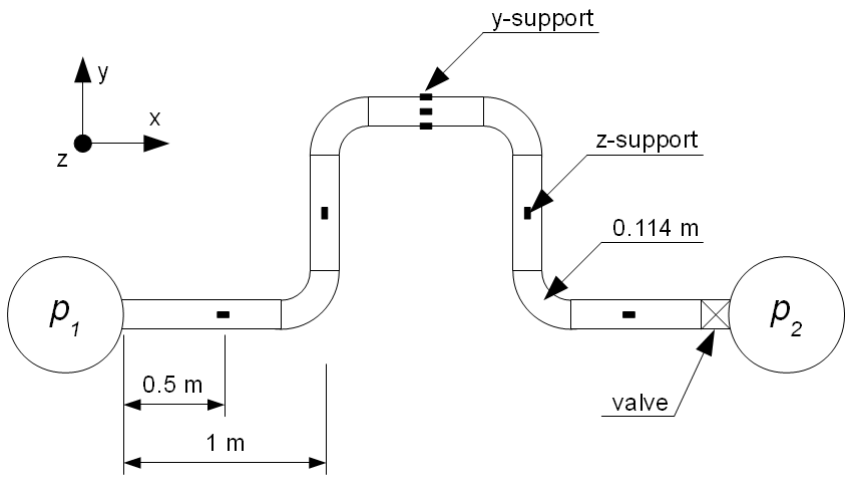

Figure 2.2: Sketch of the fictional experiment

2.2.1 Boundary conditions

The cross section of the pipe is based on an actual pipe used in nuclear powerplants and has an internal diameter of 82.8 mm and a wall thickness of 6.3 mm, the radius of the bends is 114 mm. In the middle of every straight pipe section there is a rigid support that acts in the Z-direction (gravity). On the third straight pipe section there is also a rigid support acting in the Y-direction. These supports are in place in order to restrict some of the systems movement. The pipe system goes from one tank with the pressure p_1 to another tank with the pressure p_2. The pressures of the tanks are chosen so that the fluid reaches a velocity of 2 m/s. The tanks are not really a part of the system but are needed in order to get the required fluid velocity. At the end of the pipe system, in connection with tank number two, there is a fast closing valve. The valve is modeled as a boundary condition with zero extension. In this case, the effects close

to the valve are not interesting and would make the system a lot more complicated if it were to be modeled in 3D. The effects at the start and the end of the system are also not interesting thus they are model as fixed boundaries.

The pressure in tank number two is a set to a value high enough so that the pressure wave in the system will not cause cavitation. The chosen pressure in this case is $p_2 = 10$ MPa (100 bar). According to the ASME code [3] the highest allowable internal pipe pressure is

$$p_a = \frac{2S_m t}{D_o - 2yt} \tag{2.1}$$

where

- p_a is the calculated maximum internal pipe pressure,
- t is the wall thickness,
- S_m is the maximum allowable stress intensity for the material at the design temperature, see Section 7.1,
- D_o is the outer pipe diameter,
- y is a constant that is 0.4.

The calculated maximum internal pipe pressure in this case is $p_a = 19.5$ MPa thus allowing the chosen internal pipe pressure of 10 MPa. The pressure in tank number one is regulated via a P-regulator in the Relap simulation to give the desired velocity of 2 m/s and is later used in the different simulations. The pressure in tank number one is $p_1 = 10\ 005\ 759$ Pa giving a total pressure drop of 5.759 kPa in the pipe system.

Material properties of water

The material properties of water [4], [5] are presented in Table 2.1.

Temp.	Density	Viscosity	Bulk modulus	Speed of sound
27 °C	998 kg/m^3	0.00086 Pa·s	2.2 GPa	1 500 m/s

Table 2.1: Material properties of water

Material properties of the pipe

The pipe material chosen for the fictional experiment is SS 2353, a stainless steel that is used in seamless pipes. The material properties for SS 2353 [6] are presented in Table 2.2.

Temp.	Young's modulus	Density	Yield strength	Tensile strength
27 °C	200 GPa	7850 kg/m^3	210 MPa	490 MPa

Table 2.2: Material properties of the pipe

2.3 Assumptions

All the comparisons will be made only from points in the straight parts of the pipe system which is assumed to give the most reliable results. This is because there are too many factors in the current analysis method that will effect the results in the pipe bends. Fixed points and points close to them will not be evaluated. The risk for disturbances from the fixed points is big and the results will not reflect the real solution. The length of the simulations, primarily the 3D CFD simulation and the FSI simulation will be set to 0.5 seconds. Since these are carried out with very small time steps the CPU time of the simulations will be long. 0.5 seconds is assumed to be enough to see the differences between the simulations. Phase change due to cavitation will not be a part of this dissertation. In order to assure this, a rather high internal pressure within the pipe system will be used.

Chapter 3

Theory

The most vital theory behind the CFD, FEM and FSI methods used in this dissertation will be explained here, without digging too deep. This in order to give an insight in what these analyze methods are all about.

3.1 Flow formulation

The ADINA CFD code uses Navier-Stokes equations as primary governing equations. From the ADINA manual [7] the conservative form of the Navier-Stokes equations for mass, momentums and energy, respectively, in a fixed Cartesian coordinate frame of reference is

$$\frac{\partial \rho}{\partial t} + \nabla \bullet (\rho \mathbf{v}) = 0 \tag{3.1}$$

$$\frac{\partial \rho \mathbf{v}}{\partial t} + \nabla \bullet (\rho \mathbf{v}\mathbf{v} - \boldsymbol{\tau}) = \mathbf{f}^B \tag{3.2}$$

$$\frac{\partial \rho E}{\partial t} + \nabla \bullet (\rho \mathbf{v} E - \boldsymbol{\tau} \bullet \mathbf{v} + \mathbf{q}) = \mathbf{f}^B \bullet \mathbf{v} + q^B \tag{3.3}$$

where

- t is the time,
- ρ is the density,
- $\mathbf{v}$ is the velocity vector,
- $\mathbf{f}^B$ is the body force vector of the fluid medium,
- $\boldsymbol{\tau}$ is the stress tensor, defined as in Equation (3.5),
- E is the specific total energy, defined as in Equation (3.4),
- $\mathbf{q}$ is the heat flux,
- q^B is the specific rate of heat generation.

$$E = \frac{1}{2}\mathbf{v} \bullet \mathbf{v} + e \equiv b + e \tag{3.4}$$

$$\boldsymbol{\tau} = (-p + \lambda \nabla \bullet \mathbf{v})\mathbf{I} + 2\mu\mathbf{e} \tag{3.5}$$

where

- e is the specific internal energy,
- b is the specific kinetic energy,
- p is the pressure,
- μ is the dynamic viscosity,
- λ is the kinematic viscosity,
- $\mathbf{e}$ is the velocity strain tensor defined as in Equation (3.6).

$$\mathbf{e} = \frac{1}{2}\left(\nabla\mathbf{v} + \nabla\mathbf{v}^{\mathrm{T}}\right) \tag{3.6}$$

The heat flux $\mathbf{q}$ is assumed to obey the Fourier's law of heat conduction

$$\mathbf{q} = -k\nabla\theta \tag{3.7}$$

where

- θ is the temperature,
- k is the heat conductivity coefficient.

To be able to obtain the solution, additional equations needs to be provided to correlate the variables, p, ρ, θ, and e. These equations are called state equations and are usually provided in the form of

$$\rho = \rho(p, \theta),\ e = e(p, \theta) \tag{3.8}$$

From the ADINA manual [7] the nonconservative form of the Navier-Stokes equations for mass, momentums and energy, respectively, can be expressed in a fixed Cartesian coordinate frame of reference as

$$\frac{\partial \rho}{\partial t} + \mathbf{v} \bullet \nabla \rho + \rho \nabla \bullet \mathbf{v} = 0 \tag{3.9}$$

$$\rho \frac{\partial \mathbf{v}}{\partial t} + \rho \mathbf{v} \bullet \nabla \mathbf{v} - \nabla \bullet \boldsymbol{\tau} = \mathbf{f}^B \tag{3.10}$$

$$\rho C_v \frac{\partial \theta}{\partial t} + \rho C_v \mathbf{v} \bullet \nabla \theta + \nabla \bullet \mathbf{q} = 2\mu D^2 + S_c + q^B \tag{3.11}$$

where

D is the deformation rate as defined in Equation (3.12),

S_c is the heat source due to the fluid compressibility as defined in Equation (3.13).

$$D = \sqrt{\mathbf{e} \otimes \mathbf{e}} \equiv \sqrt{e_{ij} e_{ij}} \tag{3.12}$$

$$S_c = \nabla \bullet \mathbf{v} \left(-p + \lambda \nabla \bullet \mathbf{v} \right) \tag{3.13}$$

3.1.1 Slightly compressible flow

In the general case a liquid such as water is assumed to be incompressible, this is most often a good assumption. However in some cases the compressibility of water cannot be disregarded, for example in confined flows or in situations where the fluid is subjected to a sudden load of disturbance, like a pressure surge. Alas, if the propagation of a pressure wave is to be calculated, a compressible formulation of the continuity equation is needed, as is the case in this Master's dissertation.

When using ADINA the option used is called Slightly Compressible Flow. The slightly compressible formulation is based upon the state equations, see Equation (3.8),

$$\rho_m = \rho \left(1 + \frac{p}{\kappa}\right) \tag{3.14}$$

$$e = C_v \theta \tag{3.15}$$

where

ρ_m	is the fluid density with compressibility,
ρ	is the density at $p = 0$,
p	is the current pressure,
κ	is the bulk modulus,
e	is the specific internal energy,
C_v	is the specific heat at constant volume,
θ	is the temperature.

By inserting Equation (3.14) into Equation (3.9) the nonconservative form of the continuity equation in the Navier-Stokes equations then becomes

$$\frac{\rho}{\kappa}\left(\frac{\partial p}{\partial t} + \mathbf{v} \bullet \nabla p\right) + \rho_m \nabla \bullet \mathbf{v} = 0 \tag{3.16}$$

3.2 Mode superposition

The mode superposition method [8] is used in both ADINA and Pipestress. The goal is to find a solution $\mathbf{x}$ that satisfy the modified governing equation plus calculating the mode shape $\boldsymbol{\phi}$ corresponding to an eigenfrequency up to a chosen limit. This in data will be used in Equation (3.18) of mode superposition below to sum the displacements of every mode.

$$\mathbf{M}\frac{\partial^2 \mathbf{a}}{\partial t^2} + \mathbf{C}\frac{\partial \mathbf{a}}{\partial t} + \mathbf{K}\mathbf{a} = \mathbf{F} \tag{3.17}$$

$$\mathbf{U} = \sum_{i=1}^{n} \boldsymbol{\phi}_i x_i \tag{3.18}$$

The method is based on the free vibration problem where no damping or force vector is applied to find the eigenfrequencies and mode shapes. These can then be used to eliminate the mass, stiffness and damping matrix. The governing equation, Equation (3.17), is used but because of the free vibration, without $\mathbf{C}$ and $\mathbf{F}$ in the first step

$$\mathbf{M}\frac{\partial^2 \mathbf{a}}{\partial t^2} + \mathbf{K}\mathbf{a} = \mathbf{0} \tag{3.19}$$

The first step is to find the modeshape $\boldsymbol{\phi}$ wich is done by a frequency analysis by using the general solution $\mathbf{a} = \boldsymbol{\phi} e^{\omega i t}$ in (3.19) wich leads to

$$(\mathbf{K} - \omega_i^2 \mathbf{M})\boldsymbol{\phi}_i = \mathbf{0} \tag{3.20}$$

Note that $\boldsymbol{\phi}_i$ is the vector corresponding to ω_i. By solvning $det(\mathbf{K} - \omega^2 \mathbf{M}) = \mathbf{0}$, a number of eigenfrequencies will be obtained dependning on $\mathbf{K}$ and $\mathbf{M}$. How many modes that are needed is usually depending on the frequency of the load. It is important that the modes will cover all load frequencies so that no excitation of the system will be lost. The eigenfrequencies can then be used in Equation (3.20) to obtain the eigenvector $\boldsymbol{\phi}_i$ and its mounted eigenmatrix $\boldsymbol{\phi}$ containing the mode shapes for each eigenfrequency.

From Equation (3.20) and the fact that $\boldsymbol{\phi}_i$ is M-orthogonalized the following equations, which can eliminate $\mathbf{K}$ and $\mathbf{M}$, are also obtained

$$\boldsymbol{\phi}^T \mathbf{K} \boldsymbol{\phi} = \boldsymbol{\omega}^2 \tag{3.21}$$

$$\boldsymbol{\phi}^T \mathbf{M} \boldsymbol{\phi} = \mathbf{I} \tag{3.22}$$

where

- $\mathbf{I}$ is the identity matrix,
- $\boldsymbol{\omega}$ is a diagonal matrix containing the eigenfrequencies.

The next step is to find $\mathbf{x}$. A general displacement is defined as $\mathbf{a} = \boldsymbol{\phi}\mathbf{x}$ where $\mathbf{x}$ is the solution to the problem. By applying $\mathbf{a}$ on Equation (3.17) and pre-multiply it with $\boldsymbol{\phi}^T$ the equation for a general problem is obtained

$$\boldsymbol{\phi}^T \mathbf{M} \frac{\partial^2}{\partial t^2}(\boldsymbol{\phi}\mathbf{x}) + \boldsymbol{\phi}^T \mathbf{C} \frac{\partial}{\partial t}(\boldsymbol{\phi}\mathbf{x}) + \boldsymbol{\phi}^T \mathbf{K} \boldsymbol{\phi}\mathbf{x} = \boldsymbol{\phi}^T \mathbf{F} \tag{3.23}$$

Considering the fact that $\boldsymbol{\phi}$ is not time dependent and by applying Rayleigh damping $\mathbf{C} = (\alpha\mathbf{M} + \beta\mathbf{K})$, where α and β are constants which will be explained in Section 3.4.2, the following equation can be written by combining Equation (3.21), (3.22) and (3.23)

$$\frac{\partial^2 \mathbf{x}}{\partial t^2} + (\alpha \mathbf{I} + \beta \boldsymbol{\omega}^2)\frac{\partial \mathbf{x}}{\partial t} + \boldsymbol{\omega}^2 \mathbf{x} = \boldsymbol{\phi}^T \mathbf{F} \tag{3.24}$$

The Rayleigh damping can be related to the more usual damping factor

$$\xi_i = \frac{\alpha + \beta \omega_i^2}{2\omega_i} \tag{3.25}$$

This will lead to the final form of the governing equation of mode superpositon. $\mathbf{x}$ has to be solved in order to find the nodal displacements $\mathbf{U}$ from Equation (3.18). The $\mathbf{x}$ vector contains the solution for all eigenfrequencies. To advance Equation (3.26) in time the Newmark method can be used as in ADINA. This method is explained in Section 3.3.

$$\frac{\partial^2 \mathbf{x}}{\partial t^2} + 2\boldsymbol{\xi}\boldsymbol{\omega}\frac{\partial \mathbf{x}}{\partial t} + \boldsymbol{\omega}^2 \mathbf{x} = \boldsymbol{\phi}^T \mathbf{F} \tag{3.26}$$

3.3 Direct integration

The ADINA structural code has a variety of different methods for solving a direct integration FEM simulation. The one used in this dissertation is the Newmark method. The Newmark direct integration method [8] is based on finding the node displacement at the next time step i.e. $t_{n+1} = t_n + \Delta t$ which can be written as $t = (n+1)\Delta t$ where $n =$ current time step. The system is solved at each time step.

The governing equation is seen in Equation (3.27), including $\frac{\partial^2 x}{\partial t^2}$ and $\frac{\partial x}{\partial t}$. Therefore, an expression for acceleration and velocity must be derived. Note that this method is only suitable for linear problems.

$$\mathbf{M}\frac{\partial^2 \mathbf{x}}{\partial t^2} + \mathbf{C}\frac{\partial \mathbf{x}}{\partial t} + \mathbf{K}\mathbf{x} = \mathbf{F} \tag{3.27}$$

The expression for velocity is derived. The θ term decides whether or not the velocity is obtained at the current or the next time step, $0 \leq \theta \leq 1$.

$$\frac{\partial \mathbf{x}}{\partial t}\Big|_{n+1} = \theta\frac{\partial \mathbf{x}^{(n+1)}}{\partial t} + (1-\theta)\frac{\partial \mathbf{x}^{(n)}}{\partial t} = \frac{1}{\Delta t}\left(\mathbf{x}^{(n+1)} - \mathbf{x}^{(n)}\right) \tag{3.28}$$

which leads to

$$\frac{\partial \mathbf{x}^{(n+1)}}{\partial t} = \frac{1}{\theta \Delta t}\left(\mathbf{x}^{(n+1)} - \mathbf{x}^{(n)}\right) - \frac{1-\theta}{\theta}\frac{\partial \mathbf{x}^{(n)}}{\partial t} \tag{3.29}$$

The expression for acceleration is derived

$$\frac{\partial^2 \mathbf{x}^{(n+1)}}{\partial t^2} = \theta \frac{\partial^2 \mathbf{x}^{(n+1)}}{\partial t^2} + (1-\theta)\frac{\partial^2 \mathbf{x}^{(n)}}{\partial t^2} = \frac{1}{\Delta t}\left(\frac{\mathbf{x}^{(n+1)}}{\partial t} - \frac{\mathbf{x}^{(n)}}{\partial t}\right) \tag{3.30}$$

which leads to

$$\frac{\partial^2 \mathbf{x}^{(n+1)}}{\partial t^2} = \frac{1}{\theta \Delta t}\left(\frac{\mathbf{x}^{(n+1)}}{\partial t} - \frac{\mathbf{x}^{(n)}}{\partial t}\right) - \frac{1-\theta}{\theta}\frac{\partial^2 \mathbf{x}^{(n)}}{\partial t^2} \tag{3.31}$$

Now back to Equation (3.27) where the acceleration, velocity and displacement can be applied.

$$\begin{gathered}\left[\mathbf{M}\frac{\partial^2 \mathbf{x}^{(n+1)}}{\partial t^2} + \mathbf{C}\frac{\partial \mathbf{x}^{(n+1)}}{\partial t} + \mathbf{K}\mathbf{x}^{(n+1)}\right]\theta + \\ \left[\mathbf{M}\frac{\partial^2 \mathbf{x}^{(n)}}{\partial t^2} + \mathbf{C}\frac{\partial \mathbf{x}^{(n)}}{\partial t} + \mathbf{K}\mathbf{x}^{(n)}\right](1-\theta) = \\ \theta \mathbf{f}^{(n+1)} + (1-\theta)\mathbf{f}^{(n)}\end{gathered} \tag{3.32}$$

The equation will advance in time and predict $\mathbf{x}^{(n+1)}$. All the references to velocity and acceleration at time step $(n+1)$ must therefore be eliminated by applying Equation (3.29) and (3.31) on (3.32). This will provide the following equation

$$\mathbf{M}\left[\frac{1}{\theta\Delta t}\left(\mathbf{x}^{(n+1)}-\mathbf{x}^{(n)}\right)-\frac{1-\theta}{\theta}\frac{\partial\mathbf{x}^{(n)}}{\partial t}-\frac{\partial\mathbf{x}}{\partial t}\right]+$$
$$\mathbf{C}\left[\mathbf{x}^{(n+1)}-\mathbf{x}^{(n)}\right]+\Delta t\mathbf{K}\left[\theta\mathbf{x}^{(n+1)}+(1-\theta)\mathbf{x}^{(n)}\right]= \tag{3.33}$$
$$\theta\Delta t\mathbf{f}^{(n+1)}+(1-\theta)\Delta t\mathbf{f}^{(n)}$$

Here it is possible to apply Rayleigh damping as $\mathbf{C}=\alpha\mathbf{M}+\beta\mathbf{K}$, where α and β are constants which will be explained in Section 3.4.2.

By introducing Rayleigh damping in Equation (3.33) the final equation containing only the node displacement at the next time step is produced. This means that the system can be solved using only known in data from the current time step.

$$\left[\left(\alpha+\frac{1}{\theta\Delta t}\right)\mathbf{M}+(\beta+\theta\Delta t)\mathbf{K}\right]\mathbf{x}^{(n+1)}=$$
$$\left[\left(\alpha+\frac{1}{\theta\Delta t}\right)\mathbf{M}+[\beta-(1-\theta)\Delta t]\mathbf{K}\right]\mathbf{x}^{(n)}+ \tag{3.34}$$
$$\frac{1}{\theta}\mathbf{M}\frac{\partial\mathbf{x}^{(n)}}{\partial t}+\theta\Delta t\mathbf{f}^{(n+1)}+(1-\theta)\Delta t\mathbf{f}^{(n)}$$

The parameter θ can vary as seen above and is usually stable in the range $\frac{1}{2}<\theta<1$

3.4 Damping

Damping needs to be included in the simulations to account for the natural energy losses within the system.

3.4.1 Modal damping

Modal damping is applied in a mode superposition method. The damping factor ξ_i, where i represents each mode of interest. ξ_i can be different for each mode. The damping factor can also be the same for every mode in which case $\xi_i=\xi$ for all modes.

3.4.2 Rayleigh damping

Rayleigh damping is applied in the direct integration approach. Unlike modal damping, which dampens the current mode, Rayleigh damping dampens the system at the current frequency instead. The equation of the Rayleigh damping curve is

$$\xi = \frac{\alpha}{2\omega} + \frac{\beta\omega}{2} \tag{3.35}$$

where

ξ	is the damping ratio,
α, β	are constant parameters,
ω	is the frequency.

In order to decide α and β two reference frequencies, ω_i and ω_j, are needed. The damping ratio ξ_i and ξ_j for the two reference frequencies are also needed.

$$\xi_i = \frac{\alpha}{2\omega_i} + \frac{\beta\omega_i}{2} \tag{3.36}$$

$$\xi_j = \frac{\alpha}{2\omega_j} + \frac{\beta\omega_j}{2} \tag{3.37}$$

which is the same as

$$\begin{bmatrix} \xi_i \\ \xi_j \end{bmatrix} = \begin{bmatrix} \frac{1}{2\omega_i} & \frac{\omega_i}{2} \\ \frac{1}{2\omega_j} & \frac{\omega_j}{2} \end{bmatrix} \begin{bmatrix} \alpha \\ \beta \end{bmatrix} \tag{3.38}$$

which leads to

$$\begin{bmatrix} \alpha \\ \beta \end{bmatrix} = \begin{bmatrix} \frac{1}{2\omega_i} & \frac{\omega_i}{2} \\ \frac{1}{2\omega_j} & \frac{\omega_j}{2} \end{bmatrix}^{-1} \begin{bmatrix} \xi_i \\ \xi_j \end{bmatrix} \tag{3.39}$$

and the parameters α and β can be decided.

3.5 Fluid-Structure Interaction

There are two different ways to couple the fluid and structure simulations, one-way FSI and two-way FSI [7].

In two-way FSI, basically the fluid forces affects the structural deformations and the displacement of the solid structure affects the fluid. The solid displacements are seen as a moving wall which requires an ALE-formulation to be described and this will be explained in Section 3.5.1. Two-way FSI is used to get a more accurate result than just looking at "cause and effect". These conditions must be fulfilled at the boundary between the fluid and the solid to satisfy the coupled equation

$$\mathbf{d}_f = \mathbf{d}_s \tag{3.40}$$

$$\boldsymbol{\tau}_f = \boldsymbol{\tau}_s \tag{3.41}$$

where
$\mathbf{d}_f$ is the fluid displacement,
$\mathbf{d}_s$ is the displacement of the solid,
$\boldsymbol{\tau}_f$ is the fluid stress,
$\boldsymbol{\tau}_s$ is the solid stress.

One-way FSI can be used if the deformation of the solid model is so small that it does not significantly affect the fluid. Then only the fluid loads has to be applied onto the structure and no iteration between the fluid and solid is needed. Stuctures affecting fluids without any coupling effects can also be used to simulate moving material in a fluid like a low velocity mixing blade in a low viscous medium where the medium will not significantly affect the blade.

There are a number of different methods to solve the coupled system in ADINA which will be explained shortly to show their main differences. The iterative method described in this chapter is commonly refereed to as the explicit method while the direct method is commonly refereed to as the implicit method.

- Iterative computing of two-way coupling: The fluid equations and the solid equations are solved individually, always using the latest information provided from each other in the coupled system. For each iteration the following equations of equilibrium are solved to obtain $\mathbf{X}$ at iteration $n = 1, 2, ...$ This to obtain the solution at $t + \Delta t$.

1.
$$\mathbf{F}_f[\mathbf{X}_f^{(n)}, \lambda \mathbf{d}_s^{(n-1)} + (1-\lambda)\mathbf{d}_s^{(n-2)}] = \mathbf{0} \tag{3.42}$$

This solution is obtained in the fluid analysis using the solid displacements. λ is a relaxation factor that can vary to help find convergence.

2.
$$\mathbf{F}_s[\mathbf{X}_s^{(n)}, \lambda \boldsymbol{\tau}_f^{(n)} + (1-\lambda)\boldsymbol{\tau}_f^{(n-1)}] = \mathbf{0} \tag{3.43}$$

This solution is obtained in the structure analysis using the fluid stresses. λ is also here a relaxation factor that can vary to help find convergence.

3. The stresses and displacements are checked against the tolerance. If the stress and displacement criteria is fulfilled then the result can be saved and printed otherwise it has to go back to step (1).

- Direct computing of two-way coupling: This computing method is also called the simultaneous solution method. In this direct solution method, as in the iterative method, the fluid and solid solution variables are fully coupled. The fluid equations and the solid equations are combined and handled in one matrix system like the following.

$$\begin{bmatrix} \mathbf{K}_{ff} & \mathbf{K}_{fs} \\ \mathbf{K}_{sf} & \mathbf{K}_{ss} \end{bmatrix} \begin{bmatrix} \Delta\mathbf{X}_f^n \\ \Delta\mathbf{X}_s^n \end{bmatrix} = \begin{bmatrix} \text{-}\mathbf{F}_f^n \\ \text{-}\mathbf{F}_s^n \end{bmatrix} \tag{3.44}$$

$$\text{-}\mathbf{F}_f^n = \text{-}\mathbf{F}_f[\mathbf{X}_f^{(n)}, \lambda \mathbf{d}_s^{(n-1)} + (1-\lambda)\mathbf{d}_s^{(n-2)}] \tag{3.45}$$

$$\text{-}\mathbf{F}_s^n = \text{-}\mathbf{F}_s[\mathbf{X}_s^{(n)}, \lambda \boldsymbol{\tau}_f^{(n)} + (1-\lambda)\boldsymbol{\tau}_f^{(n-1)}] \tag{3.46}$$

As can be seen it looks the same as in the iterative method. The following steps will be performed in each iteration to obtain the solutions at $t + \Delta t$.

1. Assemble the fluid and solid equations as usual followed by assembling the coupling matrices $\mathbf{K}_{sf}$ and $\mathbf{K}_{fs}$.
2. Solve the linearized equation of the coupled system and update the solution. Check the convergence criteria for displacement and stress. If convergence is obtained continue to the next step or else, go back to step (1).
3. Print and save solutions.

   The direct method is generaly faster then the iterative method but at the cost of memory usage. The direct FSI method can not be applied on the Segregated method where the fluid nodes are not directly coupled. See the ADINA fluid manual [7].

- Direct computing of one-way coupling: In this method the fluid stress is applied onto the structure while the structure has no influence on the fluid. The following will be perform in each time step:

  1. Solve the fluid model just like for a fluid model alone.
  2. Solve the solid model just like for a solid model alone with the latest calculated fluid solution.
  3. Print and save solutions.

- Indirect computing of one-way coupling: The fluid and solid models are prepared separately, so the meshes of the two models may not be compatible on the interface. In this indirect computing method, the program performs the same operations as in direct computing. The specific thing about indirect computing is that all the control parameters are specified in the individual fluid and solid model. Because of this it is possible to have differences between the fluid and solid solution step. If the fluid stresses are not available at a certain time step, a linear interpolation is performed. If the solution time of the solid exceeds the solution time of the fluid, a linear extrapolation is perform to get the fluid results when not available.

3.5.1 Arbitrary Lagrangian-Eulerian formulation

In continuum mechanics there are two important algorithms when it comes to determine the relationships between the deforming material of the con-

tinuum and the grid or mesh. Two descriptions of motion are mainly used. The Lagrangian description and the Eulerian description [9].

In the Lagrangian point of view, material particles of the continuum are followed in their motion. A grid which follows the continuum is introduced. As the model deforms, rotates and translates, the grid points always connect to the same material points. This is used in structure mechanics and the disadvantage of the Lagrangian description is that it can not handle large deformations due to the fact that large distortion of the material point will deform the mesh so that it might overlap itself and become unstable.

Two domains are specified, the material domain R_X made of material particles X and the spatial domain R_x, made of spatial points x. The motion of material points relates the material coordinates of X at the initial configuration to the spatial ones of x at the current configuration, as can be seen in Figure 3.1, and is defined by $\boldsymbol{\varphi}$ such that

$$\boldsymbol{\varphi}(X,t) = (x,t) \tag{3.47}$$

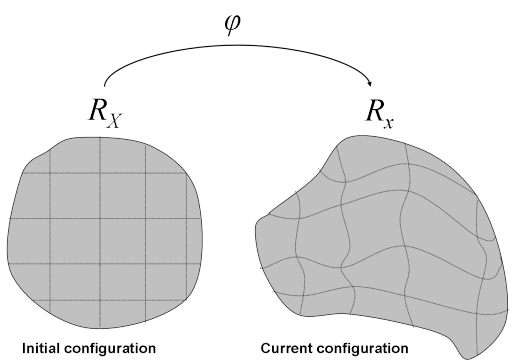

Figure 3.1: The material points at the initial configuration R_X are related to the current configuration R_x by $\boldsymbol{\varphi}$.

At every time step the mapping $\boldsymbol{\varphi}$ defines a configuration in the spatial domain. By the inverse of $\boldsymbol{\varphi}$, the reference configuration of a material point x at time t can be found and this makes it possible to keep track of the history of motion.

The Eulerian description is used in fluid dynamics. Here, the computational mesh is fixed and the particles of the continuum moves with respect to the grid. In the Eulerian description large deformation in the continuum can be handled, but at the cost of resolution in the movement of the fluid. Large distortions of the material points can be handled due to the fact that the grid is fixed and the basic idea is to look at the amount of particles passing through a fixed region of space. The mesh is therefore not deformed with respect to the deformation of the model.

Since the grid is fixed, the velocity at a specific node is the velocity that a material point has at a specific time at that specific node. With a rough mesh the lack of resolution is a fact. The velocity is expressed with respect to the fixed mesh without any reference to the initial configuration. This is why it can be hard to follow the motion with precision in the Eulerian description.

A technique has been developed, called the Arbitrary Lagrangian-Eulerian (ALE) formulation, that combines the best features of both the Lagrangian and the Eulerian description. This will give us the advantage of being able to deal with relatively large deformation at minimum cost of mesh resolution. In Figure 3.2, 3.3 and 3.4 a visualization of how the different mesh formulations work is presented.

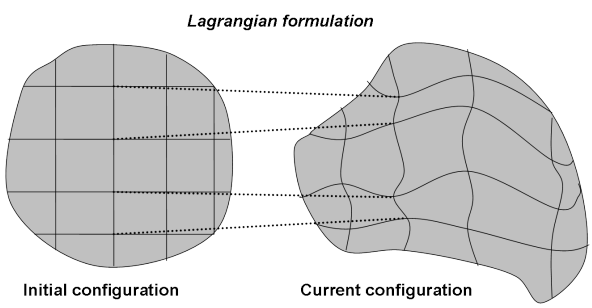

Figure 3.2: Lagrangian formulation. The grid follows the material points in its motion.

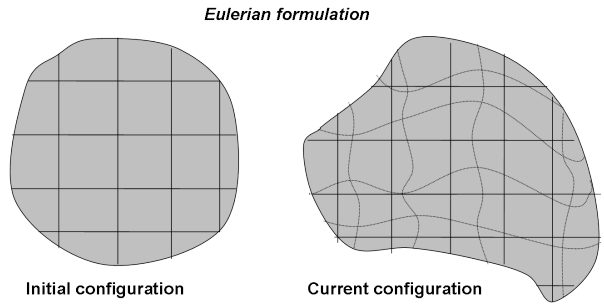

Figure 3.3: Eulerian formulation. The grid stays in position when the material points move as the model deforms.

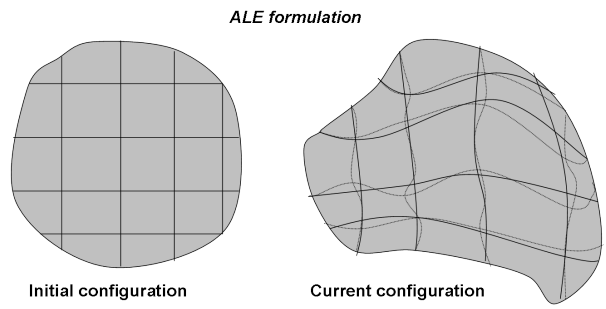

Figure 3.4: ALE formulation. The grid may be arbitrarily moved so that large deformations can be handled without the loss of high resolution.

In the ALE description of motion, neither the material or the spatial domain is referred to. A third domain is defined; the referential domain R_χ where the reference coordinates χ are introduced to identify the grid points. The referential domain is mapped into the material domain by $\mathbf{\Psi}$ and the spatial domain by $\mathbf{\Phi}$. The particle motion $\boldsymbol{\varphi}$ may then be expressed as $\boldsymbol{\varphi} = \mathbf{\Phi} * \mathbf{\Psi}^{-1}$. These mappings are not independent, as can be seen in Figure 3.5.

By using $\mathbf{\Psi} = \mathbf{I}$ or $\mathbf{\Phi} = \mathbf{I}$ a purely Lagrangian or Eulerian description, respectively can be obtained. This is why it is possible to use the advantages of the both methods when needed.

In order to move the meshes, a method of leader-follower can be used to move the follower nodes based on the movement of the leader [7]. The

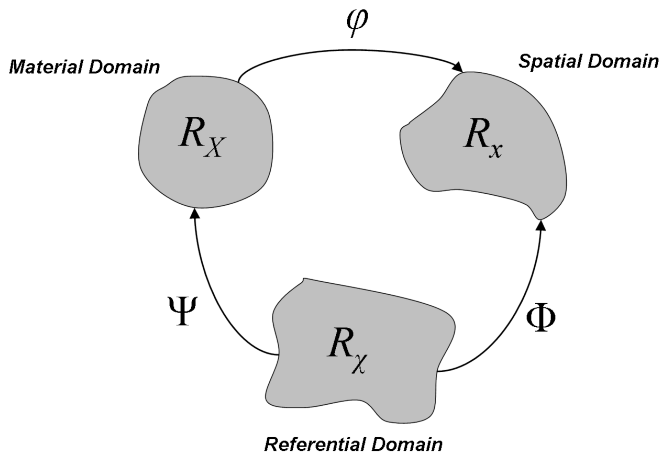

Figure 3.5: The three domains are are not independent.

leader node is connected to the boundary of the moving boundary, in this dissertation the FSI boundary, and is therefore controlled by the movement of the material points. The follower nodes must be moved in relation to its leader but not necessarily in the exact same manor. Different factors can be used to alter the relations between the movement of the leader and its follower.

There can also be boundary-followers that always must stay on the boundary while following the leader node. There are certain times when this method do not work due to overlapping of elements which will terminate the process. To avoid such problems, the elements should be as convex as possible or divided into convex sub domains to give more room for larger deformations.

Chapter 4

Software

A number of different softwares are needed in this dissertation. Here the most used are presented with a short description of their main applications to give the reader a basic understanding of what the different codes are capable of.

4.1 Relap

Relap5 [10] is a one dimensional thermo hydraulic silmulation tool developed for the United States Nuclear Regulatory Comission and used for calculations of pipesystems in nuclear powerplants. It is a code suitable for analyzing transients in Light Water Reactor systems suchs as loss of coolant accidents and a full range of operational transients. The program can also handle two-phase flow. There are a number of basic components that can be use in the simulations which includes pumps, valves, tanks, pipes, heat relesing or absorbing structures and turbines. Relap5 has been validated through a lot of experimental testing [11], [12].

4.2 Pipestress

Pipestress [13] is a program used to perform linear elastic analyzes on three-dimensional beam element piping systems with different loads such as vibrational, heat transient, force transient and pressure loads. To simulate 3D components like valves and nozzles in the beam structure ASME code [3] is used to calculate a specific stress index for that component based on the components diameter, wall thickness, rounding etc. Those indices are applied on the model to induce the stress which would have occurred in a 3D simulation. Reliable results due to the conservatism in the ASME code can therefore be achieved.

4.3 ANSA

ANSA is an advanced Computer Aided Engineering (CAE) pre-processing tool for FEM and FVM analyzes with a wide range of functionality. Everything from modeling and detailed meshing to applying loads and boundary conditions can be done in the same software. ANSA can provide full functionality in terms of preparing data for most analysis softwares used in the engineering business.

4.4 ADINA

ADINA software [14], [7] have a wide range of analysis capability. In this dissertation the FEM, CFD and the combined mode FSI (Fluid Structure Interaction) capabilities will be used.

The FEM part is used to analyze 2D and 3D structures in statics and dynamics, both linear and nonlinear applications such as material behavior, large deformations and contact conditions. It can be used to perform frequency analyzes as well as mode superposition and both explicit and implicit direct integration.

The CFD part can be used for both incompressible and compressible flows. The model may contain free surfaces, where boundary conditions are applied or moving meshes where the flow affects the solid and we get a Fluid Structure Interaction.

FSI can be done in one single program with highly nonlinear response due to large deformations, inelasticity, contact and temperature transients. There are two-way coupled (fully coupled) solutions where the response of the solid is strongly affected by the fluid, and vice versa. In one-way coupling the fluid only affects the solid, or the other way around.

Chapter 5

Relap

The setup for the Relap simulation was done by one of the employees at FS Dynamics. Mostly because there was not enough time to fully learn another software but also because the use of Relap already is a validated procedure and thus there is no need for further evaluation. In this dissertation it is merely used as a point of comparison. The basic equations that is used in Relap are mass continuity, momentum conservation and energy conservation. More about this and how the equations advance in time can be read in the Relap theory manual [10].

5.1 The model

The Relap model in this case starts with a tank followed by five straight pipes and ends with yet another tank. Each straight pipe section is divided into ten subsections, each with a length of 0.1 m. Junctions are used to connect all these components with each other. Instead of modeling bends, a loss coefficient is being used to simulate the bend. In order to achieve the desired velocity of the fluid the pressure of the first tank is regulated using a P-regulator. The pressure difference between the two tanks gives the desired velocity, in this case 2 m/s. The pressure of the second tank is chosen to be 10 MPa (100 bar), see Section 2.2.1, so that there will be no risk of cavitation in the pipe system. Via the P-regulator the pressure of the first tank will get a pressure of 10 005 759 Pa, which will give the fluid the desired velocity. After the last straight pipe section but before the second

tank there is a valve. This valve is modeled by linearly reducing the pipe area, going from an area ratio of 1 to 0 over 0.01 seconds. The fast closing valve will excite the fluid and create a pressure wave that will bounce in the pipe system. One thing that is noteworthy is that the first tank will not absorb the pressure wave but instead the pressure wave will bounce against the boundary with an inverted sign. The system boundaries are also completely rigid, which means that the fluid domain will not change during the simulation. The time step of the simulation is $5 \cdot 10^{-6}$ s.

5.2 Results

The Relap simulation will calculate a lot of different results and responses. In this dissertation only a few of these are of interest. The mass flow within the system is used for calculating the force response of the fluid excitation which later is used as a time dependent dynamic load in Pipestress. The pressure within the system is needed for comparison with the ADINA CFD simulation. It is also possible to calculate the force response using the pressure. It will be of interest for this dissertation how the mass flow changes over the valve, this in order to model the valve boundary of the ADINA CFD simulation as correctly as possible. In Figure 5.1 the mass flow change over the valve is presented.

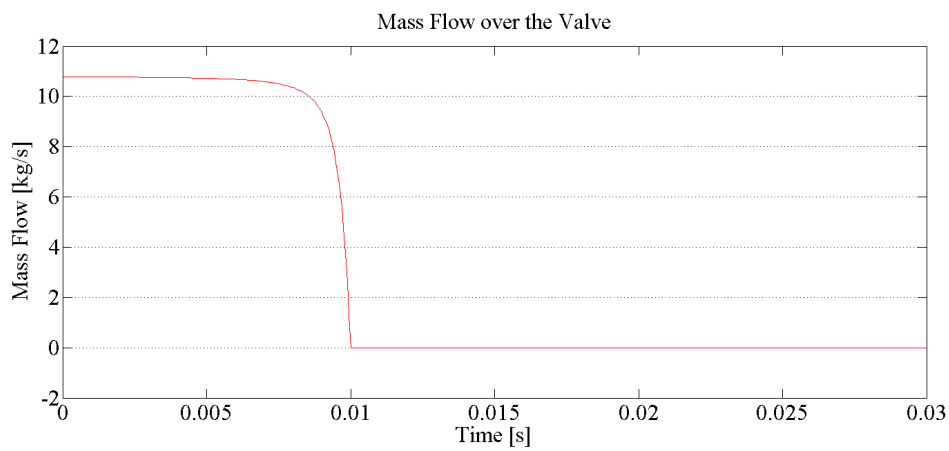

Figure 5.1: Mass flow change over the valve

5.2.1 Pressures

In Section A.1 in Appendix A the pressure calculated with Relap in some chosen points in the system are presented. The positions of the points in the fluid are presented in Figure A.1. The points are chosen to show how the pressure may vary over the range of the system. In Figure 5.2 and Figure 5.3 the pressure curves from the beginning and the end of the system are presented, respectively. The behavior of the pressure is not surprising as it is expected to bounce back and forth within the pipe and eventually dissipating.

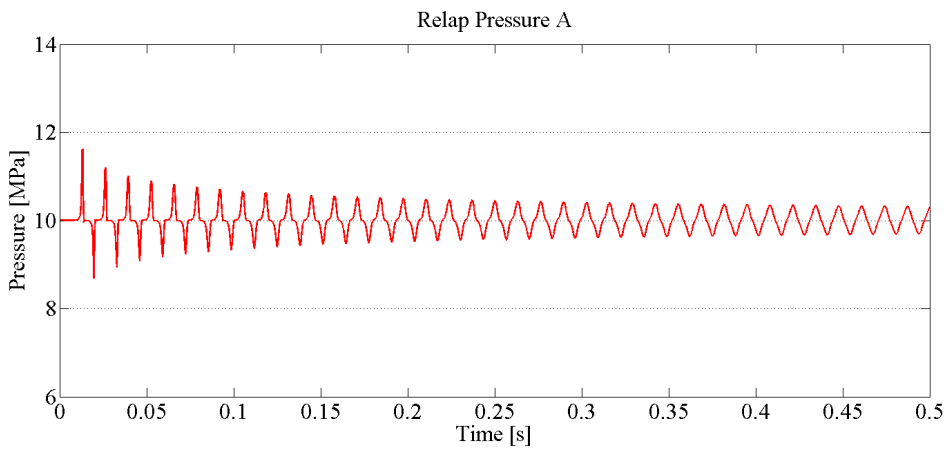

Figure 5.2: Pressure at the beginning of the system

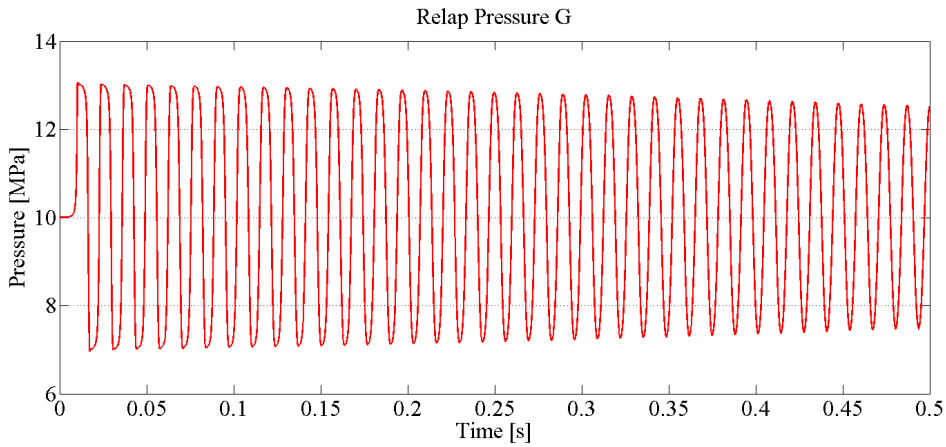

Figure 5.3: Pressure at the end of the system

5.2.2 Forces

In order to calculate the force response of the fluid excitation the change in mass flow over time is used. By taking the mean mass flow in a pipe section and deriving it with respect to time and then multiplying it with the total pipe section length the force acting on the fluid is calculated. Since the force response in the pipe is a reaction force the sign of the fluid force has to be inverted. A mathematical representation for calculating the force is presented in Equation (5.1). Repeating this for all five pipe sections, all force responses are given. The force response for all five pipe sections are presented in Section B.1 in Appendix B. Figure B.1 shows how the fluid is divided into its different sections. In Figure 5.4 below the force in the last pipe section is presented.

$$F = (-1) \cdot \frac{0.1 \sum_{i=1}^{9} \dot{m}_i + 0.05(\dot{m}_0 + \dot{m}_{10})}{\Delta t} \tag{5.1}$$

where

- F is the reaction force,
- $\dot{m}_i$ is the mass flow in junction i from the previous time step, $i = 0, ..., 10$ which is all junctions connected to a straight pipe section,
- Δt is the time step.

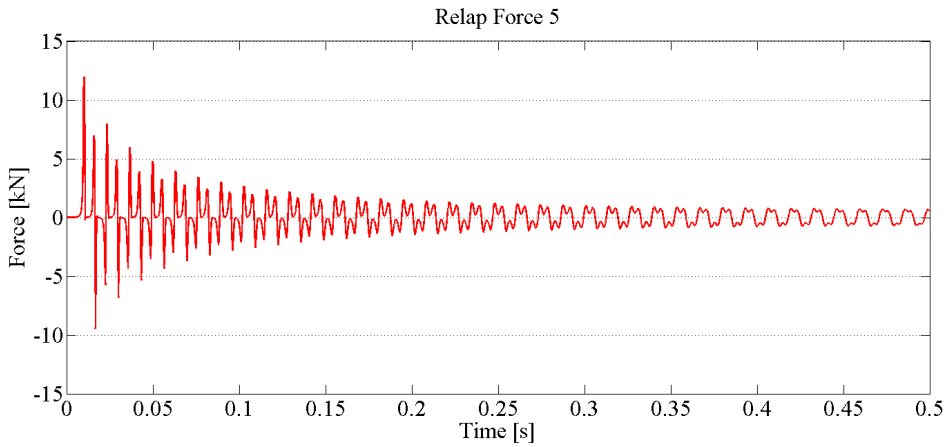

Figure 5.4: Force response in the last pipe section

Chapter 6

ADINA Fluid

6.1 The model

The ADINA CFD simulation is executed using theory for a slightly compressible flow, see Section 3.1.1 for explanation. There is the question of how to reach the steady-state before the valve closure. One option is to run the steady-state simulation and then restart the transient simulation from that point. The other option is to reach the steady-state within the transient simulation and then close the valve. The latter option is chosen for this dissertation.

This is done by ramping up the boundary conditions that control the steady-state solution, in this case the velocity at the outlet and the pressure at the inlet. At the three (3) second mark the valve closure begins. The reason why the solution runs for three seconds before to valve closure is to make sure that the entire flow have reached steady-state conditions. In all graphical representations of the result from the ADINA CFD simulation these three seconds have been removed as they are of no interest in this dissertation.

The elements used in the ADINA CFD simulation are called FCBI-C elements. These elements are 3D brick elements, i.e. eight node elements. FCBI-C means Flow Condition Based Interpolation - Center, which means that all the degrees of freedom are defined at the center of the element. The FCBI-C elements uses an iterative algorithm to solve the nonlinear fluid system that is called the Segregated method. More about the FCBI-

C elements and the Segregated method can be read in the ADINA fluid manual [7].

6.1.1 Mesh

In order to know how well resolved the fluid domain mesh needs to be a mesh convergence test is performed. Consideration of the time step size also needs to be taken. The mesh convergence test was done by doing a series of test runs on different mesh qualities, main focus was on resolving the mesh over the fluid cross section after seeing how the element lengths in the axial direction of the fluid had little effect on the solutions. Therefore, a reasonable element length was chosen so that the total number of cells in the model was kept low. Another criteria that had to be taken into consideration was the computational time. During the tests it has shown, not surprisingly, that the cpu time when dealing with increasing number of cells rapidly increases, therefore a small number of cells in the final model is desirable. Four meshes were tested. Fluid_01, Fluid_02 and Fluid_03 all have the same element length in the axial direction of the fluid but different meshes over the cross section, from course to dense respectively. Fluid_04 has the same mesh over the cross section as Fluid_01 but its element length in the axial direction of the fluid is half. All the test meshes are presented in Appendix C. A total of six test runs have been performed in order to evaluate what mesh will be suitable to solve the problem. it is assumed that if a difference in the results can be observed the result given by the denser mesh or the smaller time step is the more correct solution.

First, the simulation of Fluid_01 using different time steps was compared. An important thing to consider when deciding what time step a simulation should have is whether or not the characteristics of the transient will pass over an entire element within one time step. If it were to pass over an element in one time step the risk is significant that important information is lost within the solution. Therefore it is important to set a time step that is small enough so that the simulation will capture all information within the transient. In this case the interesting characteristics of the transient is the velocity of the pressure wave, which travels with a speed of $c = 1\ 500$ m/s, see Section 2.2.1. c is the velocity of sound in water. To know whether or not the time step is small enough it has to satisfy that the Courant Number is less than one, $C < 1$. The equation to

decide the Courant number is

$$C = \frac{v\Delta t}{l_{el}} \tag{6.1}$$

where

- C is the Courant number,
- v is the characteristic velocity of the fluid,
- Δt is the time step,
- l_{el} is the smallest element length of interest.

The time step in this case then is

$$\Delta t = C\frac{l_{el}}{c} \tag{6.2}$$

where

- c is the speed of sound in water.

In mesh Fluid_01 the smallest element length of interest is 9 mm. The Courant number $C_1 = 1$, $C_{0.1} = 0.1$ and $C_{0.075} = 0.075$ was used, which gives time steps of $\Delta t_{C_1} = 6 \cdot 10^{-6}$ s, $\Delta t_{C_{0.1}} = 6 \cdot 10^{-7}$ s and $\Delta t_{C_{0.075}} = 4.5 \cdot 10^{-7}$ s, respectively. $C_{0.075}$ is the Courant number used in the Relap simulation. In Section 5.1 it is stated that in the Relap simulation $\Delta t = 5 \cdot 10^{-6}$ s and that the element length is 0.1 m. With the velocity of sound in water, $c = 1\ 500$ m/s, a Courent number of $C = 0.075$ is obtained from Equation (6.1).

The solutions showed that the difference between C_1 and $C_{0.1}$ is significant, the difference between $C_{0.1}$ and $C_{0.075}$ is small thus concluding that $C_{0.1}$ is sufficient for this dissertation, especially considering that the cpu time is a limiting factor. In Figure 6.1 a pressure plot showing the two first oscillations with different Courant numbers is presented.

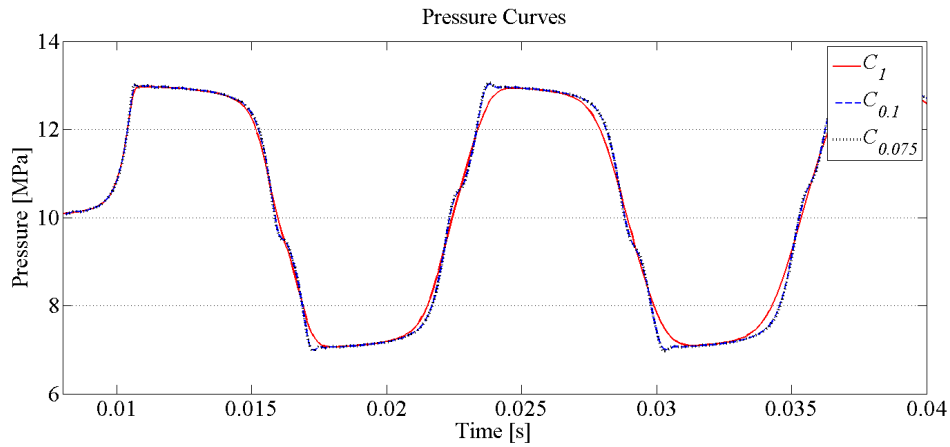

Figure 6.1: Pressure curve with different Courant numbers

When doing the test runs to compare the results from different mesh qualities the courant number is set to $C = 1$. As can be seen in Figure 6.2 the results from the simulation done with the Fluid_01 mesh and the Fluid_04 mesh are almost identical, meaning that the element length in the axial direction of the fluid in mesh Fluid_01 is sufficient.

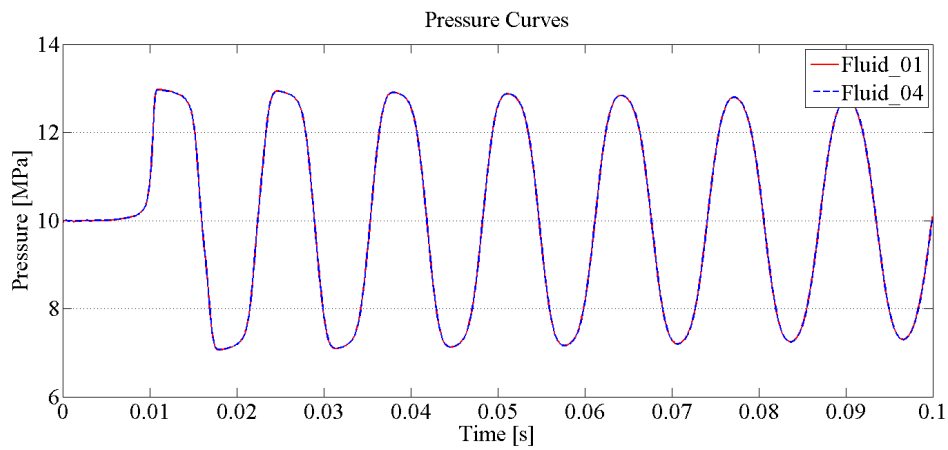

Figure 6.2: Pressure curves generated by the meshes Fluid_01 and Fluid_04

As can be seen in Figure 6.3, the denser the mesh the better the result. The difference between the mesh in Fluid_01 and the other two is big, however the difference between mesh Fluid_02 and Fluid_03 is a lot less and when considering the longer CPU time of mesh Fluid_03 it is reasonable to conclude that mesh Fluid_02 is the mesh most suitable for this dissertation.

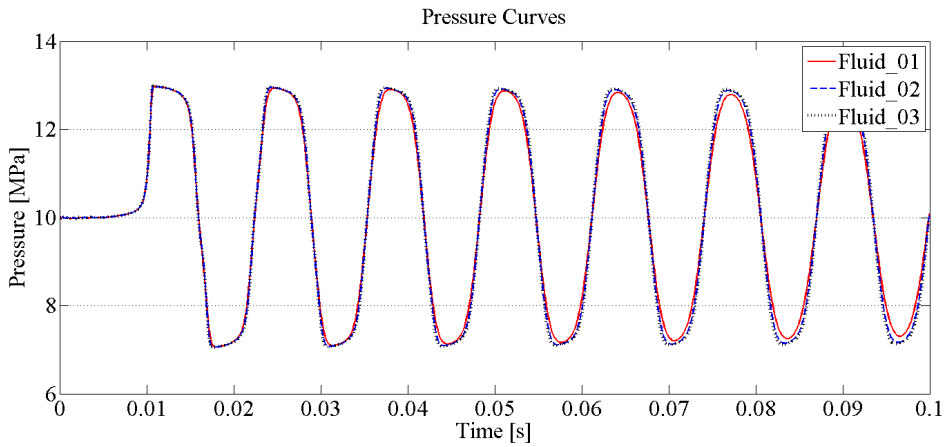

Figure 6.3: Pressure curves generated by the meshes Fluid_01, Fluid_02 and Fluid_03

Finally, the result given by Fluid_02 and Fluid_01 using the Courant number $C = 0.1$ are compared. As seen in Figure 6.4 there is a significant difference between the two results. The pressure curve generated by Fluid_01 with $C = 0.1$ gives a much more detailed result. Also, when compared with the Relap pressure the result from Fluid_01 is very similar except for the frequency, see Figure 6.5, concluding that mesh Fluid_01 with a Courant number of $C = 0.1$ is the choice of mesh for this dissertation.

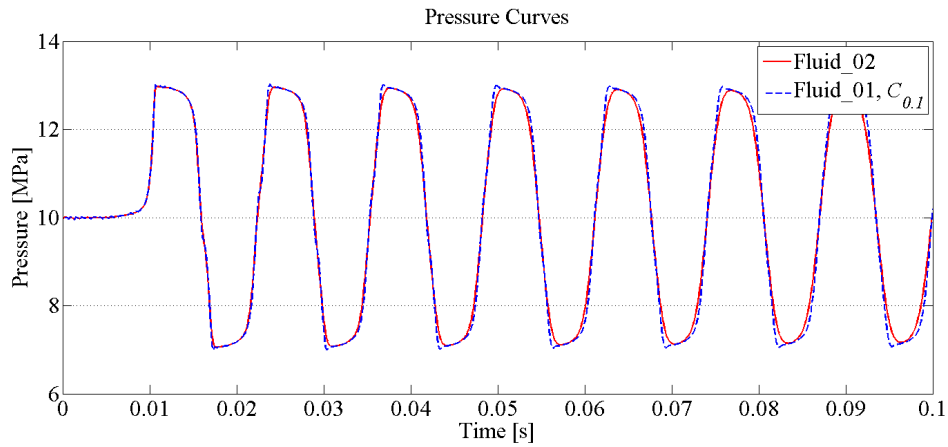

Figure 6.4: Pressure curves generated by the meshes Fluid_02 and Fluid_01 with $C = 0.1$

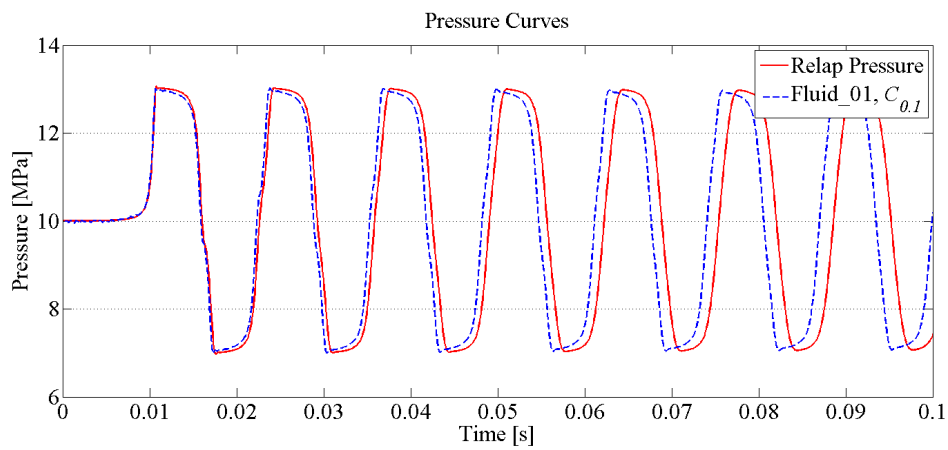

Figure 6.5: Pressure curves generated by the meshes Fluid_01 with $C = 0.1$ and Relap

6.1.2 Turbulence

A good indication of whether or not a flow should be considered turbulent or laminar is given by looking at the Reynolds number (Re) [15]. A low Reynolds number indicates that the flow is laminar and a high Reynolds

number indicates that the flow is turbulent. The equation for the Reynolds number is

$$\mathrm{Re} = \frac{\rho v D_H}{\mu} \tag{6.3}$$

where

- ρ is the density of the fluid,
- v is the mean velocity of the fluid,
- D_H is the hydraulic diameter, in this case the inside diameter of the pipe,
- μ is the dynamic viscosity.

The Reynolds number for this setup is $185.7 \cdot 10^3$ before the valve closure which clearly indicates that the flow is turbulent. However, after the valve closure the fluid will be contained within a closed space with a fixed zero velocity in all directions on one side and a high pressure boundary on the other, giving a stationary fluid. The pressure wave that will propagate through the pipe is what is interesting in this dissertation. The pressure wave will not be affected by the turbulance the same way a flowing fluid would, thus a turbulent simulation will not be needed. Also, if turbulence were to be included in the simulation the CPU time would be extensive. Due to the fine mesh required for the turbulent simulation the time step of that solution would be $\Delta t = 3.33 \cdot 10^{-8}$ s, with the Courant number needed, see Section 6.1.1. For a simulation that would run over 0.5 s that would mean a total of 15 000 000 time steps which would take a long time to complete with the available soft- and hardware.

6.1.3 Boundary conditions

One of the hardest parts of a CFD simulation is to use the correct boundary conditions. If poor boundary conditions are chosen the whole solution might be governed by them and thus yielding wrong answer. In this CFD simulation two major concerns regarding boundary conditions was raised. How were the tanks going to be modeled and how was the valve going to be modeled? The interface between the fluid and the pipe was of no big concern seeing how this solution was going to be executed using a rigid boundary. A wall with no slip condition was used giving a zero velocity at the interface and zero displacement of the fluid domain. The valve is

modeled using the X-velocity at the outlet meaning that the Y- and Z-velocity and the outlet is set to free. This means that when the X-velocity is 0 the valve will start to leak in the Y- and Z-direction due to the gravity. To avoid this the Y- and Z-velocity at the outlet is set to zero.

Valve boundary condition

In order to get the most accurate result the best thing would be to actually model the valve in 3D. If the task was to investigate what happened with the fluid close to the valve that approach would have been crucial for the solution. However, in this dissertation the behavior of the fluid close to the valve is not of interest, neither is the turbulent effects in the fluid that might be caused by the valve. A numerical boundary condition describing the behavior of the valve would be sufficient. Since there does not exist any numerical valve boundary condition it had to be described using some other parameter. The most suitable parameter was the velocity of the fluid. Controlling the fluid velocity would also present a way of giving the entire fluid its steady-state velocity of 2 m/s and also removing the problem of how to model the second tank. After looking at the fluid response over the valve in the Relap simulation and trying some different approaches it was decided that the best way of controlling the velocity was by reducing it according to the mass flow response over the valve in the Relap simulation. The mass flow response over the valve in the Relap simulation is presented in Figure 5.1.

Tank boundary condition

Much as with the valve, the best thing would have been to model the entire tank. However, since the results will be compared with the Relap simulation and the tanks was only modeled numerically resulting in the pressure wave simply bouncing against the boundary a similar solution is desired in the ADINA CFD simulation. Also, the tanks are not an important part of the system, they are merely used to get the desired velocity of the fluid and to avoid cavitation. At the inlet a pressure condition was applied as normal traction in the X-direction. This normal traction has a value of 10 005 759 Pa, which is the same as tank number one in the Relap simulation.

It would be interesting to investigate what would happen if the tanks were modeled, it is a fair estimate that the tanks would absorb some of the pressure wave which then would dissipate a lot quicker. However, there was not enough time to do this within the limits of this dissertation.

6.2 Results

6.2.1 Pressures

The results of interest from the simulation are the pressure change over time. In Section A.2 in Appendix A the pressure change over time for different cross sections is presented. The placement of the cross section is the same points used to present the results in the Relap simulation. The points are presented in Figure A.1. In Section A.4 in Appendix A the pressure curves from the ADINA CFD simulation are also presented together with their counterparts from the Relap simulation. It is easily observed that the ADINA CFD simulation gives a response with a slightly higher frequency. It is important to keep in mind that Relap executes its simulation using five straight one meter long sections while the ADINA CFD simulation accounts for the bends which will give a slightly shorter total length of the pipe system and thus a slightly higher frequency, since the pressure wave does not have to travel quite as far.

It can also be seen that the pressure curve from the ADINA CFD simulation is slightly larger and that it dissipates at a slower rate. As can be seen in Section A.4 in Appendix A, all these characteristics are true for all presented pressure curves. In Figure 6.6 to 6.9 the pressure curve from a point in the beginning and the end of the pipe system from the ADINA CFD simulation are presented, both alone and with its counterpart from the Relap simulation.

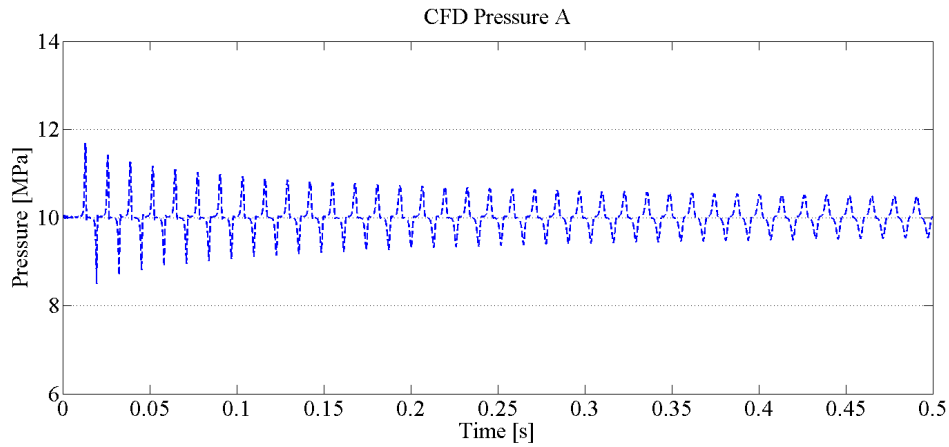

Figure 6.6: The pressure at a point in the beginning of the pipe system from the ADINA CFD simulation

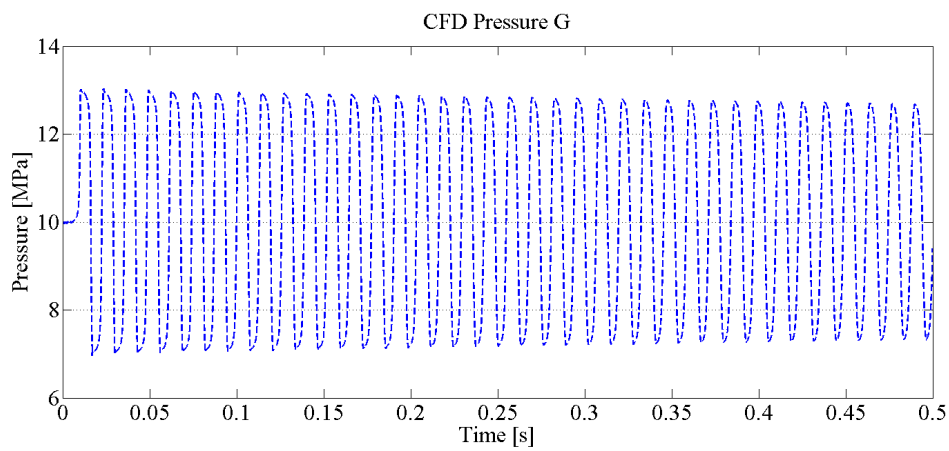

Figure 6.7: The pressure at a point in the end of the pipe system from the ADINA CFD simulation

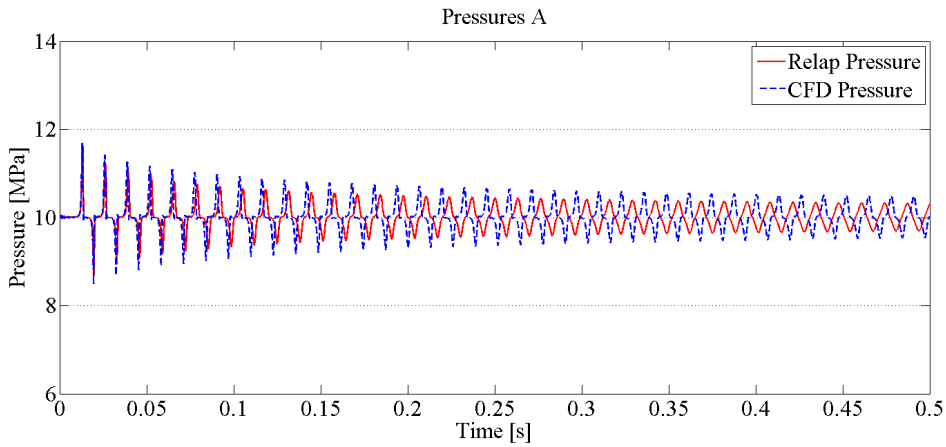

Figure 6.8: The pressure at a point in the beginning of the pipe system from the ADINA CFD and Relap simulation

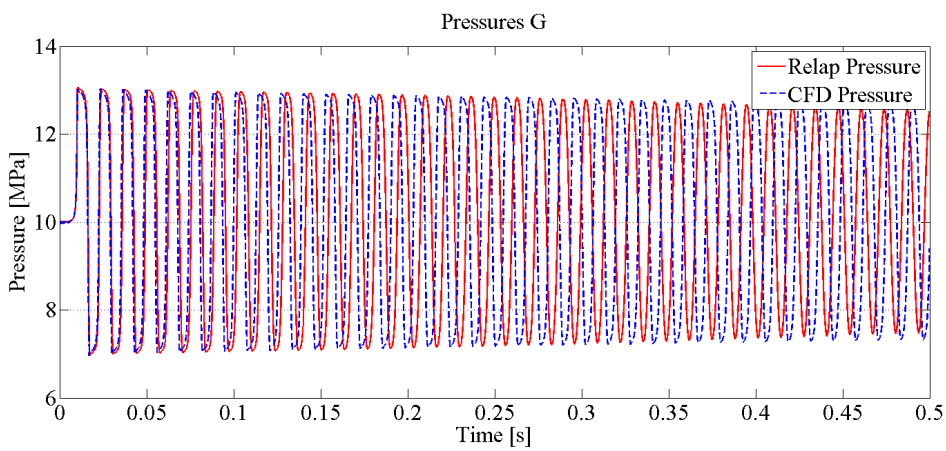

Figure 6.9: The pressure at a point in the end of the pipe system from the ADINA CFD and Relap simulation

6.2.2 Forces

In the Relap simulation the mass flow change was used to calculate the force response. In the ADINA CFD simulation the pressure change will be used instead. The equation to calculate the force response over a straight pipe is

$$F = \Delta pA \tag{6.4}$$

$$\Delta p = p_2 - p_1 \tag{6.5}$$

where

F	is the force response,
p_1, p_2	is the pressure at the first and last cross section respectively,
A	is the fluid cross section area.

A positive sign on the force mean that the force is in the direction from p_1 to p_2. Special attention has to be given to the forces in the bends. The intuitional way to turn the pressure differences in the bends into a corresponding force in a correct direction would be to use the angle with respect to the X- or Y-direction of the middle cross section in each element section. Of course, this may not be the correct way the pressure wave affects the structure but it is an approximation which turns out to give the expected result. The force in each bend has to be divided into an X-component (F_X) and a Y-component (F_Y) in order to be able to sum up the total force in each pipe section. In each bend there are a couple of element sections. Each element section will have its own force component which has to be divided into an X-component ($f_{X,i}$) and a Y-component ($f_{Y,i}$), where i is the element section.

$$f_{X,i} = \Delta p_i A \sin(v_i) \tag{6.6}$$

$$f_{Y,i} = \Delta p_i A \cos(v_i) \tag{6.7}$$

where

v_i	is the angle of element section i in the bend, defined in the middle of the element section,
Δp_i	is the pressure drop over element section i.

The total X- and Y- component in the bend then becomes

$$F_X = \sum_{i=1}^{k} f_{X,i} \tag{6.8}$$

$$F_Y = \sum_{i=1}^{k} f_{Y,i} \tag{6.9}$$

where

k is the number of element sections in the bend, in this dissertation $k = 5$.

By combining Equation (6.4) with Equation (6.8) and (6.9) the total force response can be obtained. Which of Equation (6.8) and (6.9) that needs to be used depends on the orientation of the pipe section.

For visualization, Figure 6.10 is presented. It shows each force component in their respective X- and Y-direction in each element section. The red arrows shows the f_X components and the blue arrows shows the f_Y components. The angle v is 0° when the element section normal is in the Y-direction and 90° when it is in the X-direction.

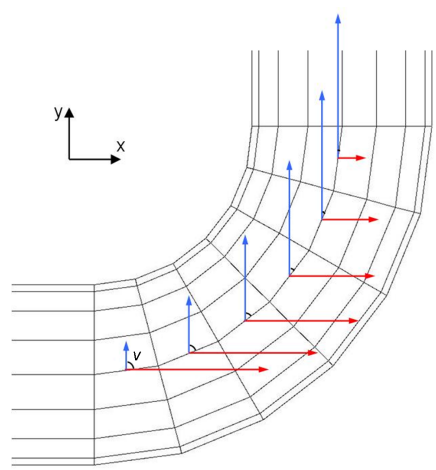

Figure 6.10: Red arrows are the f_X components, blue arrows are the f_Y components.

In Section B.2 and B.3 in Appendix B the force responses from the ADINA CFD simulation is presented both separate and together with their counterparts from the Relap simulation, respectively. In Figure 6.11 the force response in the last pipe section is presented. In Figure 6.12 the force response from both the ADINA CFD simulation and the Relap simulation in the last pipe section is presented.

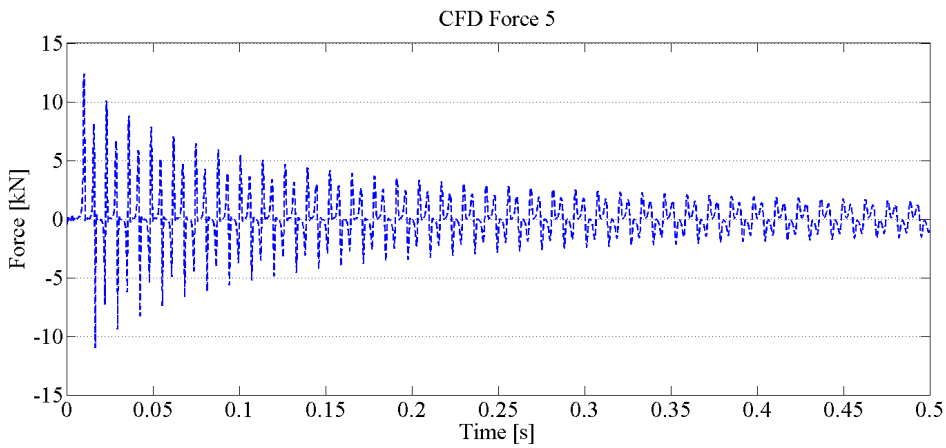

Figure 6.11: Force response in the last pipe section from the ADINA CFD simulation

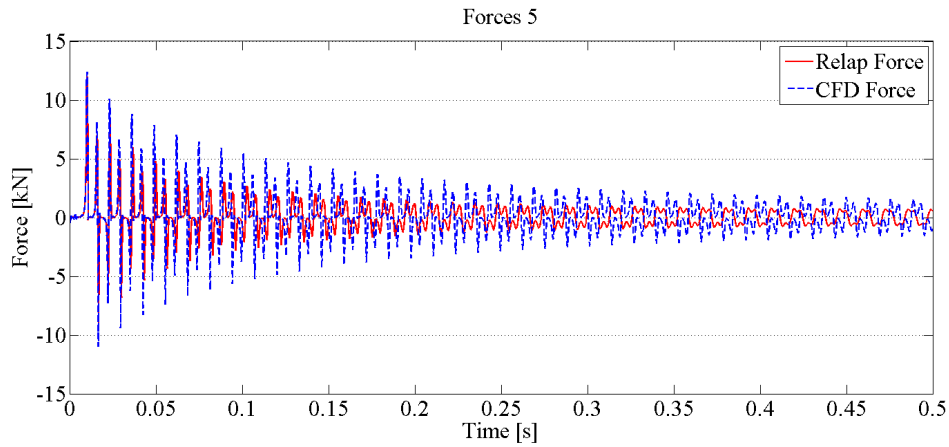

Figure 6.12: Force response from both the ADINA CFD simulation and the Relap simulation in the last pipe section

As can be seen in Figure 6.12, the force response from the ADINA CFD simulation have a slightly higher frequency than the one from the Relap simulation. It can also be seen that the force response from the ADINA CFD simulation is slightly larger and that it dissipates at a slower rate. As can be seen in Appendix B, all these characteristics are true for the force response in all five pipe sections. This is consistent with the result from Section 6.2.1.

Chapter 7

Pipestress

As mentioned in Section 4.2, the calculations that Pipestress performs are based on the ASME code [3]. The pipe system will be handled as if it were a class 1 system in the ASME code. The occasional load is within the Level A service limit.

7.1 ASME

American Society of Mechanical Engineers (ASME) have issued a code that is used world wide within the nuclear industry. This standard is referred to as the ASME code [3]. Service levels divides the system into four parts beginning with level A that contains regular cases with no big consequences when a case occurs to level D that contains incidents that are not supposed to happen. These may have devastating consequences if they do occur. Because of this, ASME allows different stresses in the different service levels with the hardest restrictions in level A since those events occurs on a regular basis and are not supposed to jeopardize the structural integrity of the system. The stresses from the system that are to be evaluated are the maximum stresses during the entire solution. The stresses in the system are evaluated against an allowable stress value which differs depending on the class and the service level of the system. The classes are divided into different parts where class 1 includes vital parts inside the reactor containment and class 2,3 and 4 are less vital parts of the nuclear power plant. In this dissertation, the stresses in the Pipestress

simulation are calculated using the ASME code NB-3600 for a class 1, level A system.

In the ASME code [3] it is stated that the maximum stresses in the pipe system due to an occasional load in a class 1 system in service level A are to be evaluated against $1.5S_m$ where S_m is decided according to Equation 7.1 according to the ASME code [16].

$$S_m = min\left(\frac{S_T}{3}, \frac{2}{3}S_Y\right) \tag{7.1}$$

where

S_T is the tensile strength,
S_Y is the yield strength.

7.2 The model

The model is basically made up of straight beam elements which are connected at a junction point. Every beam has a length, direction and an end point, the starting point of the beam is the end point of the last beam element. To be able to create the first beam element a point in space has to be defined. In this case, that point as well as the last point of the system are anchored, i.e. locked in all six degrees of freedom; X, Y, Z, -translational and -rotational. This is done to simulate the two rigid tanks. However, the anchor points have a default translational stiffness of $1.75 \cdot 10^7$ kN/mm and a rotational stiffness of $1.13 \cdot 10^9$ kNm/rad. Supports are added at the middle of every straight pipe section and they have a default stiffness of $8.75 \cdot 10^2$ kN/mm (20 000 times weaker then the anchor points). The supports act in a given direction, in this case in the Z-direction and also one support in the Y-direction. Noteworthy is that the supports act in both the positive and the negative direction since the mode superposition approach that Pipestress uses requires a linear setup. A general damping ratio for every mode is used in Pipestress, see Section 3.4.1. The damping is 5%, $\xi = 0.05$. A damping ration of $\xi = 0.05$ is commonly accepted as best practice within the Nuclear Engineering industry. In this dissertation, the number of modes used in the mode superposition solution that Pipestress uses is six. This is set by choosing up to which frequency the program should calculate the modes, which in this case is set to 200 Hz.

Then it calculates all modes from zero up to the first mode above 200 Hz, which in this case is a total of six modes.

In order to define a bend the bend radius has to be given. Using this bend radius Pipestress calculates specific stress indices in accordance with the ASME code. B_1 in order to handle the stresses due to the internal pressure and B_2 in order to handle the stresses due to the moments. According to the ASME code [3] the stress indices for a welded elbow or pipe bend is

$$h = \frac{tR}{r_m^2} \tag{7.2}$$

$$B_1 = 0.4h - 0.1 \leq 0.5 \text{ and } > 0 \tag{7.3}$$

$$B_2 = \frac{1.30}{h^{2/3}} \tag{7.4}$$

where

h	is the flexibility characteristic,
t	is the nominal pipe wall thickness,
R	is the bend radius,
r_m	is the medium radius of the pipe.

In this case $B_1 = 0.045$ and $B_2 = 2.56$ for all the bends in the pipe system. Stress indices are also used for the straight pipes, however they are, according to the ASME code [3], $B_1 = 0.5$ and $B_2 = 1$. Equation (7.3) and (7.4) have been decided empirically and might include some conservatism.

7.3 Loads

The pipe system will be subjected to a dynamic load. The load is caused by a fast valve closure. The load is calculated using both Relap and ADINA which means that the Pipestress simulation has to be made two times, one with each load, giving two separate responses. The method of how the load was calculated has been presented in the previous chapters.

7.3.1 SPECT3

SPECT3 is a Pipestress application that can evaluate the dynamic loads and calculate how much energy they contain at certain frequencies. This

is a quick way to analyze a time history load and see at which frequencies it will excite the system. Both the Relap load and the ADINA load were analyzed using SPECT3. In Figure 7.1 and Figure 7.2 the graphical representation of the SPECT3 analyze from both the Relap load and the ADINA load is presented, respectively.

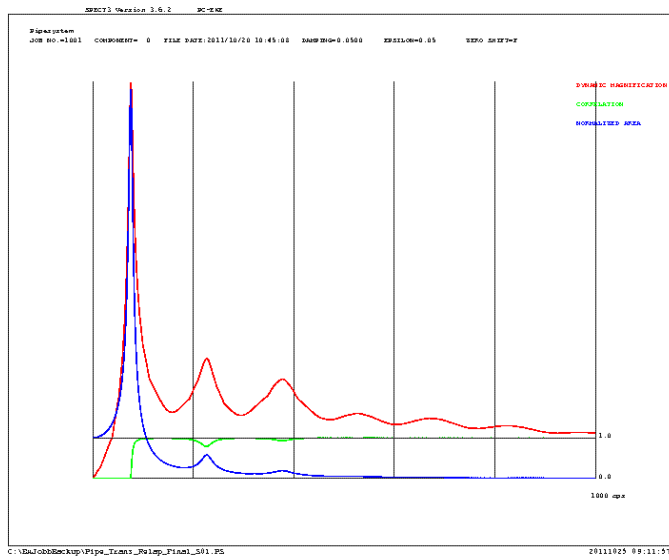

Figure 7.1: Relap force SPECT3 plot

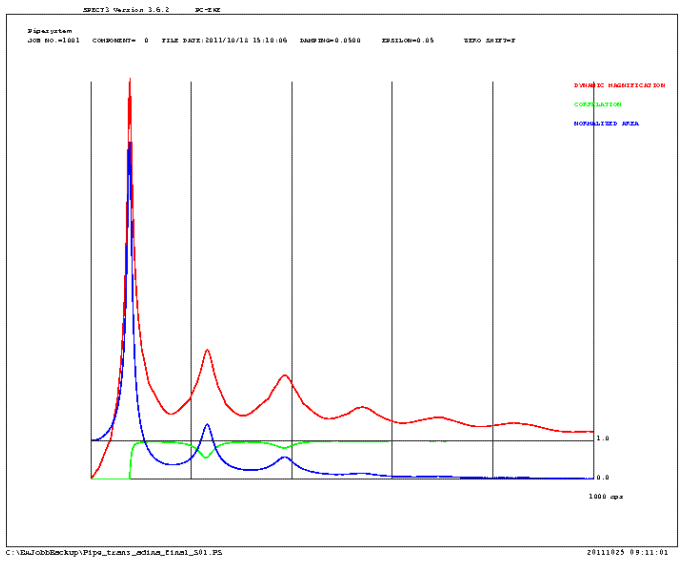

Figure 7.2: ADINA force SPECT3 plot

In Figure 7.1 and Figure 7.2 it is observed that each of the loads contain one frequency. It is difficult to see exactly which frequency that is in the graphical representations. When looking at the numerical data produced by SPECT3 it is easy to see that the Relap load has a frequency of 76 Hz while the ADINA load has a frequency of 78 Hz. This is not surprising since, as stated in section 6.2.2, the force response from the ADINA CFD simulation has a higher frequency than the force response from the Relap simulation.

7.4 Results

The results given by Pipestress are the maximum stresses for the duration of the solution in every sub part of the pipe system. In order to calculate the stresses there are several different equations available. In the case of an occasional load such as a sudden valve closure during normal operating conditions the stresses are calculated according to the ASME code [3]

$$B_1 \frac{pD_o}{2t} + B_2 \frac{D_o}{2I} M_i \leq 1.5 S_m \tag{7.5}$$

where

B_1, B_2	are the stress indices,
p	is the operating pressure in the system,
D_o	is the outside diameter of the pipe,
t	is the nominal wall thickness of the pipe,
M_i	is the resultant moment due to a combination of design mechanical loads,
I	is the moment of inertia.
S_m	is the allowable design stress intensity.

Equation (7.5) can be divided into two parts, the pressure term, $S_{Pr} = B_1 \frac{pD_o}{2t}$, and the moment term, $S_M = B_2 \frac{D_o}{2I} M_i$. The moment in a point in the pipe system contains a total of three moments, two bending moments and one torsional moment. Due to the simple setup of the pipe system the torsional moment in an arbitrary point in the system is maximum 3 Nm. This can be compared to the smallest Z-moment which is 772 Nm. When comparing the maximum torsional moment with the minimum Z-moment it is clear that the torsional moments in the system is negligible. This means that the moments acting on the pipe system due to the mechanical loads can be assumed to be pure bending moments. A bending moment that acts over a cross section only adds to the normal stress component, in this case the axial, of that cross section.

With $B_1 = 0.5$ and $B_2 = 1$ for straight pipes, see Section 7.2, Equation (7.5) for the parts of interest in this dissertation becomes

$$\frac{pD_o}{4t} + \frac{D_o}{2I} M_i \leq 1.5 S_m \tag{7.6}$$

which is the same as

$$\frac{R_o}{2t} p + \frac{R_o}{I} M_i \leq 1.5 S_m \tag{7.7}$$

where

R_o	is the outer radius of the pipe.

The pressure term, $S_{Pr} = \frac{R_o}{2t} p$, can be recognized as the equation of the stress in the axial direction of a cylindrical vessel due to internal pressure.

Frequencies	
f_1	37.92 Hz
f_2	53.44 Hz
f_3	111.66 Hz
f_4	116.96 Hz
f_5	180.24 Hz
f_6	257.61 Hz

Table 7.1: Eigenfrequencies of the pipesystem calculated with Pipestress

The moment term gives the highest stress in the axial direction of the pipe due to the bending moments over the cross section. In this case it means that for the straight pipe sections the stresses that Pipestress calculates can be assumed only to be the stress component in the axial direction. It is also clear that the stress component due to the internal pressure will be the same for all straight pipe sections. With $R_o = 47.7$ mm, $t = 6.3$ mm and $p = 10$ MPa the pressure term of Equation (7.7) will be

$$S_{Pr} = \frac{R_o}{2t} p = 37.86 \text{ MPa} \tag{7.8}$$

7.4.1 Frequencies

Since Pipestress uses a mode superposition method for calculating the stresses a frequency and mode shape analysis has to be performed in the initial step. The result of the frequency analysis is presented in Table 7.1.

7.4.2 Stresses

The stress response of the simulations made are presented in Appendix D. In Table 7.2 there are a couple of representative results presented. The placement of the points in the pipe are presented in Figure 7.3. The difference is calculated as the stress response due to the ADINA load minus the stress response due to the Relap load.

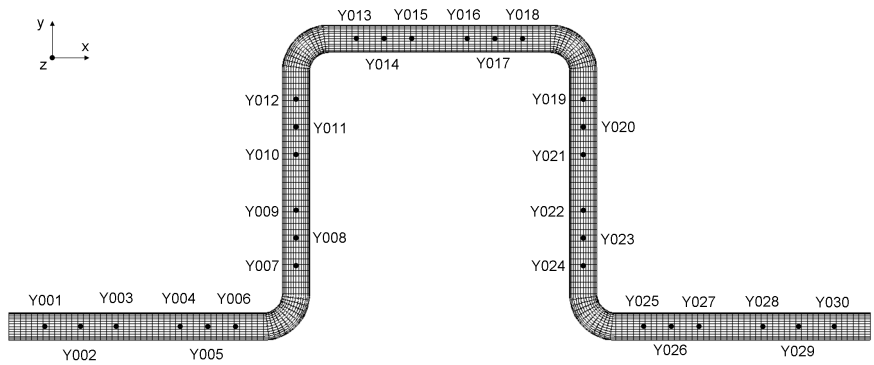

Figure 7.3: Pipe node placement

Maximum stresses in different points of the pipe system				
Point	Relap load	ADINA load	Difference	Diff., %
Y005	69.72 MPa	69.14 MPa	−0.58 MPa	−0.8 %
Y009	91.05 MPa	89.37 MPa	−1.68 MPa	−1.8 %
Y013	106.98 MPa	103.36 MPa	−3.62 MPa	−3.4 %
Y018	105.01 MPa	101.83 MPa	−3.18 MPa	−3.0 %
Y021	107.00 MPa	104.97 MPa	−2.03 MPa	−1.9 %
Y026	67.18 MPa	67.51 MPa	0.33 MPa	0.5 %

Table 7.2: Maximum stresses in different points of the pipe system

In the general case the ADINA load gives a slightly lower stress response in the pipe system. This raises a question since in section 6.2.2 it was concluded that the forces from the ADINA CFD simulation was slightly larger than the ones from the Relap simulation. This is because the frequency of the ADINA load is different from the frequency of the Relap load. In Section 7.3.1 it is concluded that the ADINA load frequency is 78 Hz and the Relap load frequency is 76 Hz. With the information from Table 7.1 it is clear that both loads are within the range of the second ($f_2 = 53.44$ Hz) and the third ($f_3 = 111.66$ Hz) eigenfrequency. The frequency that is in the middle of f_2 and f_3 is $f = 82.55$ Hz. Since the ADINA load frequency

of 78 Hz is closer to 82.55 Hz than the Relap load frequency of 76 Hz it means that it is also further away from the closest eigenfrequency and thus will excite the system less than the Relap load, giving a slightly lower stress response.

Chapter 8

ADINA Structure

The ADINA Structure simulation will be made using two different methods, a mode superposition method and an implicit direct integration method. It is of interest to see what the difference is between the two different methods. Also, the implicit direct integration method will be used in the FSI simulation.

8.1 The model

As stated in Section 2.3, all results for comparison purposes will be gathered from the straight pipe sections. For that reason, a rather course mesh in the solid simulations will be sufficient. The pipe wall will only be modeled with one element thickness. However, the elements in the solid model are of the second order so there will be a total of three nodes over the pipe thickness. As concluded in Section 7.4, stress due to moments over the cross section is due to bending moments. Because of the linear characteristics of bending moments over a cross section, one element over the pipe thickness is sufficient since the result of interest is the maximum stress component. The stress component due to internal pressure also have a linear behavior over the cross section with its maximum at the internal pipe diameter.

The nodes at the ends of the solid model are modeled as fixes with zero X-,Y- and Z-displacement. These fixes are to simulate the tanks in the system. Note that in Section 7.2 the anchor points have a default stiffness unlike the fixed points in ADINA which instead of a stiffness are modeled

with zero displacement. The same applies to the pipe supports. In ADINA the supports in Y- and Z-direction are modeled with zero displacement. This way of modeling the supports is not optimal and may cause disturbances close to the supports. However, it is sufficient for this dissertation.

The pipe system is filled with water that is under high pressure. There are two ways to account for this, either the pipe is filled with a mesh consisting of a potential based fluid element that is available in ADINA or the mass of the pipe has to be compensated for the additional weight of the water, this is possible since the entire pipe is filled with water subjected to high pressure as to not cause cavitation. The latter is chosen for this dissertation. The new density of the pipe is calculated according to

$$\rho = \rho_{\text{pipe}} + \frac{A_{\text{water}}}{A_{\text{pipe}}}\rho_{\text{water}} \tag{8.1}$$

where

ρ_{pipe}	is the original density of the pipe, se Table 2.2,
ρ_{water}	is the density of the water, se Table 2.1,
A_{water}	is the area of the water,
A_{pipe}	is the area of the pipe.

The new density of the pipe in this dissertation is $\rho = 10900$ kg/m^3.

8.2 Loads

The loads applied in the ADINA structural simulations are the same as in the Pipestress simulations, see Section 7.3 for more information about the loads.

The load on each pipe section is applied on every second node along a circle on the internal diameter of the pipe at the end of the straight pipe section. The magnitude of the load is divided by the total number of nodes that the load is applied to. The internal pressure of 10 005 759 MPa is added as a static load as well as the gravity.

8.3 Mode superposition

The mode superposition method in ADINA works like described in Section 3.2. The results of the frequency analysis is presented in Table 8.1. To solve

the transient problem ADINA applies the Newmark method, described in Section 3.3. In order to include the static internal pressure and the gravity, a static analysis needs to be made. After that, the mode superposition analysis can be restarted using the data from the static analysis. This is because the mode superposition method uses the unloaded mass and stiffness matrix calculated before the actual simulation begins and thus, if a static pressure is to be included, it needs to first be simulated statically in order for the mass and stiffness matrix to include the effects of the pressure. Five modes are being used in the simulation. In the Pipestress simulation six modes are being used. Preferably the same amount as in the Pipestress simulation should be used in the ADINA simulation, unfortunately this realization occurred when all the simulations where completed. A quick test was made by changing the number of modes in the Pipestress simulation and it showed that the results varied by up to 0.3 MPa. This variation is small and the comparison will still be made with five and six modes being used in the ADINA mode superposition simulation and the Pipestress simulation, respectively.

In the ADINA mode superposition method modal damping is applied. A general damping ratio for every mode is used, see Section 3.4.1. The chosen damping ratio is the same as in the Pipestress simulation, $\xi = 0.05$, see Section 7.2.

8.4 Direct integration

The direct integration method employed in this dissertation is an Implicit method that uses the Newmark method to solve the time integration, see Section 3.3 for detailed information about the Newmark method. Unlike the mode superposition method internal pressure and gravity can be added in the direct integration simulation without first running a static analysis. However, it is important to apply static loads in a direct integration simulation in a static time step before the dynamic solution begins otherwise the static load might add to the dynamic behavior of the structure. In the direct integration method Rayleigh damping is being used instead of modal damping. Other than that the setup of the two simulations are the same.

8.4.1 Rayleigh damping

Rayleigh damping is briefly explained in Section 3.4.2. In the ADINA direct integration simulation Rayleigh damping is applied. In order to decide the α and β parameters two reference frequencies was chosen. Also a desired damping at those frequencies were decided, $\xi = 0.05$. In Section 7.3.1 it is concluded that the load frequencies are 76 Hz and 78 Hz for the Relap load and the ADINA load, respectively. From Table 8.1 it is obvious that those load frequencies will be between $f_2 = 54.77$ Hz and $f_3 = 112.00$ Hz. f_2 and f_3 are chosen as the reference frequencies. With

$$\omega = 2\pi f \tag{8.2}$$

the α and β parameters can be calculated from Equation (3.39). In this case $\alpha = 23.11121$ and $\beta = 9.54338 \cdot 10^{-5}$. The entire Rayleigh curve is presented in Figure 8.1.

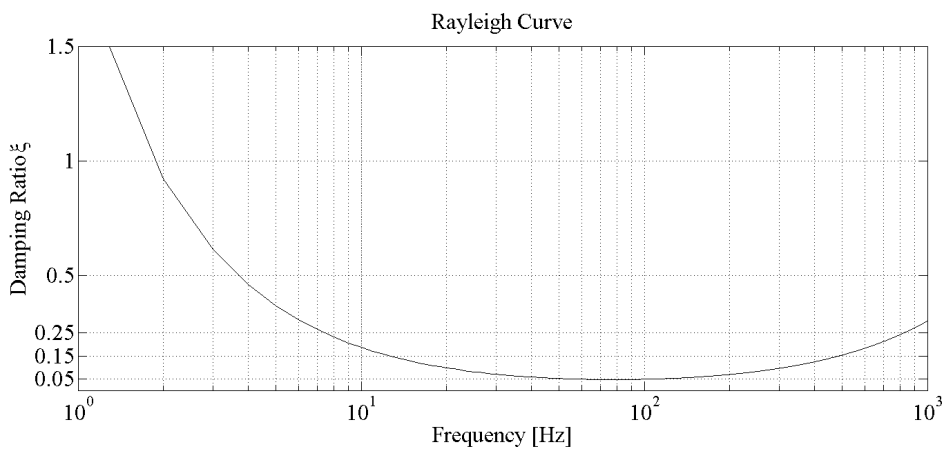

Figure 8.1: Rayleigh curve

8.5 Results

8.5.1 Frequencies

The mode superposition method of ADINA requires a frequency analysis to calculate the eigenfrequencies and the mode shapes. In Table 8.1 the

eigenfrequencies from ADINA is presented together with the frequencies from Pipestress, see Table 7.1. The difference is calculated as the eigenfrequency from ADINA minus the eigenfrequency from Pipestress. The ratio is calculated as the difference with respect to the Pipestress result.

Frequencies				
	Pipestress	ADINA	Difference	Diff., %
f_1	37.92 Hz	40.00 Hz	2.08 Hz	5.5 %
f_2	53.44 Hz	54.77 Hz	1.33 Hz	2.5 %
f_3	111.66 Hz	112.00 Hz	0.34 Hz	0.3 %
f_4	116.96 Hz	113.80 Hz	-3.16 Hz	-2.7 %
f_5	180.24 Hz	170.90 Hz	-9.34 Hz	-5.2 %

Table 8.1: Eigenfrequencies of the pipe system calculated with ADINA and Pipestress

As can be seen in Table 8.1 the eigen frequencies varies some between the ADINA analysis and the Pipestress analysis. In Section 3.2 it is stated that the equation for the free vibration only depends on the mass matrix and the stiffness matrix. Since the masses in ADINA and Pipestress are the same the only thing that can explain the difference in the eigenfrequencies are the stiffness matrix. An easy test to see if the stiffness is different between the ADINA setup and the Pipestress setup was made. One bend in the system was modeled together with two short pipe sections and subjected to a certain load. The test showed that the displacement where the load was applied differed between the test performed in ADINA and the test performed in Pipestress. The load was primarily applied so that the bend would deform the same way as it would in the simulations. Another load was applied in a different direction. This time the test showed that the difference was inverted. In Pipestress the stiffness of the bends is controlled by the flexibility factor k. According to [3] k, when the pipe bend is exposed to bending moments, is calculated as

$$k = \frac{1.65}{h}\left[\frac{1}{1 + (pr/tE)X_k}\right] \tag{8.3}$$

where

h is the flexibility characteristic according to Equation (7.2),
p is the internal pressure,
r is the mean radius of the pipe,
t is the nominal wall thickness of the pipe,
E is the modulus of elasticity,
X_k $= 6(r/t)^{4/3}(R/r)^{1/3}$.

By changing the flexibility factor in the Pipestress simulation different results can be obtained. The default flexibility factor for the bends in the pipe system in this dissertation is $k = 4.39$.

8.5.2 Stresses

Like in Section 7.1 the sought results are the maximum stress intensity over the entire solution. In the ASME code [3] it is stated that when designing pipes by FEM analysis the stress intensity is defined as twice the maximum shear stress. The stress intensity should then be evaluated against $1.5\mathrm{S_m}$, see Section 7.1 for definition of $\mathrm{S_m}$. In this dissertation the stress intensity will be compared with the results from Pipestress in order to quantify the difference between the different analysis methods. According to Handbok och formelsamling i Hållfasthetslära [17] the maximum shear stress is calculated from the principal stresses as

$$\tau_{max} = \frac{1}{2}(\sigma_1 - \sigma_3) \tag{8.4}$$

where

σ_1, σ_3 are the biggest and smallest principal stresses, respectivly.

Which leads to

$$2\tau_{max} = \sigma_1 - \sigma_3 \tag{8.5}$$

Handbok och formelsamling i Hållfasthetslära [17] states that

$$\sigma_{Tresca} = max(|\sigma_1 - \sigma_2|, |\sigma_1 - \sigma_3|, |\sigma_2 - \sigma_3|) \tag{8.6}$$

and with

$$\sigma_1 \geq \sigma_2 \geq \sigma_3 \tag{8.7}$$

Equation (8.6) can be rewritten as

$$\sigma_{Tresca} = 2\tau_{max} \tag{8.8}$$

which concludes that twice the maximum shear stress is nothing else than the Tresca stress. This can be visualized in Mohr's circle of stress, Figure 8.2.

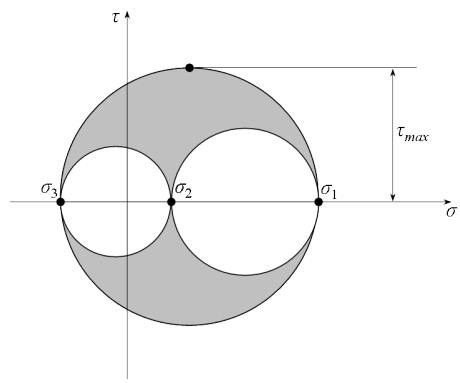

Figure 8.2: Mohr's circle of stress

The complete results from the mode superposition analysis and the direct integration analysis are presented in Appendix D. In this section the results from a selected few points in the pipe system are presented and compared with each other. As a point of reference, the results from the Pipestress simulations are also presented. The points are chosen to accurately represent the results. The conclusions presented here are done by carefully evaluating each simulation. This evaluation is not fully presented in this dissertation. However, all data needed to make the full comparison is presented in Appendix D. In Figure D.1 the placements of all the data points in the pipe system are presented.

In Table 8.2 and 8.3 the difference between the ADINA mode superposition simulations and the Pipestress simulations due to the Relap load and the ADINA load are presented. In Table 8.4 the difference between the mode superposition simulations using the Relap load and the ADINA load is presented. The difference in Table 8.2 and 8.3 are calculated as the mode superposition result minus the Pipestress result, the ratio is with

respect to the Pipestress result. In Table 8.4 the difference is calculated as the result due to the ADINA load minus the result due to the Relap load, the ratio is with respect to the results due to the Relap load.

Pipestress and Mode Superposition results due to the Relap calculated load				
Point	Pipestress	Mode Superposition	Difference	Diff., %
Y005	69.72 MPa	85.99 MPa	16.27 MPa	23.3 %
Y009	91.05 MPa	88.76 MPa	−2.29 MPa	−2.5 %
Y013	106.98 MPa	102.02 MPa	−4.96 MPa	−4.6 %
Y018	105.01 MPa	102.03 MPa	−2.98 MPa	−2.8 %
Y021	107.00 MPa	89.16 MPa	−17.84 MPa	−16.7 %
Y026	67.18 MPa	86.65 MPa	19.47 MPa	29.0 %

Table 8.2: Pipestress and Mode Superposition results due to the Relap calculated load

Pipestress and Mode Superposition results due to the ADINA calculated load				
Point	Pipestress	Mode Superposition	Difference	Diff., %
Y005	69.14 MPa	85.85 MPa	16.71 MPa	24.2 %
Y009	89.37 MPa	88.68 MPa	−0.69 MPa	−0.8 %
Y013	103.36 MPa	101.53 MPa	−1.83 MPa	−1.8 %
Y018	101.83 MPa	100.58 MPa	−1.25 MPa	−1.2 %
Y021	104.97 MPa	88.99 MPa	−15.98 MPa	−15.2 %
Y026	67.51 MPa	86.67 MPa	19.16 MPa	28.4 %

Table 8.3: Pipestress and Mode Superposition results due to the ADINA calculated load

Mode Superposition results due to the Relap and the ADINA calculated load				
Point	Relap load	ADINA load	Difference	Diff., %
Y005	85.99 MPa	85.85 MPa	−0.14 MPa	−0.2 %
Y009	88.76 MPa	88.68 MPa	−0.08 MPa	−0.1 %
Y013	102.02 MPa	101.53 MPa	−0.49 MPa	−0.5 %
Y018	102.03 MPa	100.58 MPa	−1.45 MPa	−1.4 %
Y021	89.16 MPa	88.99 MPa	−0.17 MPa	−0.2 %
Y026	86.65 MPa	86.67 MPa	0.02 MPa	0.0 %

Table 8.4: Mode Superposition results due to the Relap and the ADINA calculated load

The ADINA mode superposition simulation gives a lower result than the Pipestress simulation in about two thirds of the points. It is difficult to say if the mode superposition approach gives a lower result in the general case. Consistent with what has been seen in Section 7.4.2 the ADINA load generates lower stresses than the Relap load in the mode superposition method, although the difference is not that significant. The maximum stresses occurs within the first 0.05 seconds of the solution.

In Table 8.5 and 8.6 the ADINA direct integration simulations are compared to the Pipestress simulations using the Relap load and the ADINA load. In Table 8.7 the direct integration simulations are compared using the Relap load and the ADINA load. The difference in Table 8.5 and Table 8.6 are calculated as the direct integration result minus the Pipestress result, the ratio is with respect to the Pipestress result. In Table 8.7 the difference is calculated as the result due to the ADINA load minus the result due to the Relap load, the ratio is with respect to the results due to the Relap load.

Pipestress and Direct Integration results due to the Relap calculated load				
Point	Pipestress	Direct Integration	Difference	Diff., %
Y005	69.72 MPa	85.92 MPa	16.20 MPa	23.2 %
Y009	91.05 MPa	88.59 MPa	−2.46 MPa	−2.7 %
Y013	106.98 MPa	102.27 MPa	−4.71 MPa	−4.4 %
Y018	105.01 MPa	101.89 MPa	−3.12 MPa	−3.0 %
Y021	107.00 MPa	89.00 MPa	−18.00 MPa	−16.8 %
Y026	67.18 MPa	86.58 MPa	19.40 MPa	28.9 %

Table 8.5: Pipestress and Direct Integration results due to the Relap calculated load

Pipestress and Direct Integration results due to the ADINA calculated load				
Point	Pipestress	Direct Integration	Difference	Diff., %
Y005	69.14 MPa	85.78 MPa	16.64 MPa	24.1 %
Y009	89.37 MPa	88.54 MPa	−0.83 MPa	−0.9 %
Y013	103.36 MPa	101.78 MPa	−1.58 MPa	−1.5 %
Y018	101.83 MPa	101.41 MPa	−0.42 MPa	−0.4 %
Y021	104.97 MPa	88.91 MPa	−16.06 MPa	−15.3 %
Y026	67.51 MPa	86.62 MPa	19.11 MPa	28.3 %

Table 8.6: Pipestress and Direct Integration results due to the ADINA calculated load

Direct Integration results due to the Relap and the ADINA calculated load				
Point	Relap load	ADINA load	Difference	Diff., %
Y005	85.92 MPa	85.78 MPa	−0.14 MPa	−0.2 %
Y009	88.59 MPa	88.54 MPa	−0.05 MPa	−0.1 %
Y013	102.27 MPa	101.78 MPa	−0.49 MPa	−0.5 %
Y018	101.89 MPa	101.41 MPa	−0.48 MPa	−0.5 %
Y021	89.00 MPa	88.91 MPa	−0.09 MPa	−0.1 %
Y026	86.58 MPa	86.62 MPa	0.04 MPa	0.1 %

Table 8.7: Direct Integration results due to the Relap and the ADINA calculated load

Like the comparison between the results from the Pipestress simulation and the mode superposition simulation the direct integration simulation also gives lower results than the Pipestress simulation in about two thirds of the points. The ADINA calculated load also generates slightly lower stresses than the Relap calculated load in the direct integration simulation, as in the comparison between the results from the Pipestress simulation and the mode superposition simulation. Like with the mode superposition method, the peak stresses in the direct integration method occurs within the first 0.05 seconds of the solution.

In Table 8.8 and 8.9 the mode superposition method and the direct integration method is compared using the Relap and the ADINA loads. The difference is calculated as the direct integration result minus the mode superposition result. The ratio is with respect to the mode superposition result.

At about two thirds of the points in the pipe system the direct integration method generates slightly lower results than the mode superposition method.

As were concluded in Section 7.4 the results calculated by Pipestress only consist of the axial stress component. In all the ADINA simulations the total Tresca stress component have been calculated. Due to the orientation of the pipe system it is easy to get the stress component in the axial direction over a cross section at any given point in the straight pipe sections. In Table 8.10 and 8.11 some of these results have been presented

Mode Superposition and Direct Integration results due to the Relap calculated load				
Point	Mode Superposition	Direct Integration	Difference	Diff., %
Y005	85.99 MPa	85.92 MPa	−0.07 MPa	−0.1 %
Y009	88.76 MPa	88.59 MPa	−0.17 MPa	−0.2 %
Y013	102.02 MPa	102.27 MPa	0.25 MPa	0.2 %
Y018	102.03 MPa	101.89 MPa	−0.14 MPa	−0.1 %
Y021	89.16 MPa	89.00 MPa	−0.16 MPa	−0.2 %
Y026	86.65 MPa	86.58 MPa	−0.07 MPa	−0.1 %

Table 8.8: Mode Superposition and Direct Integration results due to the Relap calculated load

Mode Superposition and Direct Integration results due to the ADINA calculated load				
Point	Mode Superposition	Direct Integration	Difference	Diff., %
Y005	85.85 MPa	85.78 MPa	−0.07 MPa	−0.1 %
Y009	88.68 MPa	88.54 MPa	−0.14 MPa	−0.2 %
Y013	101.53 MPa	101.78 MPa	0.25 MPa	0.2 %
Y018	100.58 MPa	101.41 MPa	0.83 MPa	0.8 %
Y021	88.99 MPa	88.91 MPa	−0.08 MPa	−0.1 %
Y026	86.67 MPa	86.62 MPa	−0.05 MPa	−0.1 %

Table 8.9: Mode Superposition and Direct Integration results due to the ADINA calculated load

together with their Pipestress calculated counterparts. A complete list of all these results can be found in Appendix D.

Pipestress and Mode Superposition axial component results due to the Relap calculated load				
Point	Pipestress	Direct Integration	Difference	Diff., %
Y005	69.72 MPa	51.77 MPa	−17.95 MPa	−25.7 %
Y009	91.05 MPa	66.52 MPa	−24.53 MPa	−26.9 %
Y013	106.98 MPa	78.77 MPa	−28.21 MPa	−26.4 %
Y018	105.01 MPa	68.69 MPa	−36.32 MPa	−34.6 %
Y021	107.00 MPa	79.11 MPa	−27.89 MPa	−26.1 %
Y026	67.18 MPa	52.16 MPa	−15.02 MPa	−22.4 %

Table 8.10: Pipestress and Mode Superposition axial component results due to the Relap calculated load

Pipestress and Direct Integration axial component results due to the Relap calculated load				
Point	Pipestress	Direct Integration	Difference	Diff., %
Y005	69.72 MPa	60.77 MPa	−8.95 MPa	−12.8 %
Y009	91.05 MPa	77.00 MPa	−14.05 MPa	−15.4 %
Y013	106.98 MPa	82.58 MPa	−24.40 MPa	−22.8 %
Y018	105.01 MPa	70.17 MPa	−34.84 MPa	−33.2 %
Y021	107.00 MPa	78.26 MPa	−28.74 MPa	−26.9 %
Y026	67.18 MPa	63.21 MPa	−3.97 MPa	−5.9 %

Table 8.11: Pipestress and Direct Integration axial component results due to the Relap calculated load

When comparing the axial stress component from either the mode superposition analysis or the direct integration analysis it is clear that it calculates a lower result than Pipestress. When deciding whether or not either method will give lower results from an ASME point of view this comparison is not really of interest since it is the Tresca stress component that is of interest. However, it is of interest from a mathematical point of view since

the more refined analysis methods generates lower results when the components compared actually contains the same things. Only the stress results from the simulations done with the Relap calculated loads are presented here, that's because the Relap calculated load generates higher results than the ADINA calculated load and thus if the results are lower than Pipestress results when using the Relap calculated load, they will also be lower when using the ADINA calculated loads.

Chapter 9

ADINA Fluid Structure Interaction

9.1 The model

The difference in setting up the ADINA Fluid Structure Interaction (FSI) simulation compared to setting up the individual structure and fluid simulations are small. Basically, if the structure and the fluid simulations work separately, they should work together. In this dissertation the only differences are the wall boundary condition of the fluid simulation and the internal pressure boundary of the structure simulation. The fluid simulation used in the FSI simulation is the same used in the pure fluid simulation, see Chapter 6. The difference is that the rigid wall boundary condition have been changed to a FSI boundary condition. In the structure, the internal pressure have also been changed to a FSI boundary condition. The software will then recognize the two boundaries and link them together in the FSI simulation. For example, if the structure domain gets deformed, the fluid domain will follow that deformation. More about the theory behind FSI and moving-mesh can be found in Section 3.5. The structure simulation used is the direct integration approach, see Chapter 8. One important difference in the structure setup is the modified density, see Equation (8.1). When doing the FSI simulation the original density of the pipe needs to be used, see Table 2.2, since in this case, the water actually is being simulated. In an FSI simulation the master commands are set in the fluid setup. For

example, the time step of the solution will be governed by the fluid setup.

This means that in order to simulate the whole process over 0.5 seconds, about 800 000 time steps needs to be calculated, in both the fluid and the structure. This process is time consuming and due to unforeseen events with the servers the simulation never completed the whole 0.5 seconds. However, about 0.14 seconds of the solution was recovered and is presented in this dissertation. In earlier simulations it has shown that the maximum stress occurs in the beginning of the simulation (within the first 0.05 seconds). 0.05 seconds is well within the 0.14 seconds of the FSI simulation. As have been stated in Section 7.1, the maximum stress is the sought data and thus this solution is sufficient.

In Section 3.5 it is stated that the direct two-way FSI method can not be used with the Segregated method. In Section 6.1 it is stated that the FCBI-C element used in the CFD simulation uses the Segregated method. This means that the iterative two-way FSI method has to be used in the simulation in this dissertation, see Section 3.5 for more information about the direct and the iterative two-way FSI.

9.2 Results

For convenience purposes, the FSI simulation will only be compared to the previous simulations done using the ADINA load. As have been seen, the ADINA load gives a slightly lower stress response and thus, it is sufficient to compare the different simulations this way. If the FSI simulation gives lower results than the simulations done with the ADINA load, then it will also give lower results than the simulations done with the Relap load, see Table 7.2.

9.2.1 Pressures

In Figure 9.1 and 9.3 the pressure curves from the beginning and the end of the pipe system are presented. In Figure 9.2 and 9.4 they are presented together with the pressure curves from the ADINA CFD simulation and the Relap simulation. The rest of the pressure curve plots can be found in Appendix A.

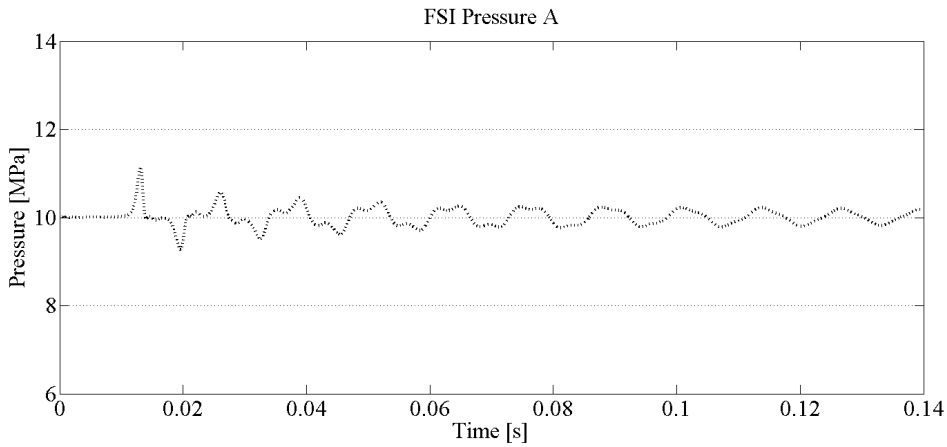

Figure 9.1: The pressure at a point in the beginning of the pipe system from the FSI simulation

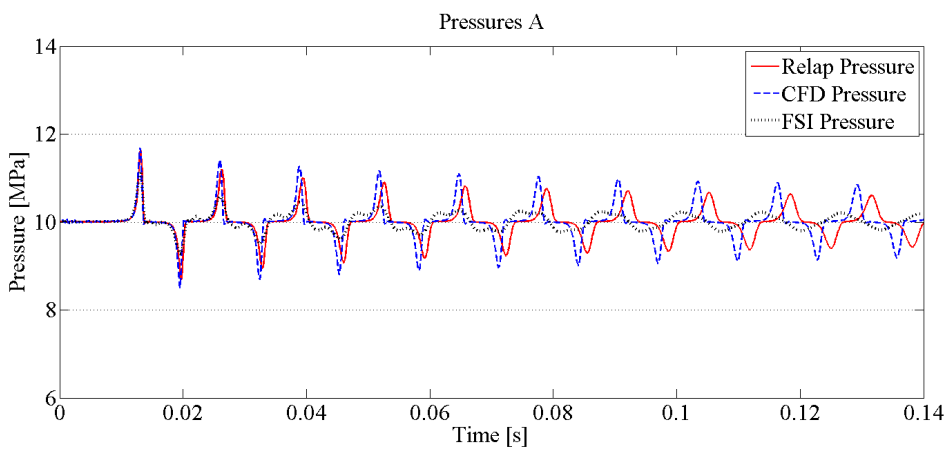

Figure 9.2: The pressure at a point in the beginning of the pipe system from the FSI simulation

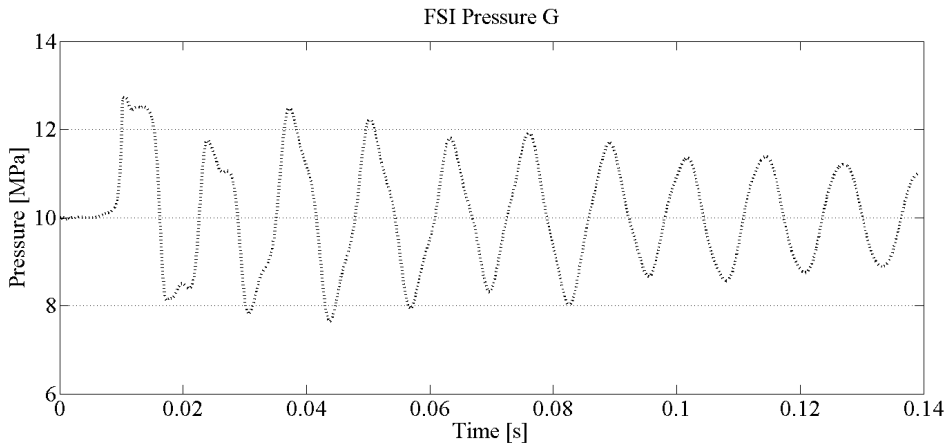

Figure 9.3: The pressure at a point in the end of the pipe system from the FSI simulation

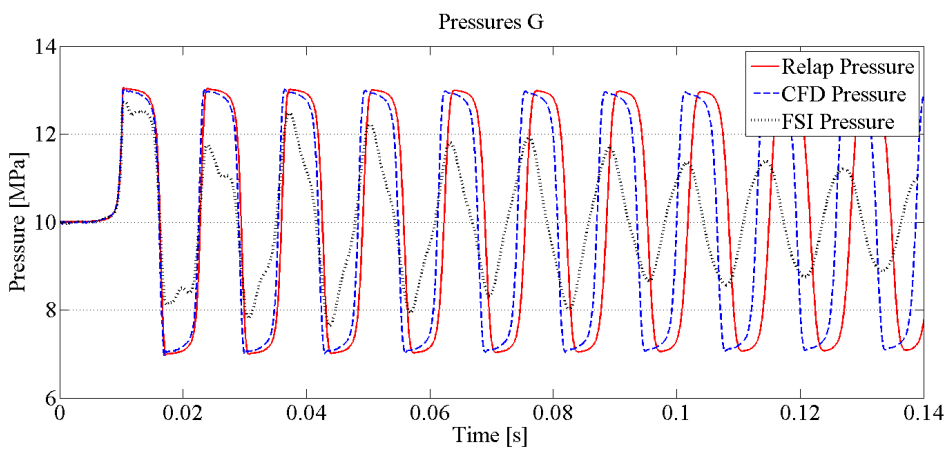

Figure 9.4: The pressure at a point in the end of the pipe system from the FSI simulation

As can be observed, the maximum pressure of the FSI simulation is lower than the maximum pressure of the other two simulations. It also dissipates at a faster rate plus there are additional micro variations in the pressure curves. It still have the same frequency as the ADINA CFD pressure curve.

9.2.2 Stresses

The FSI calculated results are compared with the Pipestress, the mode superposition and the direct integration calculated results due to the ADINA calculated loads. The difference is calculated as the FSI result minus the result from the other method. The ratio is calculated as the difference with respect to the result from the other method.

Pipestress results due to the ADINA calculated load and FSI results				
Point	Pipestress	FSI	Difference	Difference, %
Y005	69.14 MPa	98.28 MPa	29.14 MPa	42.1 %
Y009	89.37 MPa	107.20 MPa	17.83 MPa	20.0 %
Y013	103.36 MPa	107.05 MPa	3.69 MPa	3.6 %
Y018	101.83 MPa	108.44 MPa	6.61 MPa	6.5 %
Y021	104.97 MPa	109.48 MPa	4.51 MPa	4.3 %
Y026	67.51 MPa	106.00 MPa	38.49 MPa	57.0 %

Table 9.1: Pipestress results due to the ADINA calculated load and FSI results

Mode Superposition results due to the ADINA calculated load and FSI results				
Point	Mode Superposition	FSI	Difference	Difference, %
Y005	85.85 MPa	98.28 MPa	12.44 MPa	14.5 %
Y009	88.68 MPa	107.2 MPa	18.52 MPa	20.9 %
Y013	101.53 MPa	107.05 MPa	5.52 MPa	5.4 %
Y018	100.58 MPa	108.44 MPa	7.86 MPa	7.8 %
Y021	88.99 MPa	109.48 MPa	20.49 MPa	23 %
Y026	86.67 MPa	106 MPa	19.33 MPa	22.3 %

Table 9.2: Mode Superposition results due to the ADINA calculated load and FSI results

Direct Integration results due to the ADINA calculated load and FSI results				
Point	Direct Integration	FSI	Difference	Difference, %
Y005	85.78 MPa	98.28 MPa	12.5 MPa	14.6 %
Y009	88.54 MPa	107.2 MPa	18.66 MPa	21.1 %
Y013	101.78 MPa	107.05 MPa	5.27 MPa	5.2 %
Y018	101.41 MPa	108.44 MPa	7.03 MPa	6.9 %
Y021	88.91 MPa	109.48 MPa	20.57 MPa	23.1 %
Y026	86.62 MPa	106.00 MPa	19.38 MPa	22.4 %

Table 9.3: Direct Integration results due to the ADINA calculated load and FSI results

As can be seen in Table 9.1 to 9.3 the FSI results are higher than the other methods. That the FSI method gives higher result than Pipestress is not that surprising. In Section 8.5.2 it was stated that the Pipestress result does not contain all stress components and that the ADINA simulations contain the Tresca stress component, as does the FSI simulation. The fact that the FSI simulation gives higher results than the other ADINA methods is because of the difference in the maximum internal pressure of the system. In the mode superposition and the direct integration method the internal pressure is set to a fixed value of 10 MPa, see Section 8.2. This pressure gives a maximum Tresca stress value of $\sigma_{Tresca}^{10MPa} = 81.07$ MPa calculated using Equation (8.6) and the equations

$$\sigma_1 = \sigma_\phi = \frac{d^2}{D^2 - d^2}\left(1 + \frac{D^2}{4r_{min}^2}\right)p \tag{9.1}$$

$$\sigma_2 = \sigma_z = \frac{d^2}{D^2 - d^2}p \tag{9.2}$$

$$\sigma_3 = \sigma_r = \frac{d^2}{D^2 - d^2}\left(1 - \frac{D^2}{4r_{min}^2}\right)p \tag{9.3}$$

where

$\sigma_1, \sigma_2, \sigma_3$	are the principal stresses,
σ_r	is the radial stress,
σ_ϕ	is the angular stress,
σ_z	is the axial stress,
d	is the inner diameter of the pipe,
D	is the outer diameter of the pipe,
r_{min}	is the inner radius of the pipe,
p	is the internal pressure.

In the FSI simulation the internal pressure will vary with time. However, since the maximum stress is sought, only the maximum internal pressure will be of interest. With a maximum pressure varying between about 11 MPa and 12.5 MPa depending on which pipe section and with a mean of about 12.2 MPa the mean maximum Tresca stress will be $\sigma_{Tresca}^{FSI,max} = 98.91$ MPa. With a stress difference of $\sigma_{Tresca}^{FSI,max} - \sigma_{Tresca}^{10MPa} = 17.84$ MPa it is not surprising that the FSI simulation generates higher stress results. There are also some other dynamic effects that generates stress responses in the

structure and will change the total Tresca stress component. However, the lowest stress possible is still the stress due to the internal pressure.

In Table 9.4 to 9.6 the results at some points in the pipe system have been presented in their respective axial stress component. The difference is calculated as the FSI result minus the result from the other method. The ratio is calculated as the difference with respect to the result from the other method.

Pipestress results due to the ADINA calculated load and FSI axial component results				
Point	Pipestress	FSI	Difference	Difference, %
Y005	69.14 MPa	50.19 MPa	−18.95 MPa	−27.4 %
Y009	89.37 MPa	75.11 MPa	−14.26 MPa	−16.0 %
Y013	103.36 MPa	69.52 MPa	−33.84 MPa	−32.7 %
Y018	101.83 MPa	58.25 MPa	−43.58 MPa	−42.8 %
Y021	104.97 MPa	76.13 MPa	−28.84 MPa	−27.5 %
Y026	67.51 MPa	57.00 MPa	−10.51 MPa	−15.6 %

Table 9.4: Pipestress results due to the ADINA calculated load and FSI axial component results

Mode Superposition results due to the ADINA calculated load and FSI axial component results				
Point	Mode Supo-erposition	FSI	Difference	Difference, %
Y005	50.78 MPa	50.19 MPa	−0.60 MPa	−1.2 %
Y009	64.79 MPa	75.11 MPa	10.32 MPa	15.9 %
Y013	78.01 MPa	69.52 MPa	−8.49 MPa	−10.9 %
Y018	65.48 MPa	58.25 MPa	−7.23 MPa	−11.0 %
Y021	78.56 MPa	76.13 MPa	−2.42 MPa	−3.1 %
Y026	52.16 MPa	57.00 MPa	4.84 MPa	9.3 %

Table 9.5: Mode Superposition results due to the ADINA calculated load and FSI axial component results

Direct Integration results due to the ADINA calculated load and FSI axial component results				
Point	Direct Integration	FSI	Difference	Difference, %
Y005	60.20 MPa	50.19 MPa	−10.02 MPa	−16.6 %
Y009	77.47 MPa	75.11 MPa	−2.36 MPa	−3.0 %
Y013	81.90 MPa	69.52 MPa	−12.38 MPa	−15.1 %
Y018	70.16 MPa	58.25 MPa	−11.91 MPa	−17.0 %
Y021	77.68 MPa	76.13 MPa	−1.55 MPa	−2.0 %
Y026	63.78 MPa	57.00 MPa	−6.78 MPa	−10.6 %

Table 9.6: Direct Integration results due to the ADINA calculated load and FSI axial component results

In Table 9.4 it is clear that the FSI simulation generates lower results than the Pipestress simulation, much like with the mode superposition method and the direct integration method, see Section 8.5.2. The FSI simulation also generates lower stresses than the other ADINA methods, keep in mind that the axial stress component due to internal pressure still contain the difference explained in the paragraph above, although only the axial part of it.

Chapter 10

Conclusion

10.1 Pressures

In order to get a better overview of the results the peak pressure at each of the measure points are presented in Table 10.1. The pressures are presented in MPa. In Figure 10.1 all three pressure curves at the same point are presented.

Code	Peak A	Peak B	Peak C	Peak D	Peak E	Peak F	Peak G
Relap	11.62	12.62	12.99	13.05	13.06	13.07	13.07
ADINA CFD	11.69	12.66	12.94	13.00	13.03	13.03	13.04
ADINA FSI	11.15	12.16	12.47	12.55	12.63	12.60	12.74

Table 10.1: Pressures

The difference of the pressure curves are not the main focus in this dissertation. However, they are an important part of the results since the force loads in the pipe system are derived directly from the pressure curves. As can be seen the ADINA CFD simulation generates lower pressure peaks from the second straight pipe section to the valve. The ADINA FSI simulation generates lower pressure peaks all through the pipe system. By looking at the pressure curves in Appendix A it is easy to see that the AD-

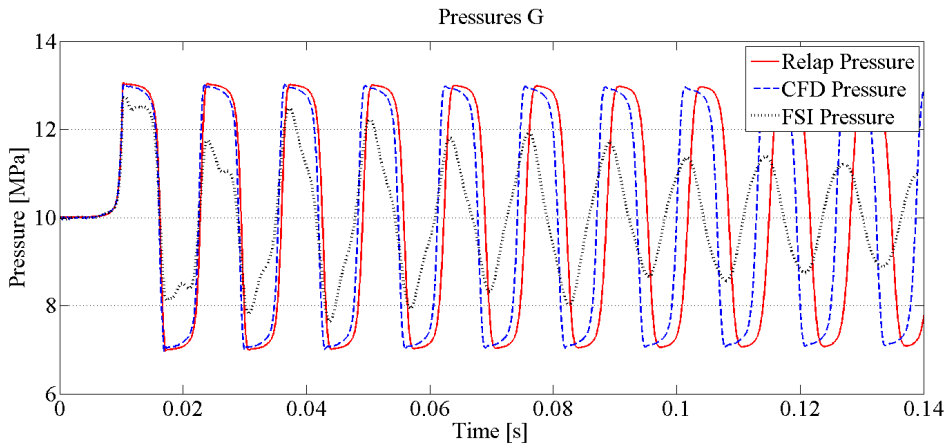

Figure 10.1: The pressure at point G of the pipe system

INA CFD and FSI calculated pressures have a slightly higher frequency than the Relap calculated pressures. The ADINA CFD pressure curves have the lowest dissipation rate while the ADINA FSI pressure curves have the highest dissipation rate.

10.2 Forces

In order to get a better overview of the results, the peak force at each of the measure points and the frequencies of the forces for each of the simulations are presented in Table 10.2. In Figure 10.2 the force curves at the same point are presented. The forces are presented in Newton (N).

Code	Pipe 1	Pipe 2	Pipe 3	Pipe 4	Pipe 5	Freq
Relap	14699	11647	11600	11850	11994	76 Hz
ADINA CFD	14729	11859	11826	11867	12358	78 Hz

Table 10.2: The force response due to Relap, ADINA CFD and ADINA FSI

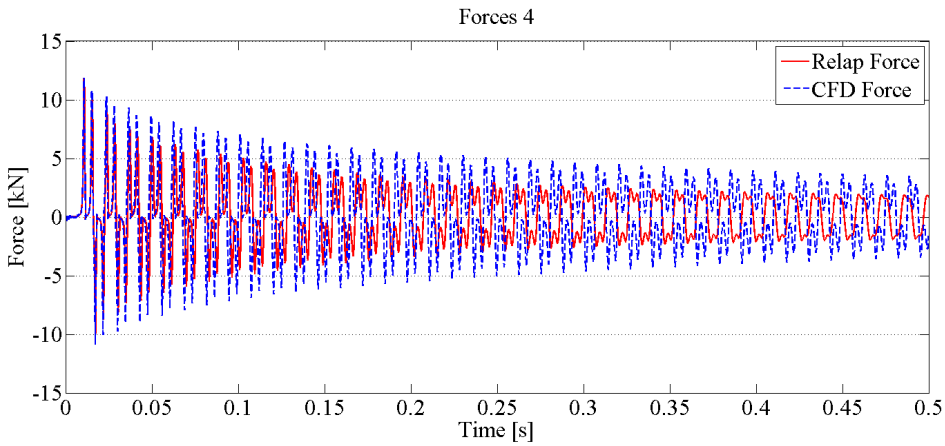

Figure 10.2: The force curve at the fourth straight pipe section

The ADINA CFD simulation generates a slightly higher force response than the Relap simulation. Much like the pressure curves, the frequencies of the different simulations vary. The ADINA CFD force frequency is higher than the Relap force. The dissipation rates of the force curves also follow the same pattern as the pressure curves, with the ADINA CFD force having the slowest dissipation rate and the Relap force having the fastest. All force curves are presented in Appendix B.

10.3 Stresses

In Table 10.3 the stress results from the different simulations are presented. The measure points are the same as presented in previous Chapters in this report. Only the simulation combinations that are of interested are presented. As stated in Section 9.2 the simulations using the ADINA CFD calculated loads generates lower stresses in the pipe system. As stated in Section 8.5.2 the stress needed for evaluation of the pipe system when analysing it using FEM is the Tresca stress. For Pipestress the stress is calculated according to Equation (7.5). These two different ways of calculating the stress results do not contain the same components, but since they, according to the ASME code [3], are to be evaluated against the same criteria we still compare them to each other.

Code	Y005	Y009	Y013	Y018	Y021	Y026
Relap and Pipestress	69.72	91.05	106.98	105.01	107.00	67.18
ADINA Mode Superposition and CFD	85.85	88.68	101.53	100.58	88.99	86.67
ADINA Direct Integration and CFD	85.78	88.54	101.78	101.41	88.91	86.62
ADINA FSI	98.28	107.20	107.05	108.44	109.48	106.00

Table 10.3: Comparison of stress components due to different simulation combinations

Since the values presented in Table 10.3 are a couple of sample points, the rest of the values are presented in Appendix D, Table D.1 - D.3. It's clear to see that the FSI simulation generates higher stresses in the pipe system than the other methods. As was argued in Section 9.2.2, since we are interested in the peak stresses and the FSI simulation is the only method where the internal pressure changes over time the maximum stresses due to the internal pressure will be higher using the FSI method and thus generating higher stresses in the pipe system. At about one third of the points, the Relap and Pipestress method generates lower stresses in the

pipe system compared to the ADINA FEM and CFD methods.

In Section 9.2.2 it was argued that the different methods don't calculate the same stress components. In Table 10.4 the axial stress results from the different simulations are presented. The measure points are the same as in Table 10.3. The results at the rest of the measure points are presented in Appendix D, Table D.4 - D.6, the Pipestress stress results are presented in D.1.

Code	Y005	Y009	Y013	Y018	Y021	Y026
Relap and Pipestress	69.72	91.05	106.98	105.01	107.00	67.18
ADINA Mode Superposition and CFD	50.78	64.79	78.01	65.48	78.56	52.16
ADINA Direct Integration and CFD	60.20	77.47	81.90	70.16	77.68	63.78
ADINA FSI	50.19	75.11	69.52	58.25	76.13	57.00

Table 10.4: Comparison of axial stress components due to different simulation combinations

The axial stress components are being compared in order to decide whether or not the Relap - Pipestress method is conservative. The stresses generated by Pipestress are higher than those generated by any of the other methods. The FSI simulation still contains the axial stress component from the higher internal pressure.

In conclusion, the Relap - Pipestress method is conservative, as can be seen in Table 10.4. It is not fully possible to determine if the fully coupled FSI simulation is appropriate to use as an additional tool in evaluating the pipe system. The increased pressure caused by the fact that the internal pressure changes over time causes higher stresses in the pipe when compared to the other methods. As can be seen in Table 10.4 the FSI simulation calculates lower stresses when the contributions from the internal pressure is reduced. It would be interesting to do the other simulations using the same peak pressure in each pipe section as the pipe in the FSI simulation is subjected to. The more refined CFD and FEM methods

might be an option as an additional tool in evaluating loads and stresses in a pipe system. However, from the results in this dissertation it is not really possible to determine to what extent.

10.4 Source of error

In Section 2.3 some assumptions were presented. Some of these might directly or indirectly be a source of some deviations in the solutions. In real life there are no such things as a fix point. Both the tanks and the pipe supports are modeled as completely fixed in the ADINA FEM models when they in fact should have some kind of stiffness. This results in numerical concentrations of the stresses in these points. It also results in increased stresses in the vicinity of the fix points. If the stiffness is included in the simulation the stresses in the vicinity will not increase as much.

In Pipestress only the beginning and the end of a pipe bend is simulated using a stress index. In a FEM simulation, the entire pipe bend is calculated and the increased stresses will affect the pipe in the vicinity of the bend.

10.5 Future work

There are different ways to continue the work in this Master's dissertation. The assumptions presented in Section 2.3 shows some of the problems that would be interesting to examine. One problem that was encountered was the long cpu time. Even though the number of cells wasn't that high the cpu time was too long to be of any commercial use. Different codes like Star CCM+ and Abaqus might increase the performance and togheter with a better calculation hardware setup the time needed might be decreased.

The contribution to the stress from the internal pressure was high. Redoing the simulations using lower internal pressure would be very interesting. The chosen pressure is reasonable in regards to what the nuclear power plants are subjected to but the effect of the refined simulations are somewhat concealed because of it. The results from this dissertation also contributes to the ongoing discussion within the nuclear industry, whether or not the maximum or the avarage pressure should be used in the simulations.

It would also be of interest to model the pipe using shell elements rather than a full 3D solid model. To model the pipe supports, either with springs simulating the stiffness or model the support which will give the stiffness within the model. A special examination of the pipe bends would also be interesting.

Bibliography

[1] A.G.T.J. Heinsbroek, "Fluid-structure interaction in non-rigid pipeline systems", Nuclear Engineering and Design, vol. 172, no. 1-2, p. 123-135, July 1997.

[2] A.S. Tijsseling, A.E. Vardy and D. Fan, "Fluid-Structure Interaction and cavitation in a Single-Elbow pipe system", Journal of Fluids and Structures, vol. 10, no. 4, p. 395-420, May 1996.

[3] The American Society of Mechanical Engineers, "2007 ASME Boiler & Pressure Vessel Code", Section III NB, July 1, 2007.

[4] "Water - Thermal Properties", The Engineering ToolBox, [Online]: http://www.engineeringtoolbox.com/water-thermal-properties-d_162.html
[November 2011]

[5] "Water - Speed of Sound", The Engineering ToolBox, [Online]: http://www.engineeringtoolbox.com/sound-speed-water-d_598.html
[November 2011]

[6] Swedish Standards Institute, Stainless steels Part 1: List of stainless steels, SS-EN 10088-1:2005, edition 2, October 2005.

[7] ADINA R&D, Inc. "ADINA Theory and Modeling Guide", Volume III: ADINA CFD & FSI, Report ARD 10-9, June 2010.

[8] Dr C. Greenough, Rutherford Appleton Laboratory "The Finite Element Library", Release 4.0, Level 1 User Documentation, September 20, 2001.

http://www.softeng.rl.ac.uk/st/projects/felib4/Docs/html/Intro/doc-intro.pdf
[September 2012]

[9] J. Donea, Antonio Huerta, J.-Ph. Ponthot and A. Rodrguez-Ferran, "Arbitrary Lagrangian-Eulerian Methods", vol. 1, chapter 14. http://eu.wiley.com/legacy/wileychi/ecm/pdfs/Volume_1_Chapter_14.pdf
[September 2012]

[10] The RELAP5 Code Development Team, U. S. Nuclear Regulatory Commission (NRC), "RELAP5/MOD3 CODE MANUAL, VOLUME I: CODE STRUCTURE, SYSTEM MODELS, AND SOLUTION METHODS", Idaho, June 1995. http://www.edasolutions.com/old/RELAP5/manuals/rv1.pdf
[September 2012]

[11] THCentral, "RELAP5", Thermal-Hydraulics, [Online]: http://www.thcentral.com/relap5.htm
[September 2012]

[12] Paul Scherrer Institute, "RELAP5", Thermal-hydraulic Research for Reactor Safety, [Online]: http://lth.web.psi.ch/codes/RELAP5.htm
[September 2012]

[13] DST Computer Services SA, "Pipestress User's Manual", Version 3.6.2, September 2009.

[14] ADINA R&D, Inc. "ADINA Theory and Modeling Guide", Volume I: ADINA, Report ARD 10-7, June 2010.

[15] "Reynolds Number", The Engineering ToolBox, [Online]: http://www.engineeringtoolbox.com/reynolds-number-d_237.html
[September 2012]

[16] The American Society of Mechanical Engineers, "2007 ASME Boiler & Pressure Vessel Code", Section II Part D, July 1, 2007.

[17] Bengt Sundström, "Handbok och formelsamling i Hållfasthetslära", Institutionen för hållfasthetslära KTH, 2005.

Appendix A

Pressures

In this appendix all the pressure curves from the different simulations are presented. In Figure A.1 all the points in the fluid where the different pressure curves are extracted from are presented. The pressure is extracted by taking the average pressure over the cross section at the points. The pressure curves are divided into different sections depending on which simulation they originate from.

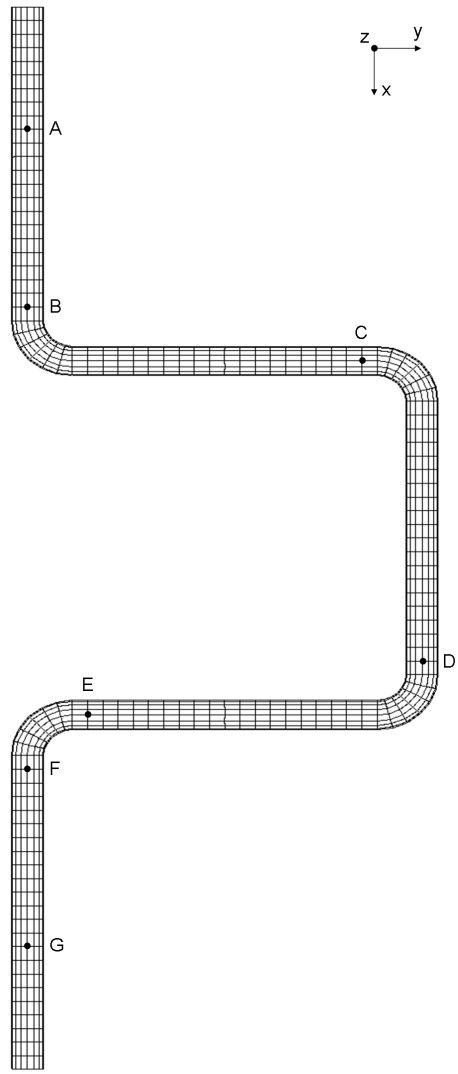

Figure A.1: Fluid node placement

A.1 Relap pressure curves

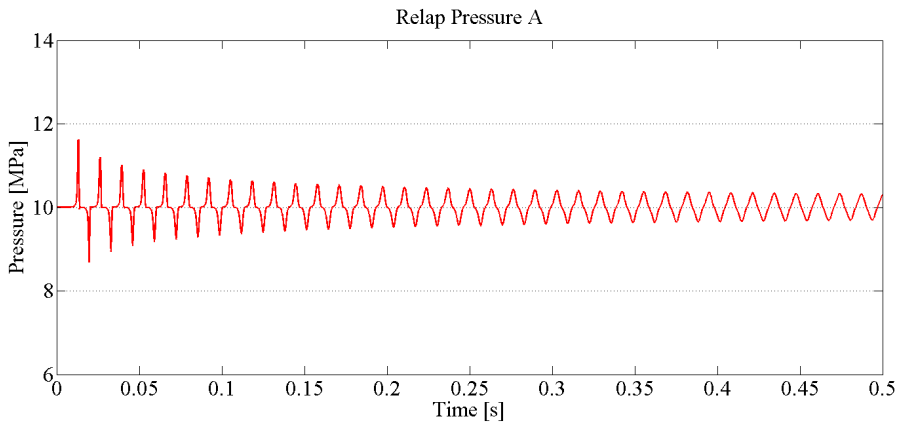

Figure A.2: Relap pressure curve at point A

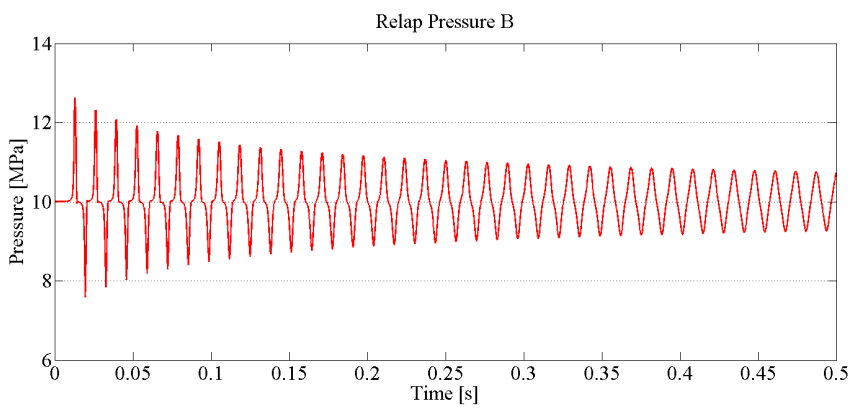

Figure A.3: Relap pressure curve at point B

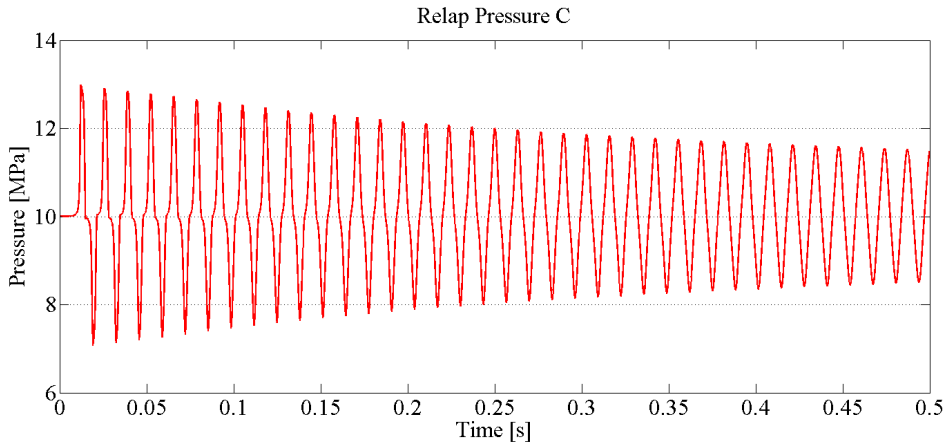

Figure A.4: Relap pressure curve at point C

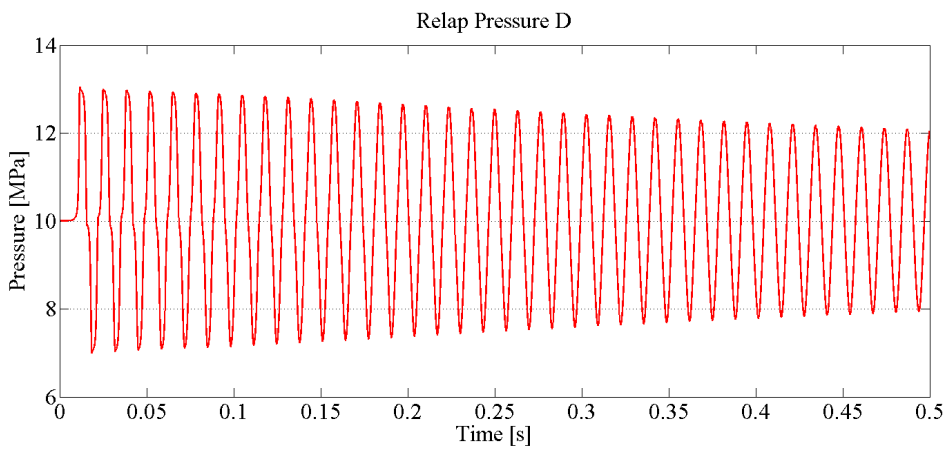

Figure A.5: Relap pressure curve at point D

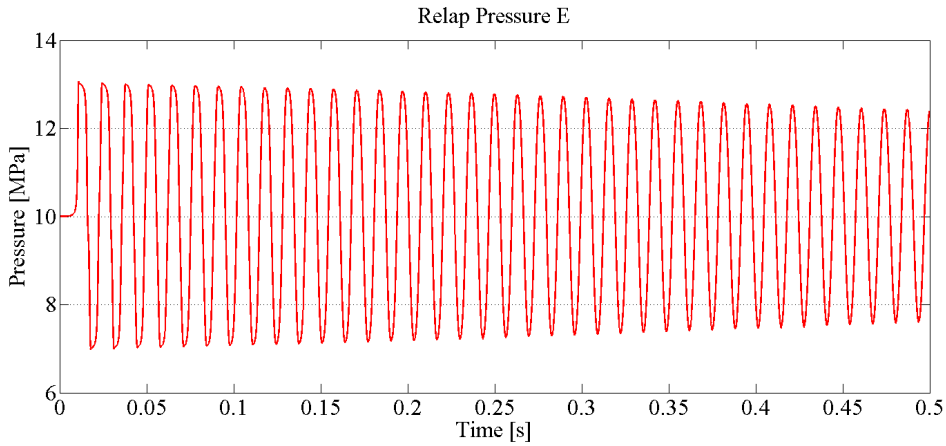

Figure A.6: Relap pressure curve at point E

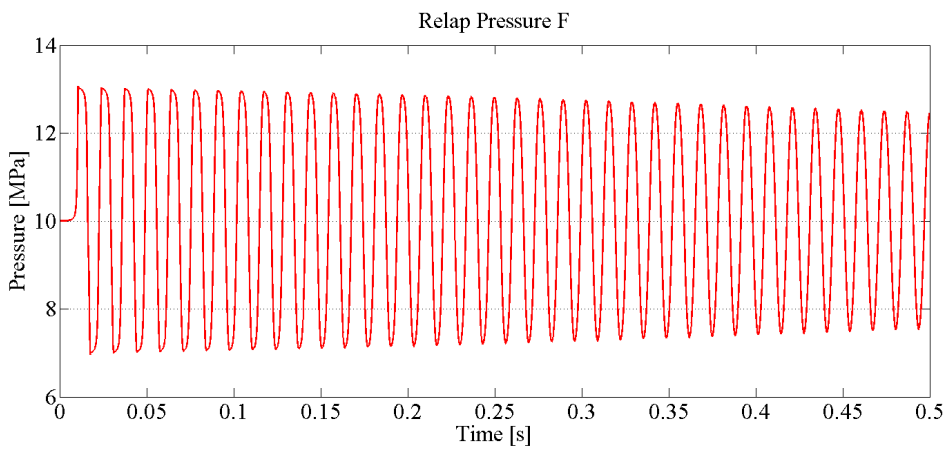

Figure A.7: Relap pressure curve at point F

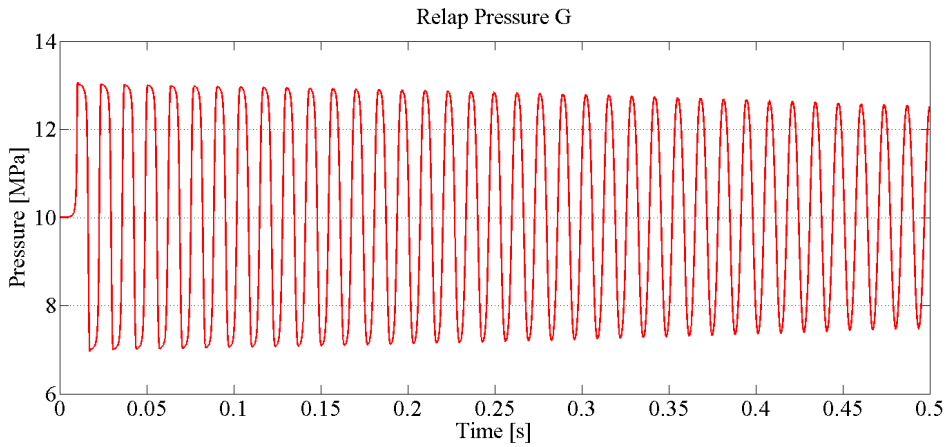

Figure A.8: Relap pressure curve at point G

A.2 ADINA pressure curves

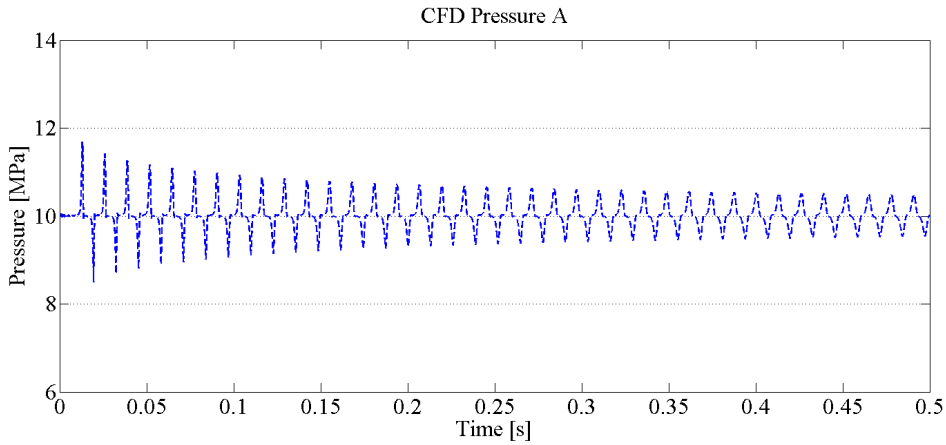

Figure A.9: ADINA Fluid pressure curve at point A

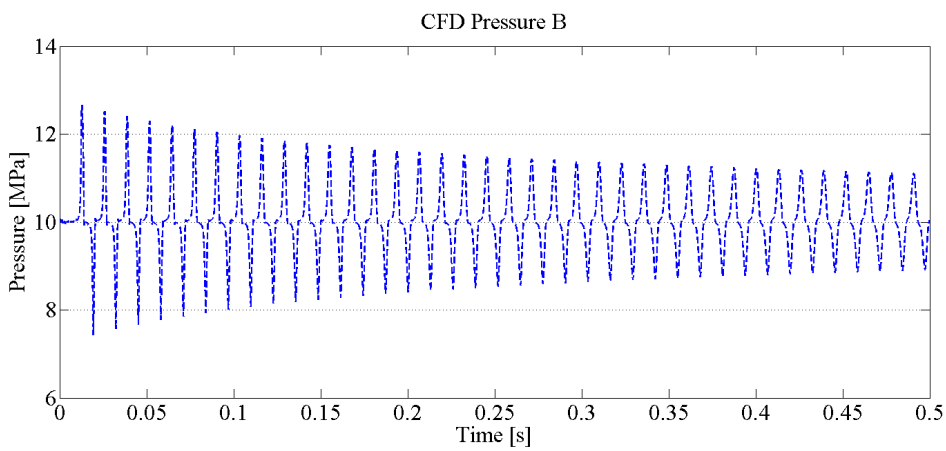

Figure A.10: ADINA Fluid pressure curve at point B

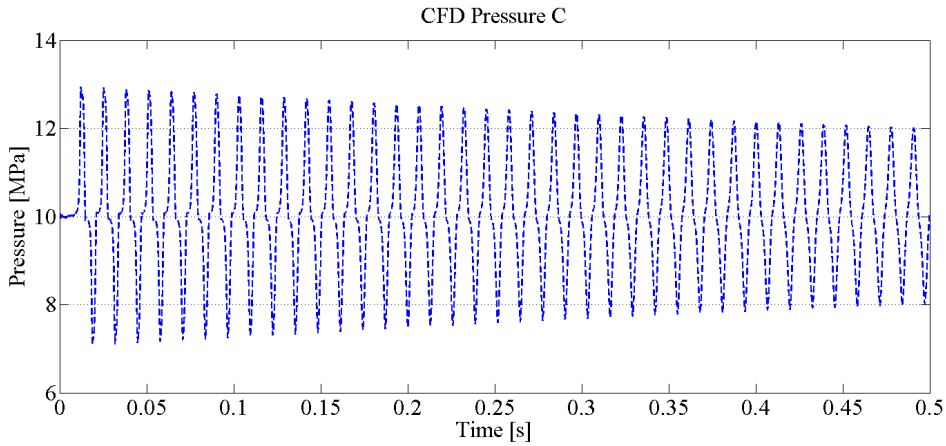

Figure A.11: ADINA Fluid pressure curve at point C

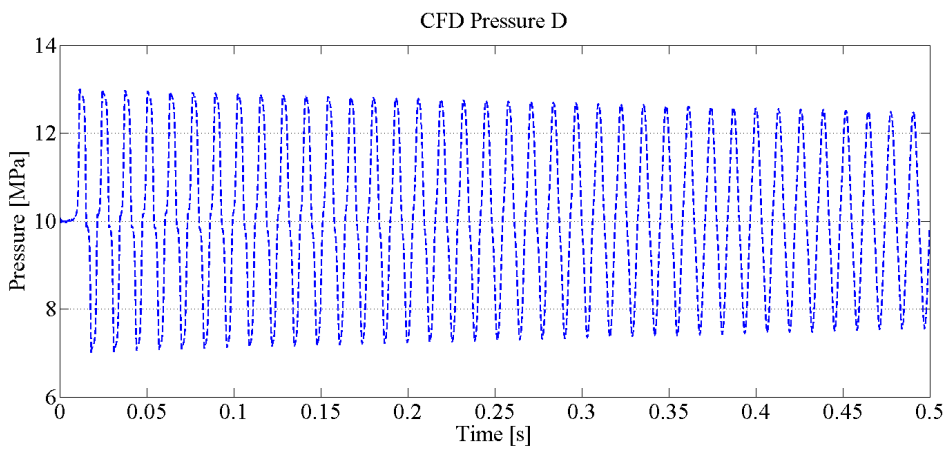

Figure A.12: ADINA Fluid pressure curve at point D

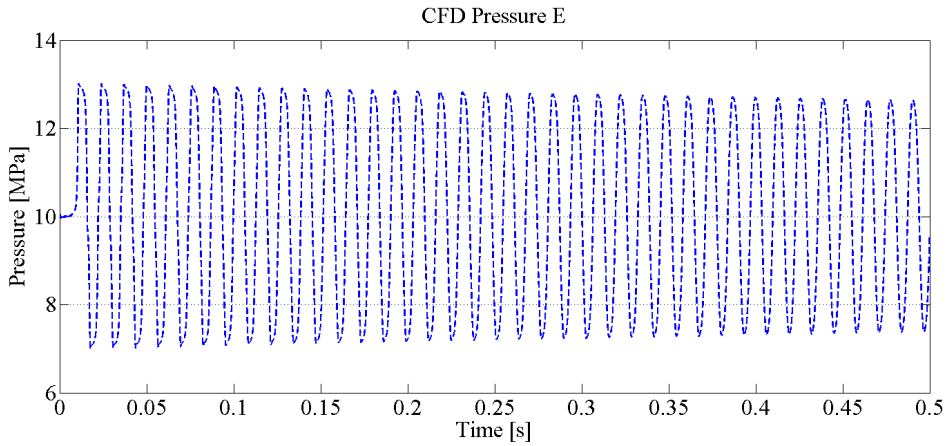

Figure A.13: ADINA Fluid pressure curve at point E

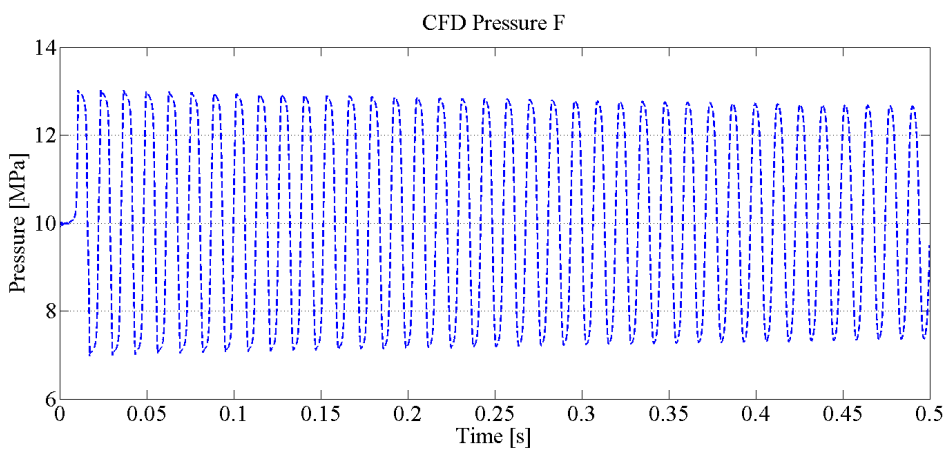

Figure A.14: ADINA Fluid pressure curve at point F

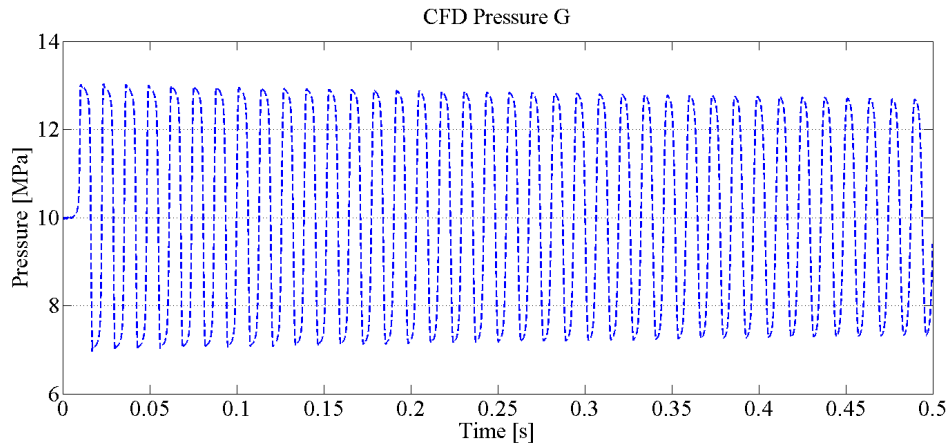

Figure A.15: ADINA Fluid pressure curve at point G

A.3 FSI pressure curves

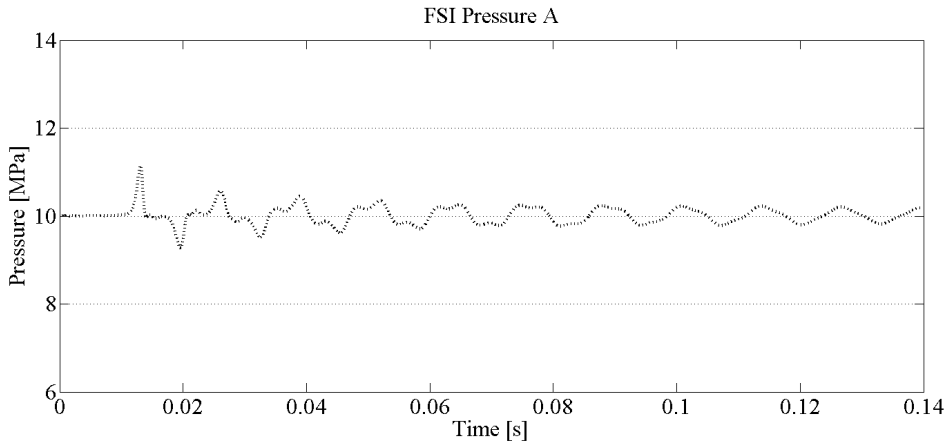

Figure A.16: ADINA FSI pressure curve at point A

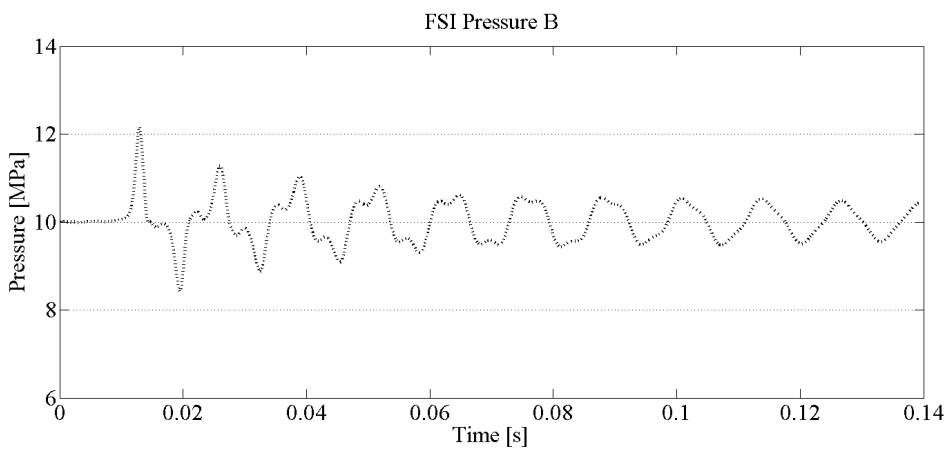

Figure A.17: ADINA FSI pressure curve at point B

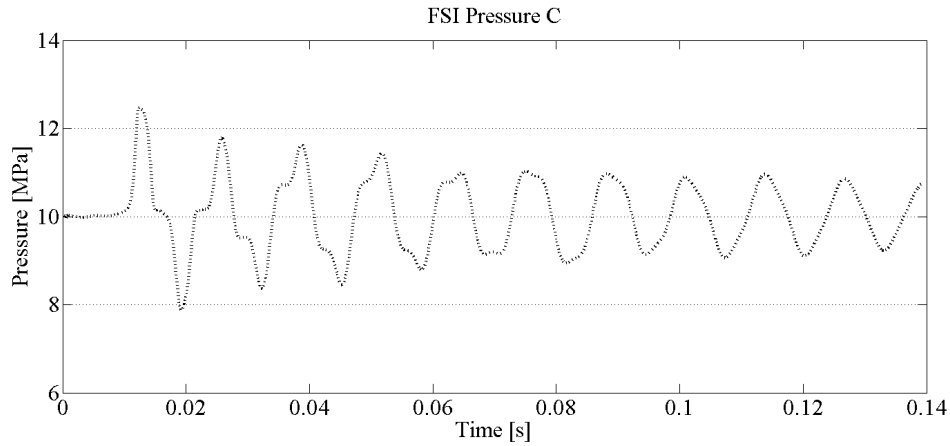

Figure A.18: ADINA FSI pressure curve at point C

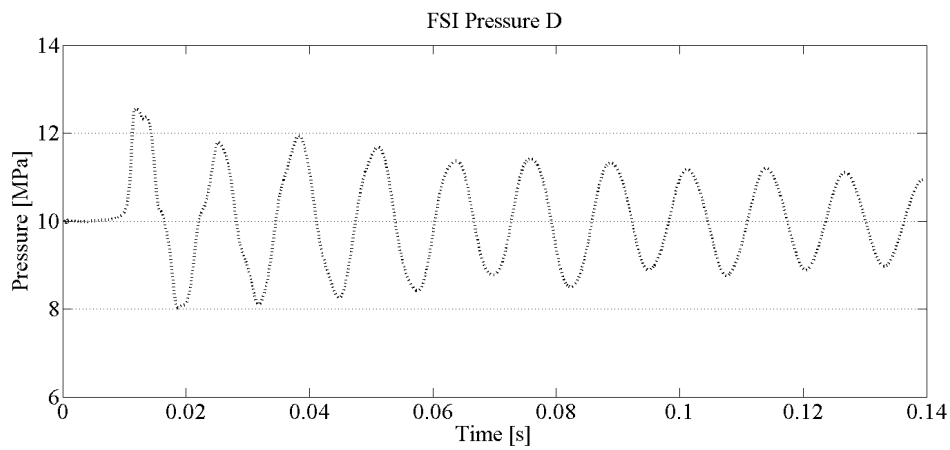

Figure A.19: ADINA FSI pressure curve at point D

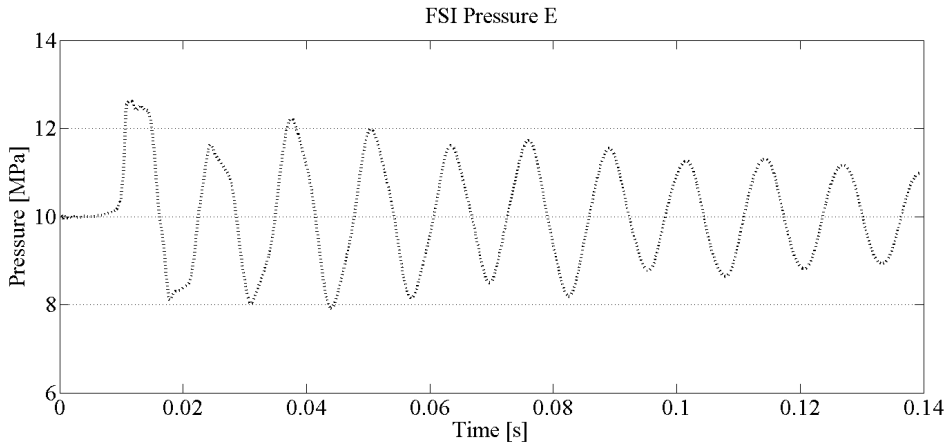

Figure A.20: ADINA FSI pressure curve at point E

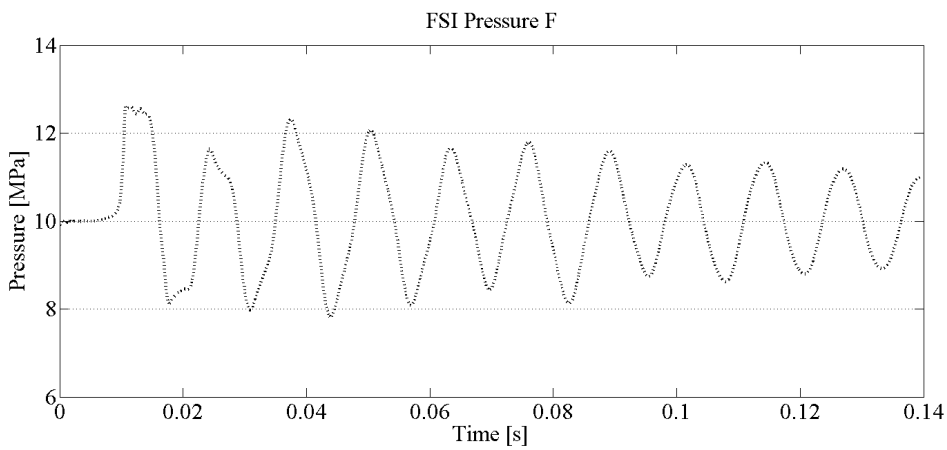

Figure A.21: ADINA FSI pressure curve at point F

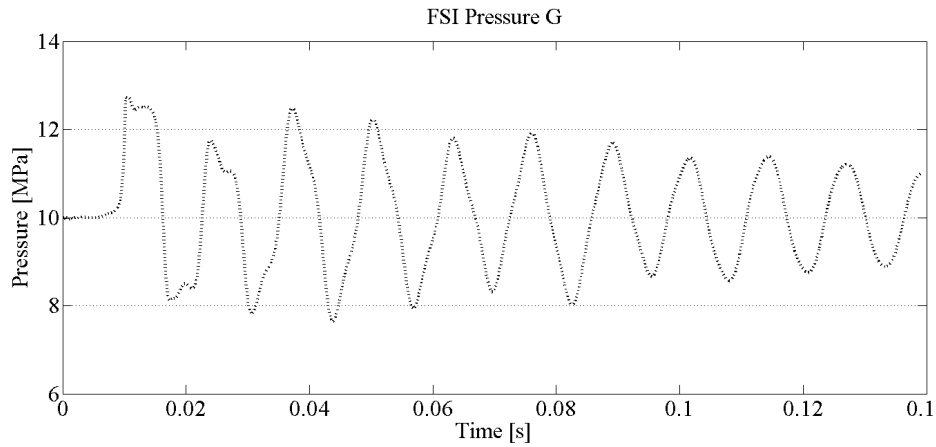

Figure A.22: ADINA FSI pressure curve at point G

A.4 Combined pressure curves

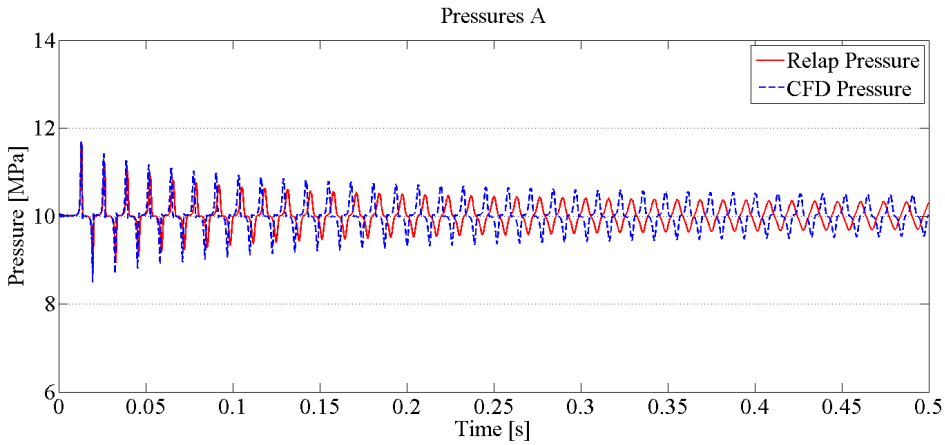

Figure A.23: Relap and AFINA CFD pressure curve at point A

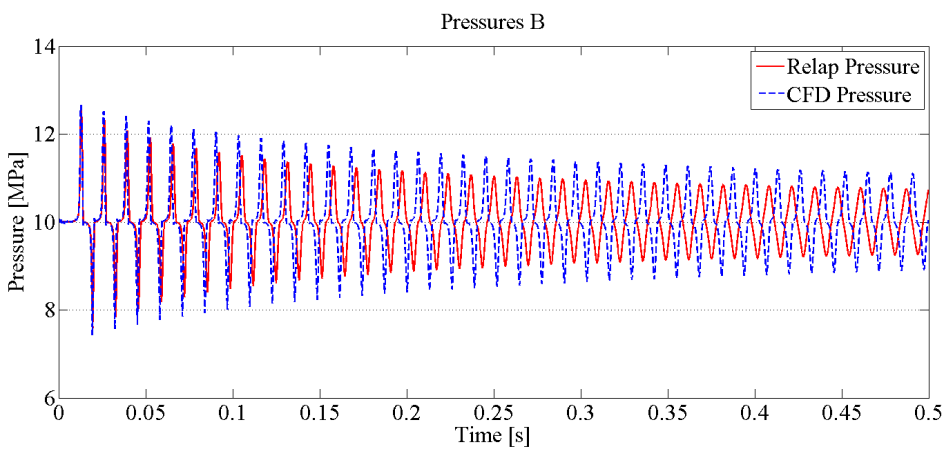

Figure A.24: Relap and AFINA CFD pressure curve at point B

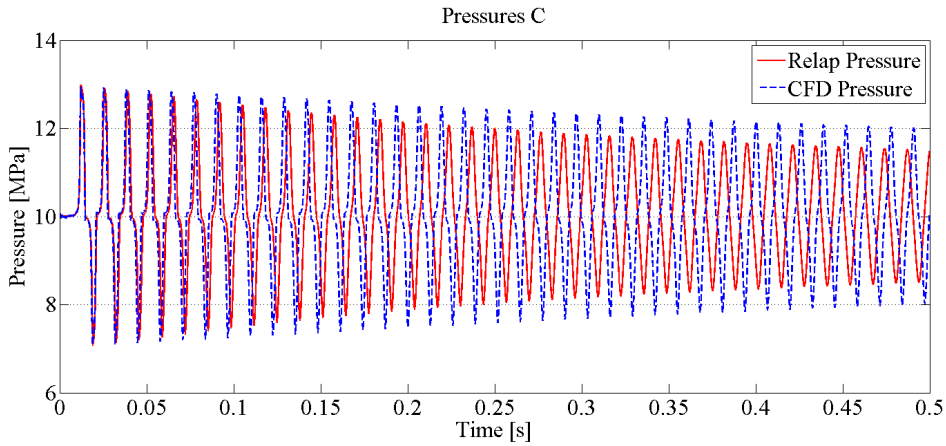

Figure A.25: Relap and AFINA CFD pressure curve at point C

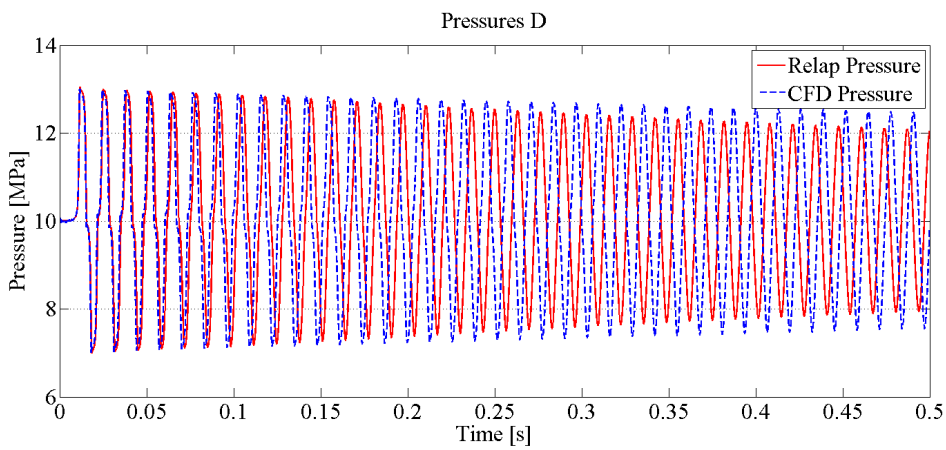

Figure A.26: Relap and AFINA CFD pressure curve at point D

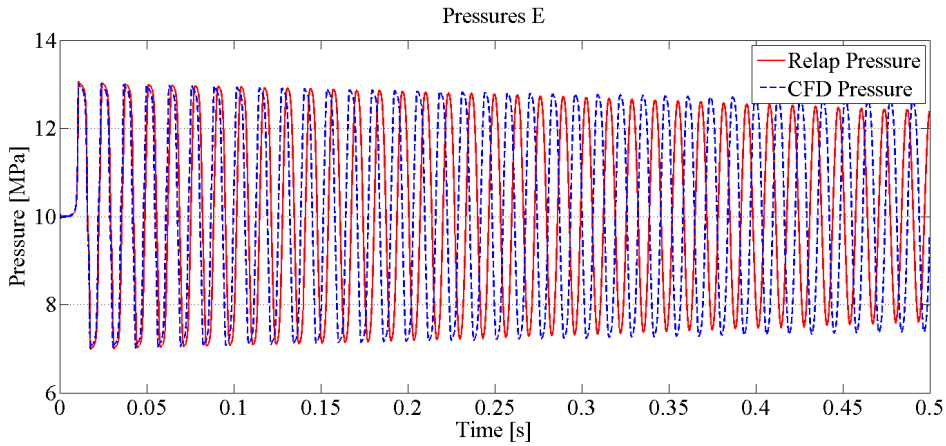

Figure A.27: Relap and AFINA CFD pressure curve at point E

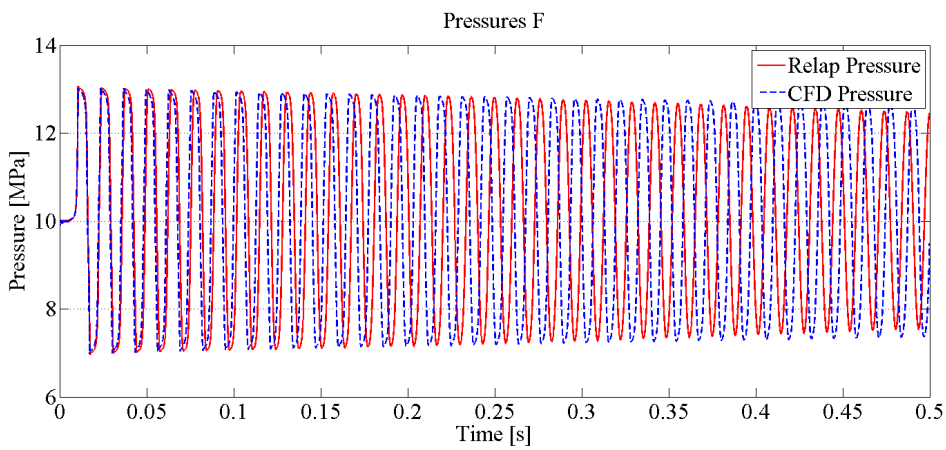

Figure A.28: Relap and AFINA CFD pressure curve at point F

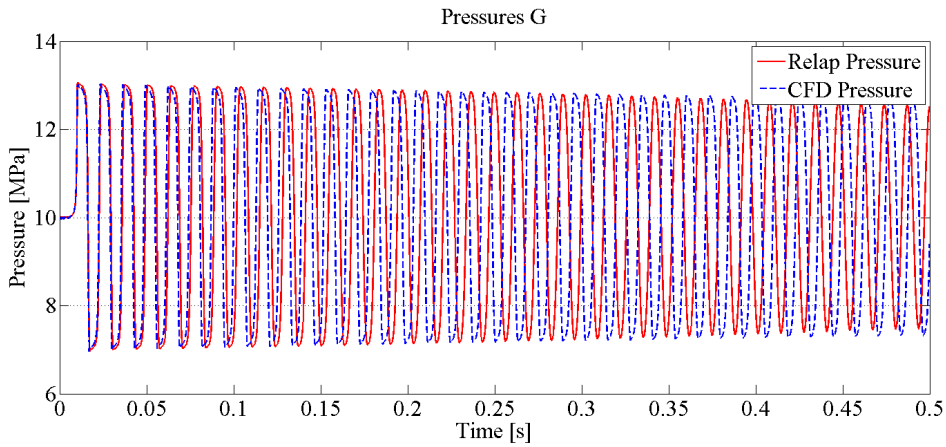

Figure A.29: Relap and AFINA CFD pressure curve at point G

A.5 Combined pressure curves - FSI

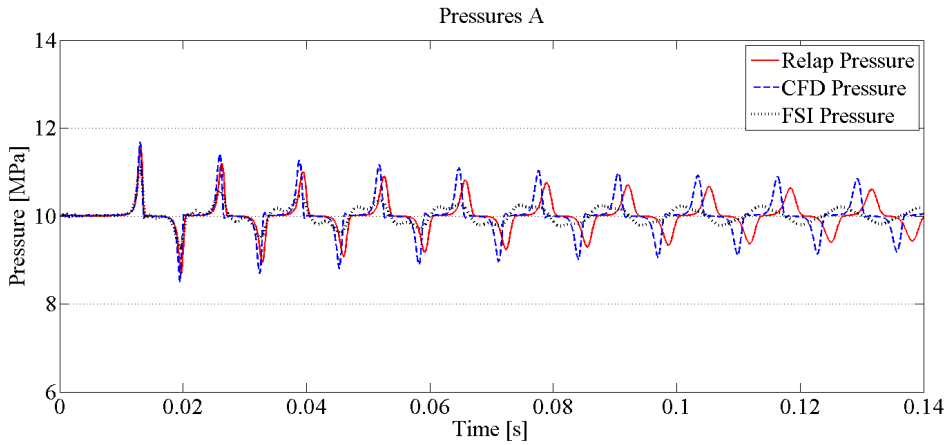

Figure A.30: Relap, ADINA Fluid and ADINA FSI pressure curve at point A

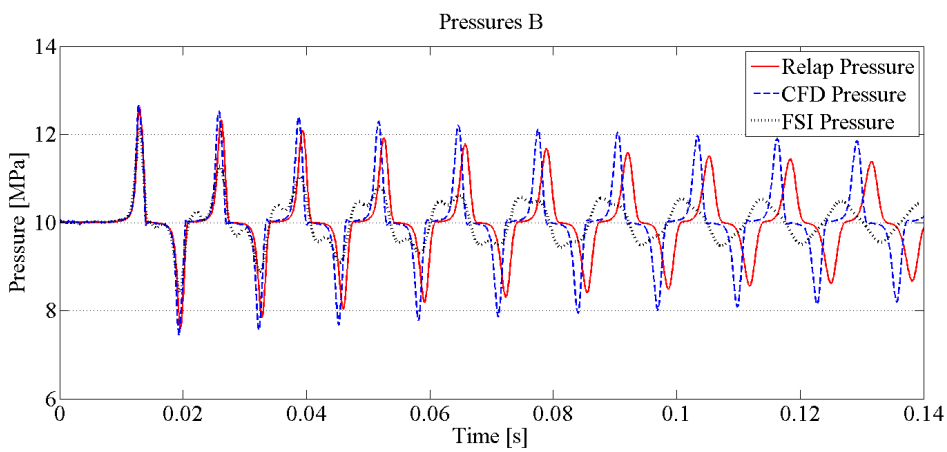

Figure A.31: Relap, ADINA Fluid and ADINA FSI pressure curve at point B

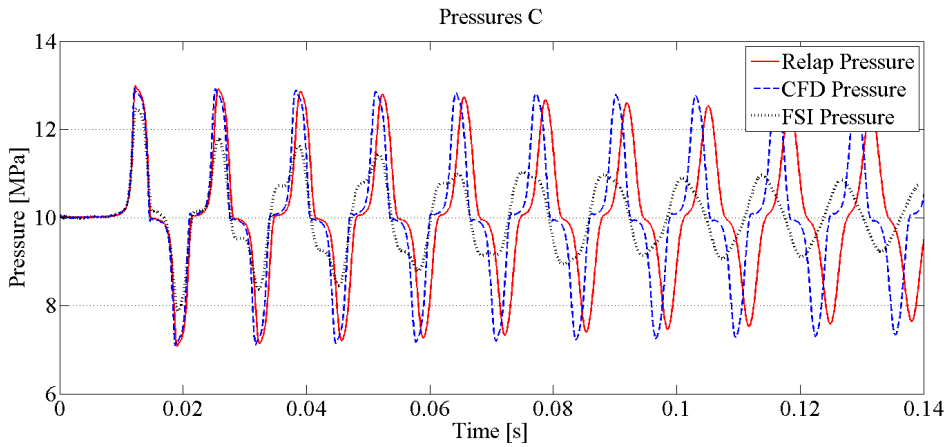

Figure A.32: Relap, ADINA Fluid and ADINA FSI pressure curve at point C

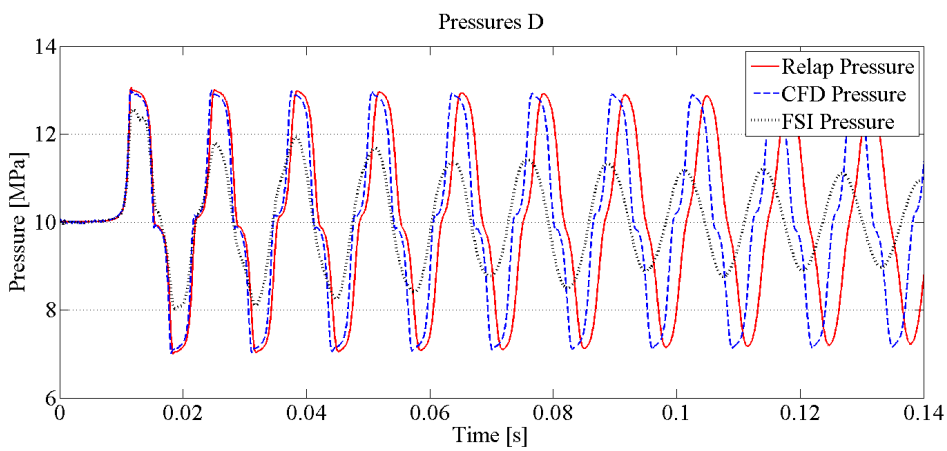

Figure A.33: Relap, ADINA Fluid and ADINA FSI pressure curve at point D

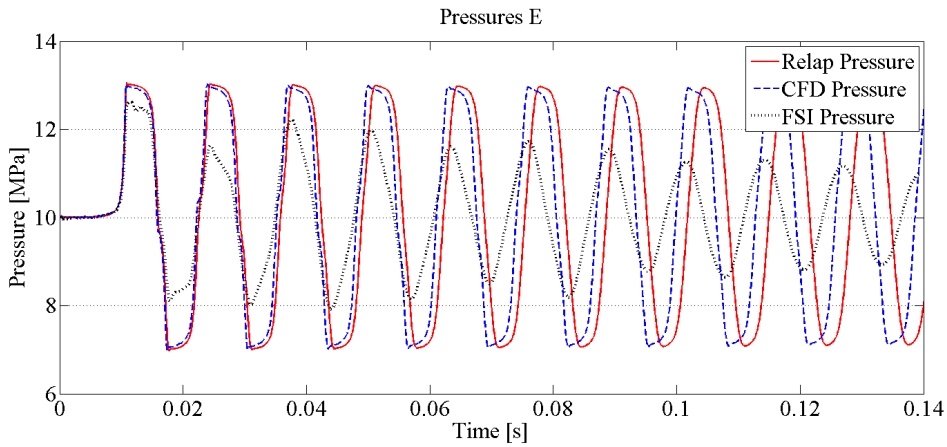

Figure A.34: Relap, ADINA Fluid and ADINA FSI pressure curve at point E

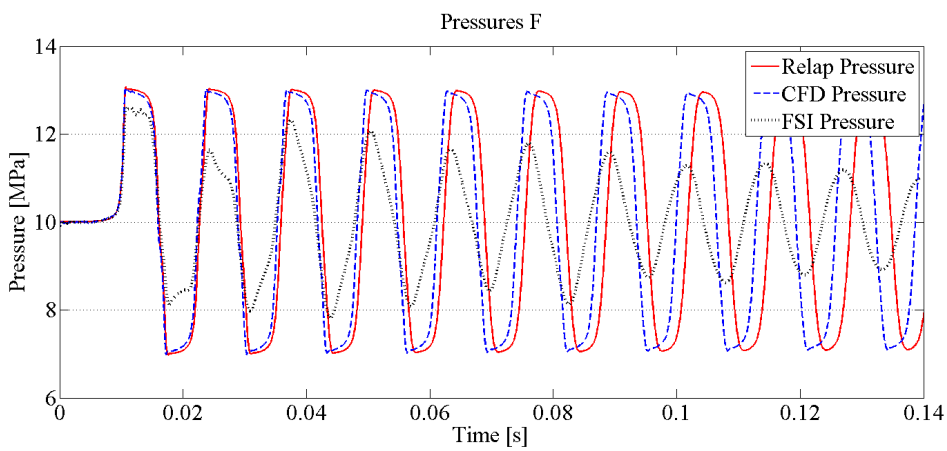

Figure A.35: Relap, ADINA Fluid and ADINA FSI pressure curve at point F

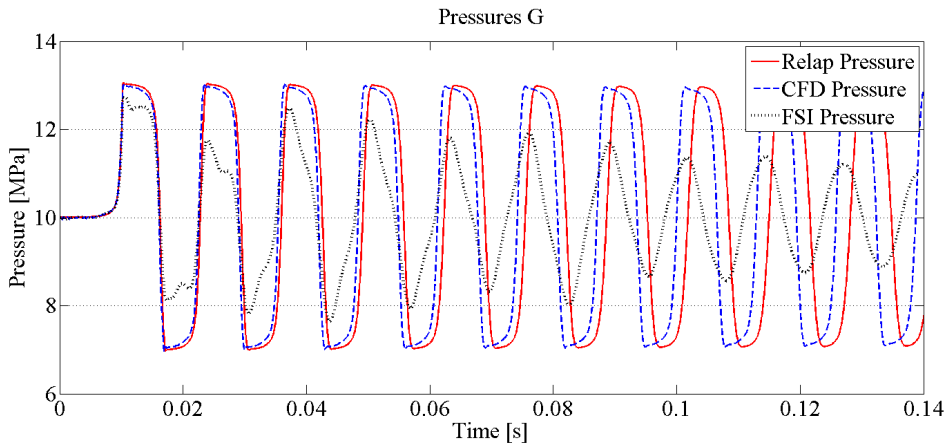

Figure A.36: Relap, ADINA Fluid and ADINA FSI pressure curve at point G

Appendix B

Forces

In this appendix all the force responses are presented. All force responses are divided into different pipe sections, section 1 to 5. In Figure B.1 these different sections are presented. If the force has a positive sign it means it goes in either the positive X- or Y-direction, depending on the orientation of that particular section. The force responses are divided into different sections depending on which simulation they originate from.

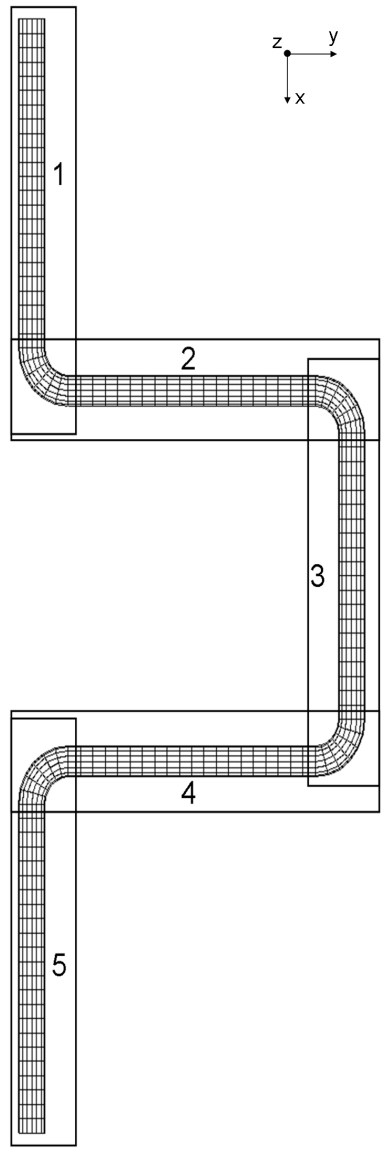

Figure B.1: Fluid divided into pipe sections

B.1 Relap force curves

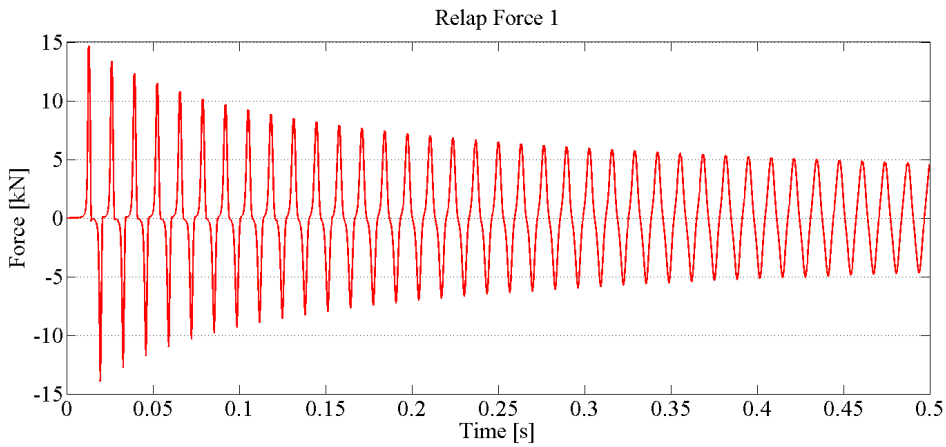

Figure B.2: Relap calculated force in the first pipe section

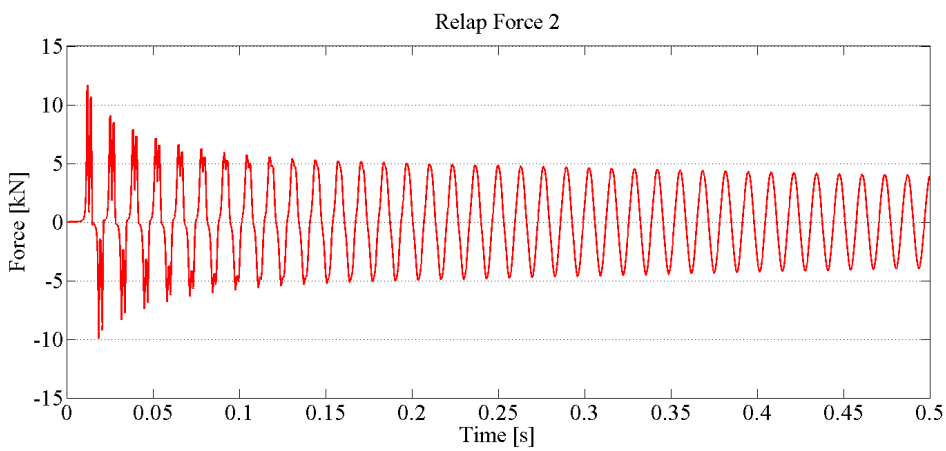

Figure B.3: Relap calculated force in the second pipe section

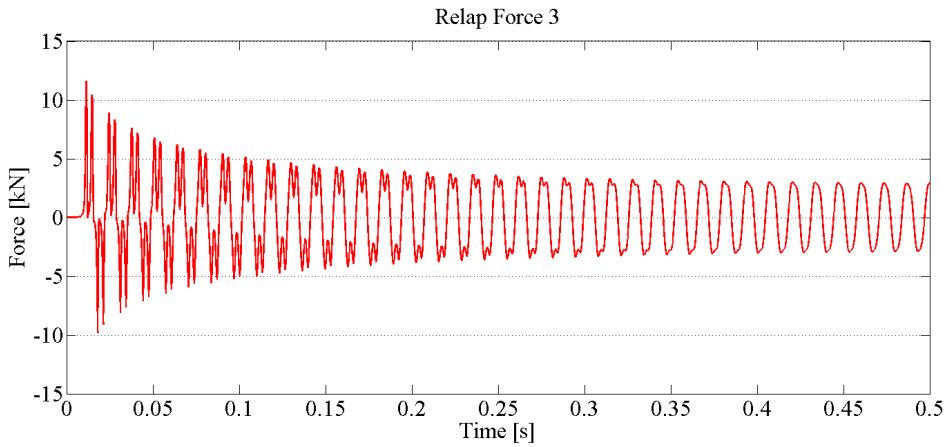

Figure B.4: Relap calculated force in the third pipe section

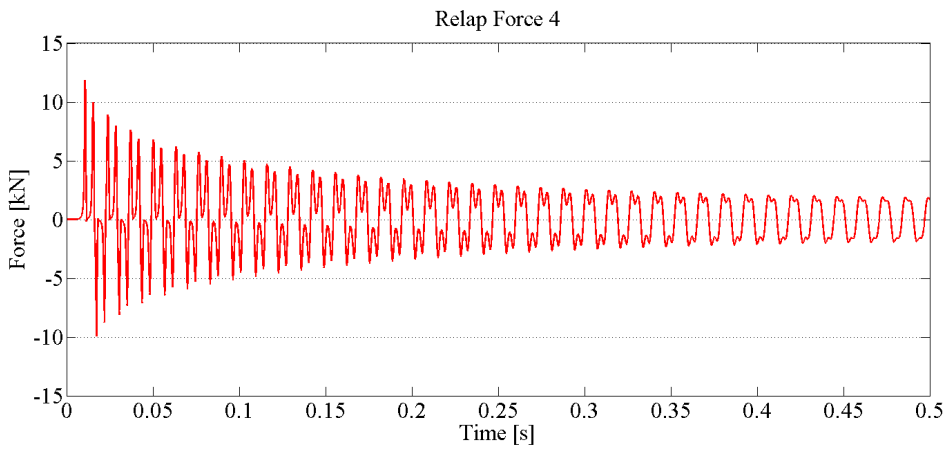

Figure B.5: Relap calculated force in the fourth pipe section

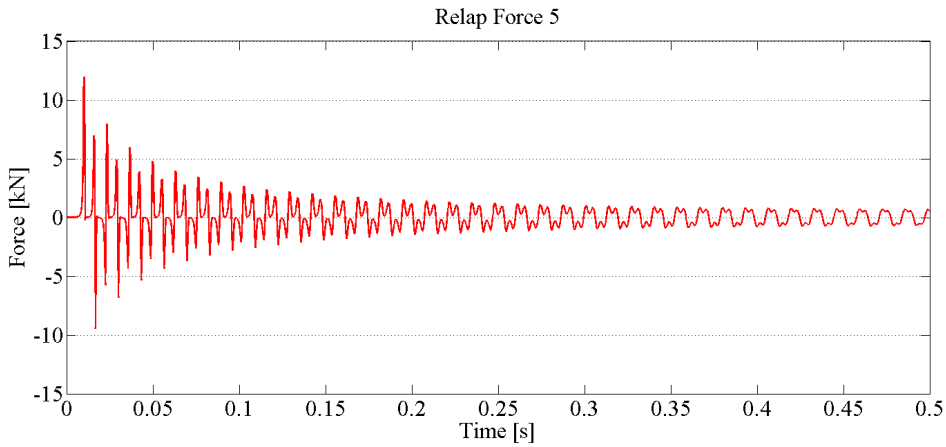

Figure B.6: Relap calculated force in the fifth pipe section

B.2 ADINA force curves

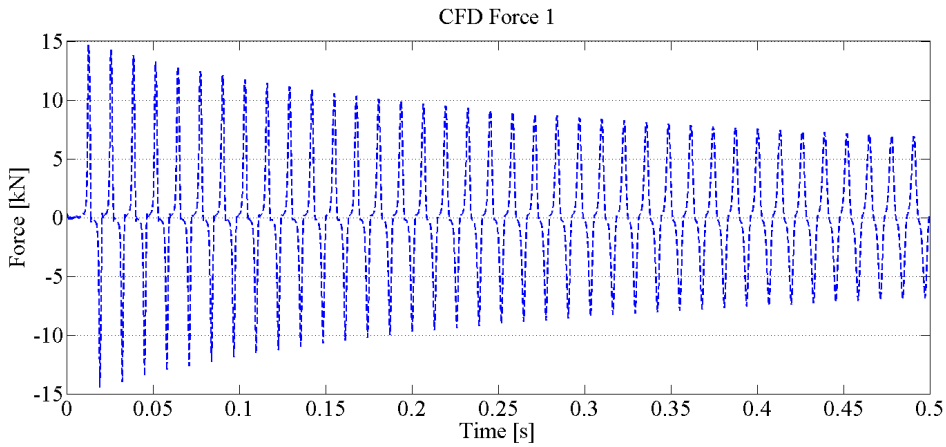

Figure B.7: ADINA Fluid calculated force in the first pipe section

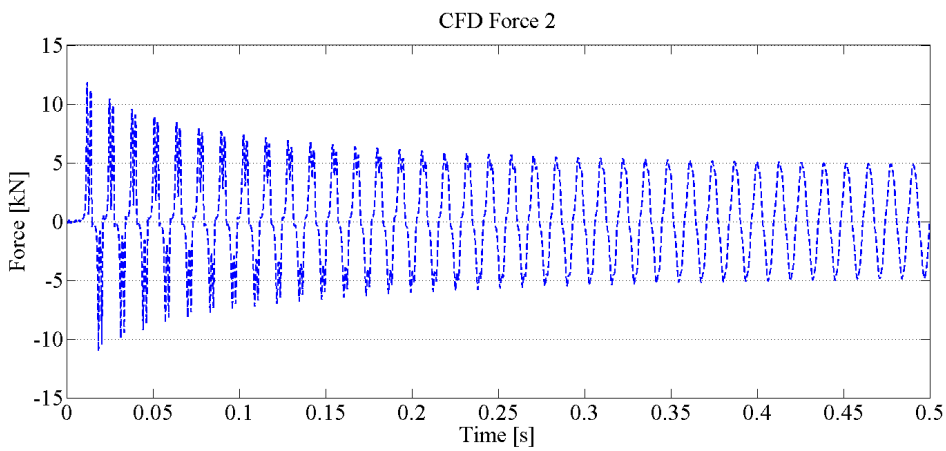

Figure B.8: ADINA Fluid calculated force in the second pipe section

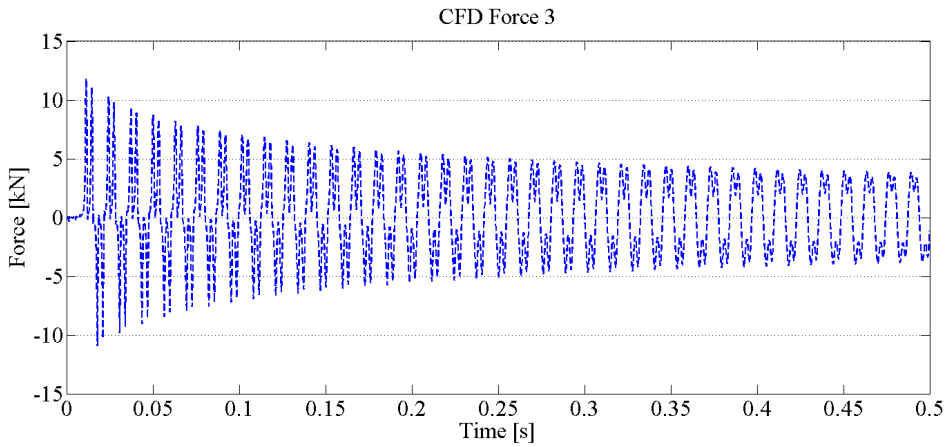

Figure B.9: ADINA Fluid calculated force in the third pipe section

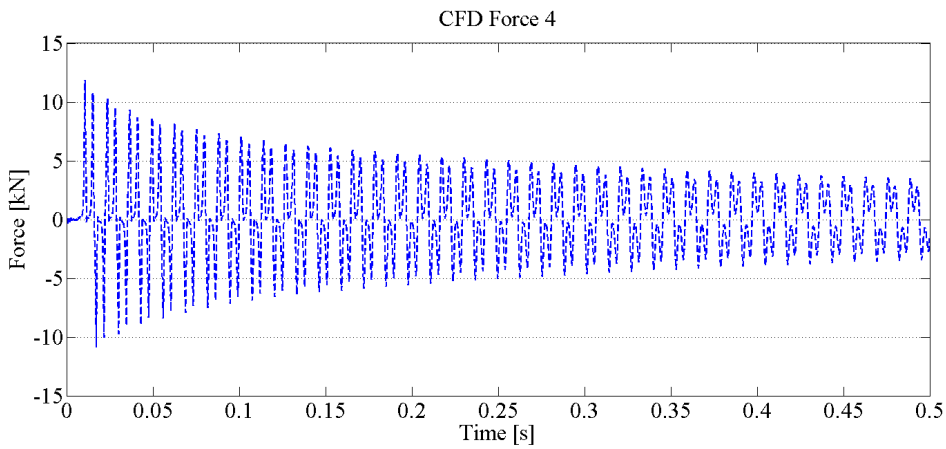

Figure B.10: ADINA Fluid calculated force in the fourth pipe section

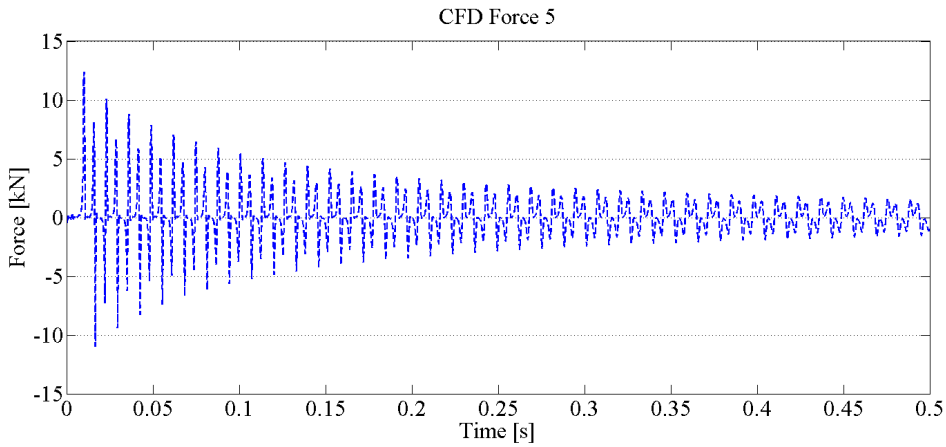

Figure B.11: ADINA Fluid calculated force in the fifth pipe section

B.3 Combined force curves

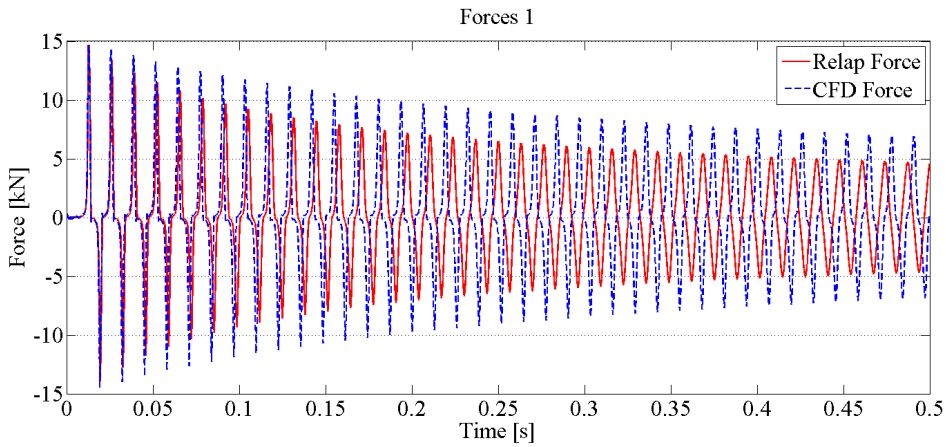

Figure B.12: Relap and AFINA CFD calculated force in the first pipe section

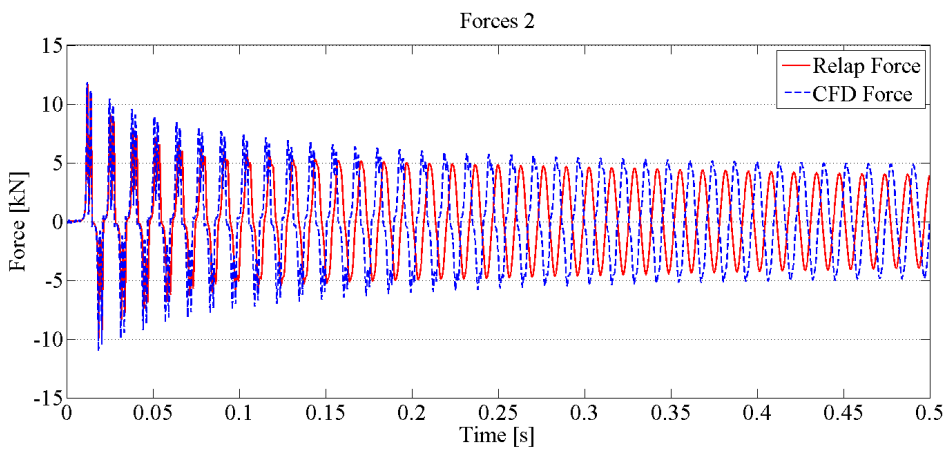

Figure B.13: Relap and AFINA CFD calculated force in the second pipe section

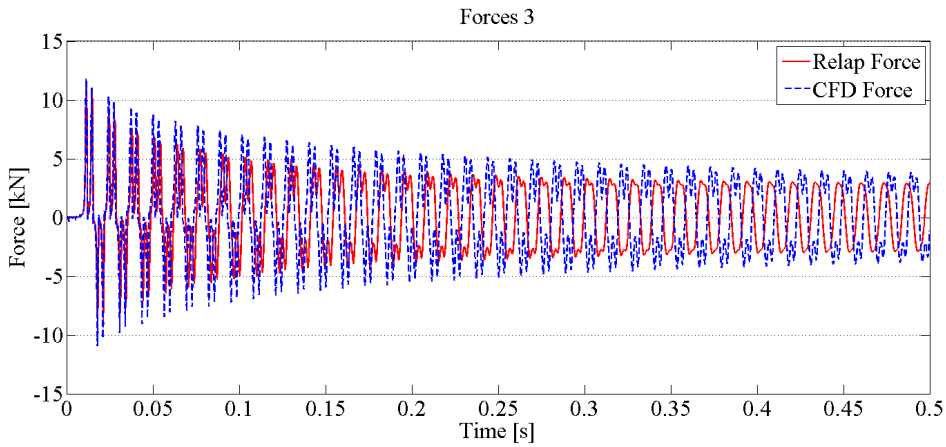

Figure B.14: Relap and AFINA CFD calculated force in the third pipe section

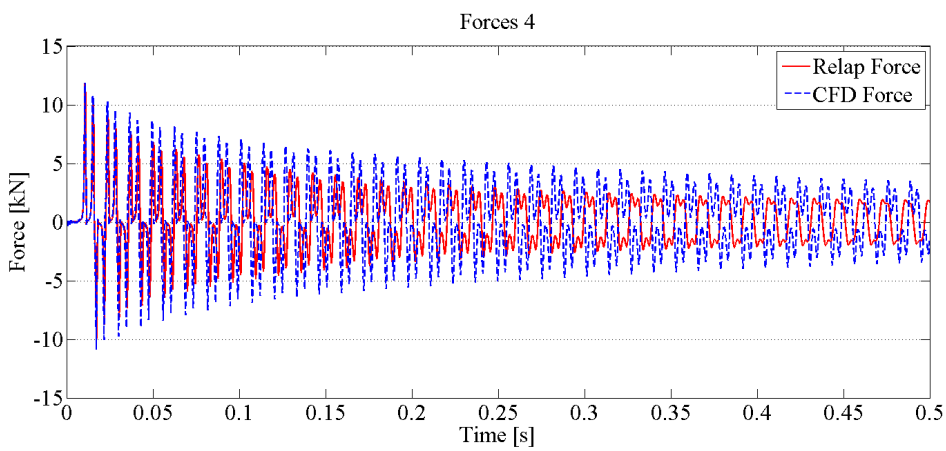

Figure B.15: Relap and AFINA CFD calculated force in the fourth pipe section

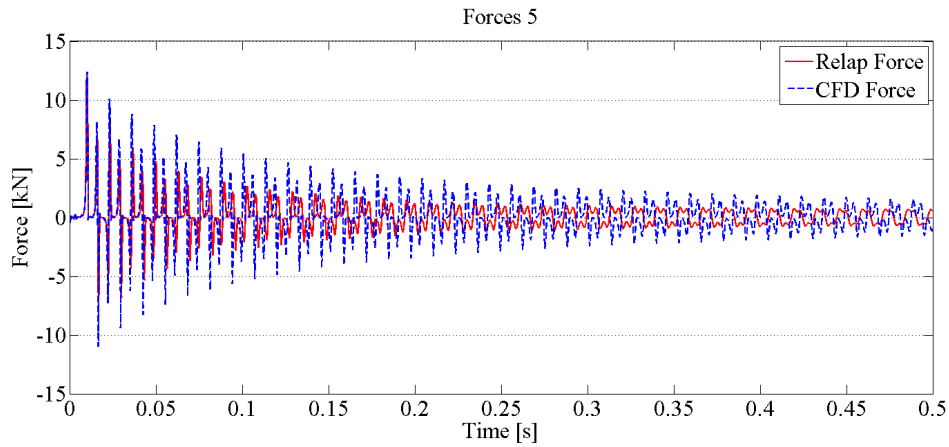

Figure B.16: Relap and AFINA CFD calculated force in the fifth pipe section

Appendix C

Mesh

In this appendix the meshes used in the mesh convergence test, see Section 6.1.1, are presented. The figures show the mesh over the fluid cross section. It also gives a basic view of the mesh in tha axial direction of the fluid.

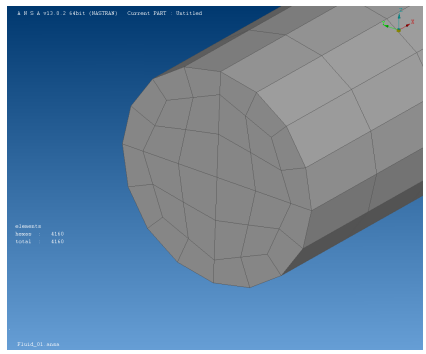

(a) Fluid_01

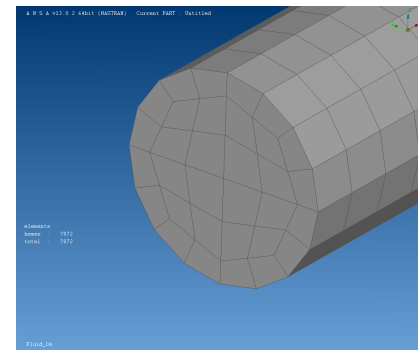

(b) Fluid_04

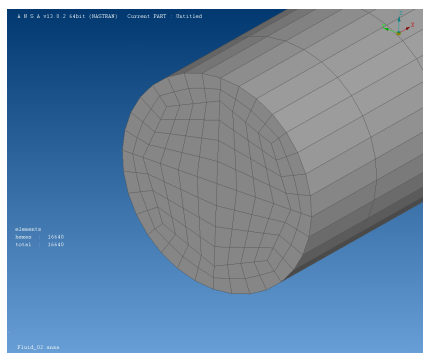

(c) Fluid_02

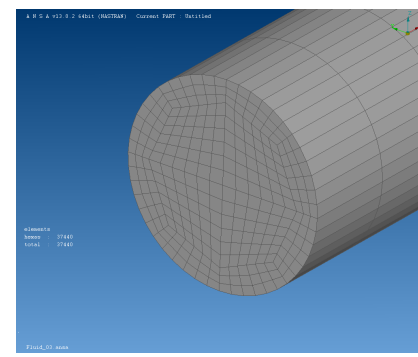

(d) Fluid_03

Figure C.1: The different meshes used in the mesh convergence test

Appendix D

Stresses

In this appendix all the different stress responses from all the different simulations are presented. They are presented alone without being compared to any of the other simulations.

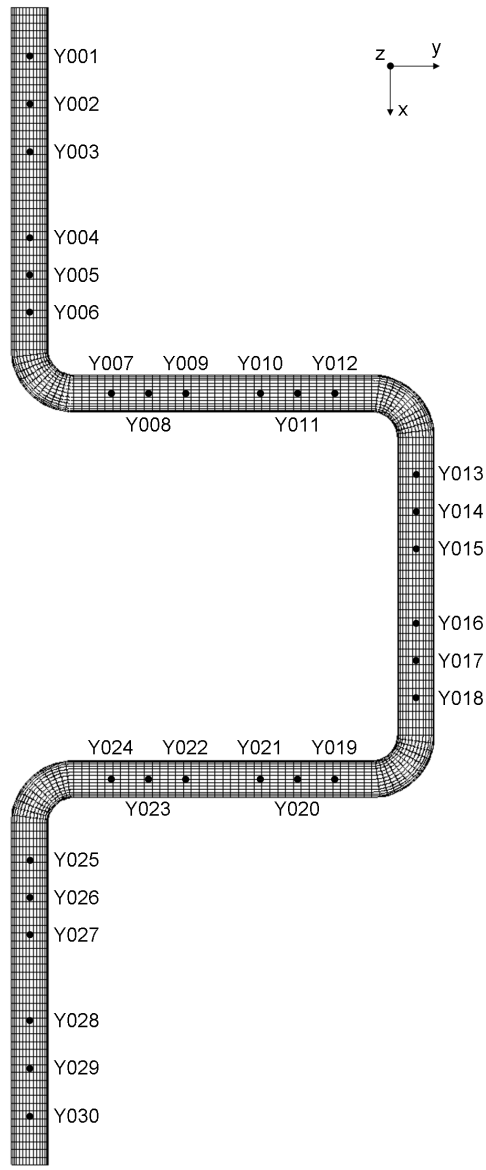

Figure D.1: Pipe node placement

Stress results due to the Relap calculated load			
Point	Pipestress	ADINA Mode Superposition	ADINA Direct Integration
Y001	153.78 MPa	112.05 MPa	115.22 MPa
Y002	125.96 MPa	93.07 MPa	94.38 MPa
Y003	99.61 MPa	85.85 MPa	86.19 MPa
Y004	59.08 MPa	89.18 MPa	89.17 MPa
Y005	69.72 MPa	85.99 MPa	85.92 MPa
Y006	88.68 MPa	101.31 MPa	101.09 MPa
Y007	95.90 MPa	103.40 MPa	102.61 MPa
Y008	92.89 MPa	85.34 MPa	85.19 MPa
Y009	91.05 MPa	88.76 MPa	88.59 MPa
Y010	99.40 MPa	88.66 MPa	88.55 MPa
Y011	104.28 MPa	85.29 MPa	85.29 MPa
Y012	108.45 MPa	103.66 MPa	102.00 MPa
Y013	106.98 MPa	102.02 MPa	102.27 MPa
Y014	94.45 MPa	85.57 MPa	85.16 MPa
Y015	82.65 MPa	85.55 MPa	85.35 MPa
Y016	75.73 MPa	86.53 MPa	86.47 MPa
Y017	77.01 MPa	86.53 MPa	86.44 MPa
Y018	105.01 MPa	102.03 MPa	101.89 MPa
Y019	120.50 MPa	105.11 MPa	105.01 MPa
Y020	113.69 MPa	86.11 MPa	86.23 MPa
Y021	107.00 MPa	89.16 MPa	89.00 MPa
Y022	93.68 MPa	89.05 MPa	89.00 MPa
Y023	94.89 MPa	86.03 MPa	85.59 MPa
Y024	99.64 MPa	102.94 MPa	102.5 MPa
Y025	89.19 MPa	101.69 MPa	101.37 MPa
Y026	67.18 MPa	86.65 MPa	86.58 MPa
Y027	61.89 MPa	89.82 MPa	89.75 MPa
Y028	104.69 MPa	87.46 MPa	87.64 MPa
Y029	128.72 MPa	102.29 MPa	101.00 MPa
Y030	160.42 MPa	126.31 MPa	128.12 MPa

Table D.1: Stress results due to the Relap calculated load

Stress results due to the ADINA calculated load			
Point	Pipestress	ADINA Mode Superposition	ADINA Direct Integration
Y001	150.77 MPa	110.42 MPa	114.69 MPa
Y002	123.32 MPa	92.09 MPa	92.61 MPa
Y003	97.05 MPa	85.78 MPa	86.17 MPa
Y004	58.47 MPa	89.05 MPa	89.07 MPa
Y005	69.14 MPa	85.85 MPa	85.78 MPa
Y006	86.95 MPa	100.62 MPa	100.4 MPa
Y007	94.27 MPa	102.69 MPa	101.89 MPa
Y008	88.26 MPa	85.25 MPa	85.09 MPa
Y009	89.37 MPa	88.68 MPa	88.54 MPa
Y010	98.57 MPa	88.59 MPa	88.48 MPa
Y011	103.05 MPa	85.22 MPa	85.19 MPa
Y012	106.02 MPa	102.75 MPa	101.07 MPa
Y013	103.36 MPa	101.53 MPa	101.78 MPa
Y014	90.44 MPa	85.33 MPa	84.93 MPa
Y015	85.09 MPa	85.37 MPa	85.21 MPa
Y016	75.59 MPa	86.30 MPa	86.26 MPa
Y017	77.30 MPa	86.21 MPa	86.22 MPa
Y018	101.83 MPa	100.58 MPa	101.41 MPa
Y019	116.45 MPa	103.30 MPa	102.75 MPa
Y020	111.22 MPa	85.54 MPa	85.65 MPa
Y021	104.97 MPa	88.99 MPa	88.91 MPa
Y022	93.83 MPa	89.05 MPa	89.03 MPa
Y023	94.15 MPa	85.65 MPa	85.63 MPa
Y024	98.72 MPa	103.02 MPa	102.61 MPa
Y025	87.89 MPa	101.77 MPa	101.57 MPa
Y026	67.51 MPa	86.67 MPa	86.62 MPa
Y027	61.65 MPa	89.83 MPa	89.77 MPa
Y028	101.12 MPa	87.37 MPa	87.56 MPa
Y029	126.83 MPa	101.24 MPa	99.99 MPa
Y030	160.41 MPa	124.48 MPa	126.45 MPa

Table D.2: Stress results due to the ADINA calculated load

Stress results from the Fluid Structure Interaction simulation	
Point	Stress
Y001	103.41 MPa
Y002	89.38 MPa
Y003	95.57 MPa
Y004	100.28 MPa
Y005	98.28 MPa
Y006	105.15 MPa
Y007	109.96 MPa
Y008	102.94 MPa
Y009	107.20 MPa
Y010	108.05 MPa
Y011	103.78 MPa
Y012	106.83 MPa
Y013	107.05 MPa
Y014	103.57 MPa
Y015	103.28 MPa
Y016	103.61 MPa
Y017	104.07 MPa
Y018	108.44 MPa
Y019	110.87 MPa
Y020	104.99 MPa
Y021	109.48 MPa
Y022	110.15 MPa
Y023	105.79 MPa
Y024	113.09 MPa
Y025	113.23 MPa
Y026	106.00 MPa
Y027	110.37 MPa
Y028	109.35 MPa
Y029	105.99 MPa
Y030	115.25 MPa

Table D.3: Fluid Structure Interaction results

Axial stress component results due to the Relap calculated load			
Point	Pipestress	ADINA Mode Superposition	ADINA Direct Integration
Y001	153.78 MPa	109.48 MPa	115.00 MPa
Y002	125.96 MPa	87.69 MPa	90.48 MPa
Y003	99.61 MPa	69.26 MPa	71.25 MPa
Y004	59.08 MPa	48.08 MPa	53.13 MPa
Y005	69.72 MPa	51.77 MPa	60.77 MPa
Y006	88.68 MPa	67.22 MPa	76.05 MPa
Y007	95.90 MPa	82.19 MPa	82.01 MPa
Y008	92.89 MPa	73.72 MPa	74.23 MPa
Y009	91.05 MPa	66.52 MPa	77.00 MPa
Y010	99.40 MPa	75.55 MPa	73.81 MPa
Y011	104.28 MPa	82.11 MPa	78.69 MPa
Y012	108.45 MPa	88.02 MPa	82.82 MPa
Y013	106.98 MPa	78.77 MPa	82.58 MPa
Y014	94.45 MPa	71.07 MPa	75.93 MPa
Y015	82.65 MPa	67.56 MPa	67.09 MPa
Y016	75.73 MPa	68.42 MPa	66.79 MPa
Y017	77.01 MPa	62.42 MPa	60.93 MPa
Y018	105.01 MPa	68.69 MPa	70.17 MPa
Y019	120.50 MPa	89.10 MPa	86.78 MPa
Y020	113.69 MPa	81.91 MPa	80.50 MPa
Y021	107.00 MPa	79.11 MPa	78.26 MPa
Y022	93.68 MPa	78.41 MPa	76.90 MPa
Y023	94.89 MPa	74.11 MPa	72.34 MPa
Y024	99.64 MPa	79.57 MPa	77.08 MPa
Y025	89.19 MPa	67.76 MPa	75.21 MPa
Y026	67.18 MPa	52.16 MPa	63.21 MPa
Y027	61.89 MPa	48.81 MPa	52.39 MPa
Y028	104.69 MPa	77.79 MPa	79.84 MPa
Y029	128.72 MPa	100.32 MPa	99.81 MPa
Y030	160.42 MPa	125.90 MPa	126.86 MPa

Table D.4: Axial stress component results due to the Relap calculated load

Axial stress component results due to the ADINA calculated load			
Point	Pipestress	ADINA Mode Superposition	ADINA Direct Integration
Y001	150.77 MPa	107.98 MPa	114.48 MPa
Y002	123.32 MPa	86.81 MPa	89.84 MPa
Y003	97.05 MPa	67.78 MPa	68.60 MPa
Y004	58.47 MPa	47.78 MPa	53.05 MPa
Y005	69.14 MPa	50.78 MPa	60.20 MPa
Y006	86.95 MPa	65.72 MPa	74.90 MPa
Y007	94.27 MPa	80.50 MPa	80.53 MPa
Y008	88.26 MPa	72.58 MPa	73.24 MPa
Y009	89.37 MPa	64.79 MPa	77.47 MPa
Y010	98.57 MPa	72.79 MPa	73.44 MPa
Y011	103.05 MPa	79.39 MPa	77.51 MPa
Y012	106.02 MPa	85.44 MPa	81.65 MPa
Y013	103.36 MPa	78.01 MPa	81.90 MPa
Y014	90.44 MPa	71.60 MPa	76.32 MPa
Y015	85.09 MPa	66.52 MPa	68.50 MPa
Y016	75.59 MPa	67.74 MPa	67.68 MPa
Y017	77.30 MPa	63.46 MPa	61.00 MPa
Y018	101.83 MPa	65.48 MPa	70.16 MPa
Y019	116.45 MPa	84.16 MPa	81.71 MPa
Y020	111.22 MPa	80.10 MPa	79.16 MPa
Y021	104.97 MPa	78.56 MPa	77.68 MPa
Y022	93.83 MPa	77.59 MPa	76.07 MPa
Y023	94.15 MPa	73.20 MPa	70.98 MPa
Y024	98.72 MPa	79.68 MPa	76.81 MPa
Y025	87.89 MPa	67.85 MPa	75.74 MPa
Y026	67.51 MPa	52.16 MPa	63.78 MPa
Y027	61.65 MPa	48.42 MPa	52.33 MPa
Y028	101.12 MPa	77.01 MPa	80.52 MPa
Y029	126.83 MPa	99.03 MPa	99.06 MPa
Y030	160.41 MPa	124.00 MPa	124.75 MPa

Table D.5: Axial stress component results due to the ADINA calculated load

Axial stress component results due to the Fluid Structure Interaction simulation	
Point	Stress
Y001	103.07 MPa
Y002	82.05 MPa
Y003	65.53 MPa
Y004	47.01 MPa
Y005	50.19 MPa
Y006	63.24 MPa
Y007	78.38 MPa
Y008	72.96 MPa
Y009	75.11 MPa
Y010	71.80 MPa
Y011	66.76 MPa
Y012	70.54 MPa
Y013	69.52 MPa
Y014	67.35 MPa
Y015	67.63 MPa
Y016	61.47 MPa
Y017	57.86 MPa
Y018	58.25 MPa
Y019	80.74 MPa
Y020	78.73 MPa
Y021	76.13 MPa
Y022	73.62 MPa
Y023	70.98 MPa
Y024	76.83 MPa
Y025	69.50 MPa
Y026	57.00 MPa
Y027	45.23 MPa
Y028	76.46 MPa
Y029	92.97 MPa
Y030	113.12 MPa

Table D.6: Axial stress component results due to the Fluid Structure Interaction simulation